# 雲と大気大循環

惑星の雲・エアロゾル

金星

地球成層圏エアロゾル

初期地球
初期火星

系外惑星

- 惑星のアルベドを支配
- 散乱温室効果
- 上層大気へ輸送され宇宙空間への散逸に至る化学種を制限

H$_2$SO$_4$ clouds of Venus
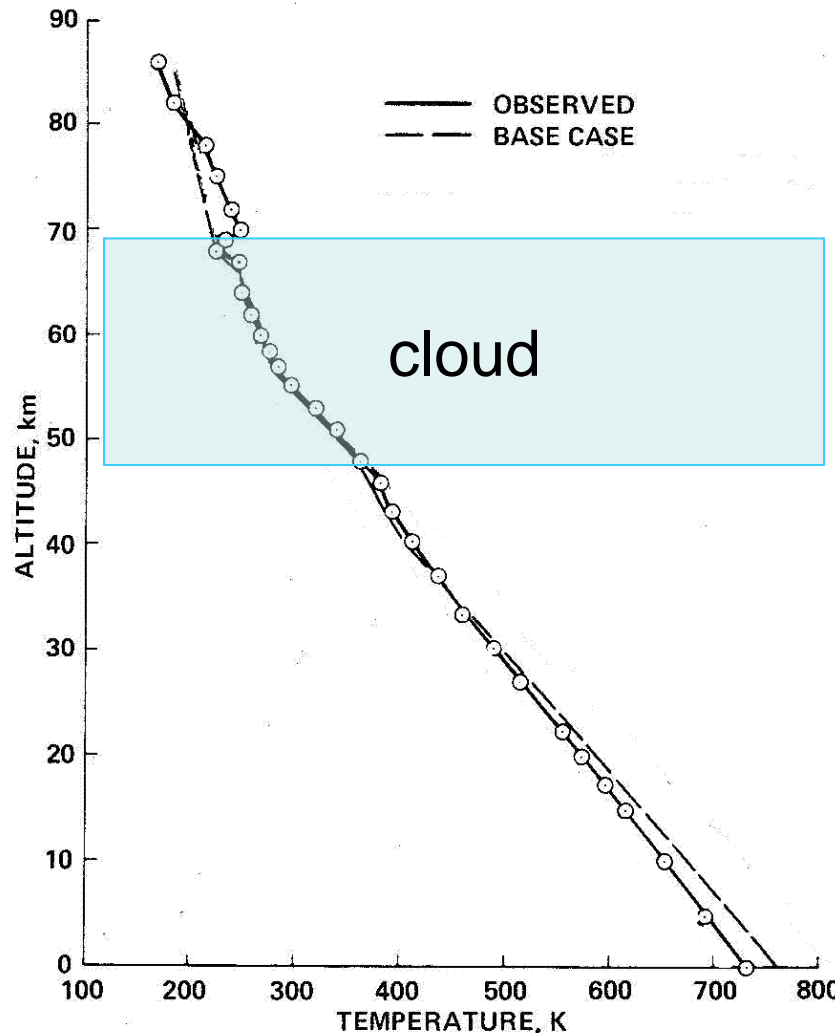
Fig. 2. Comparison between the observed temperature structure of Venus' lower atmosphere and that of several models, which are described in the main text.
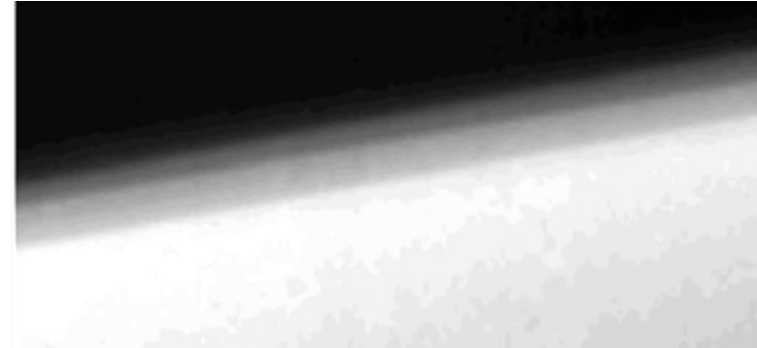
- Solar energy flux reaching the Venus surface (17W/m^2) is much less than that of the Earth (168W/m^2).

- Greenhouse effect of massive CO$_2$ and small amount of H$_2$O explains the high temperature.

Pollack et al. (1980)

Polarization of sunlight reflected by Venus

Horizontal Linear Polarization
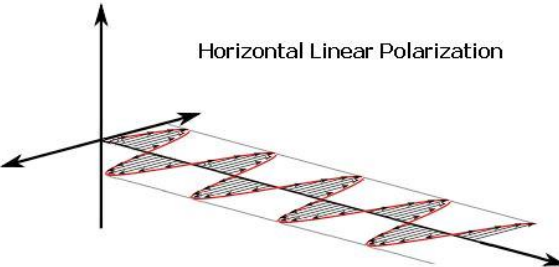
Vertical Linear Polarization

Hansen & Hovenier (1974)

FIG. 7. Observations and theoretical computations of the polarization of sunlight reflected by Venus at $\lambda = 0.99\ \mu m$. The observations were made with an intermediate bandwidth filter, the X's being obtained by Coffeen and Gehrels (1969) in 1959–67 and by Coffeen (cf. Dollfus and Coffeen, 1970) from 1967 to March 1969, and the O's being obtained by Coffeen (cf. Dollfus and Coffeen, 1970) in May–July, 1969. The theoretical curves are for spherical particles having the size distribution (8) with $b = 0.07$. The different theoretical curves are for various refractive indices, the effective particle radius being selected in each case to yield closest agreement with the observations for all wavelengths.

Refractive index = 1.44

→ consistent with H_2SO_4-H_2O solution

Effective radius ~ 1 μm

Microphysical properties of Venus clouds

- H_2SO_4-H_2O droplets with radii $r < 5$ μm
- Smallest mode (including sub-cloud haze) might be condensation nuclei whose composition is unknown.
- Size distribution is variable.

Pioneer Venus LCPS (54 km)

MODE 1 LOG-NORMAL

Mode 1

Mode 2

Mode 3

Ncm^{-3}μm^{-1}

0.1   1 DIAMETER (μm)   10

Diameter (μm)

Venera-13 Lander

P

S

Cl

60   55   50   47

Cl ? S ? P ?
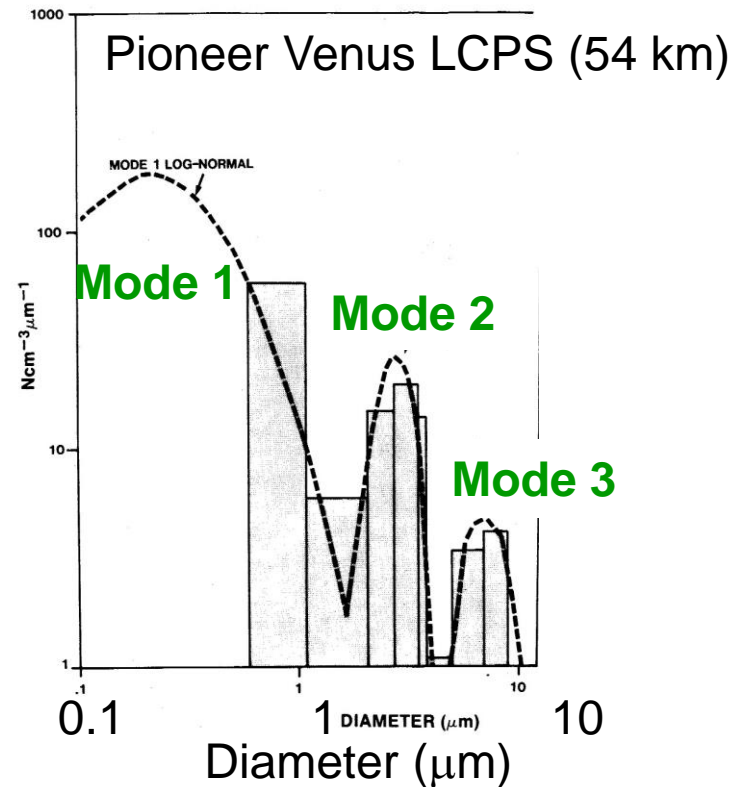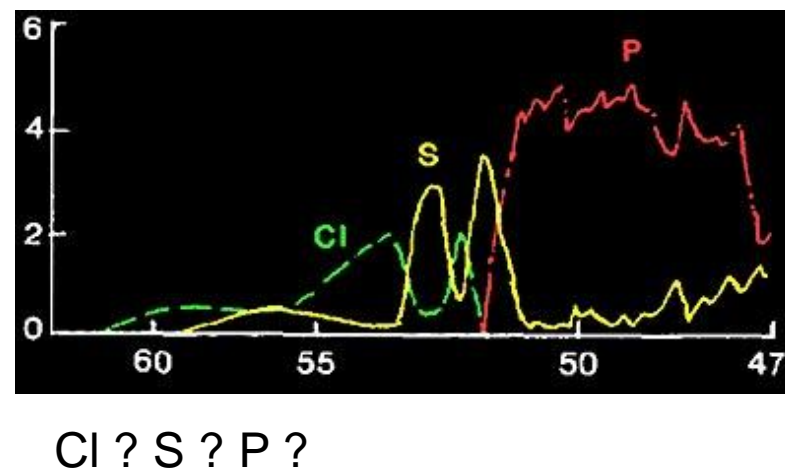
微物理的性質

- H_2SO_4-H_2O液滴、r < 5 μm
- 最小モード (sub-cloud hazeを含む)は凝結核である可能性あり。凝結核の組成は不明。
- 粒径分布は測るたびに違う
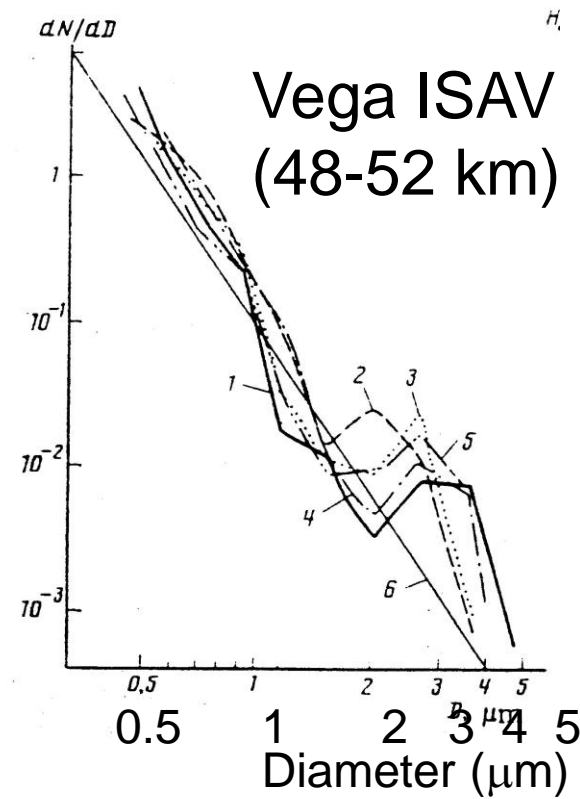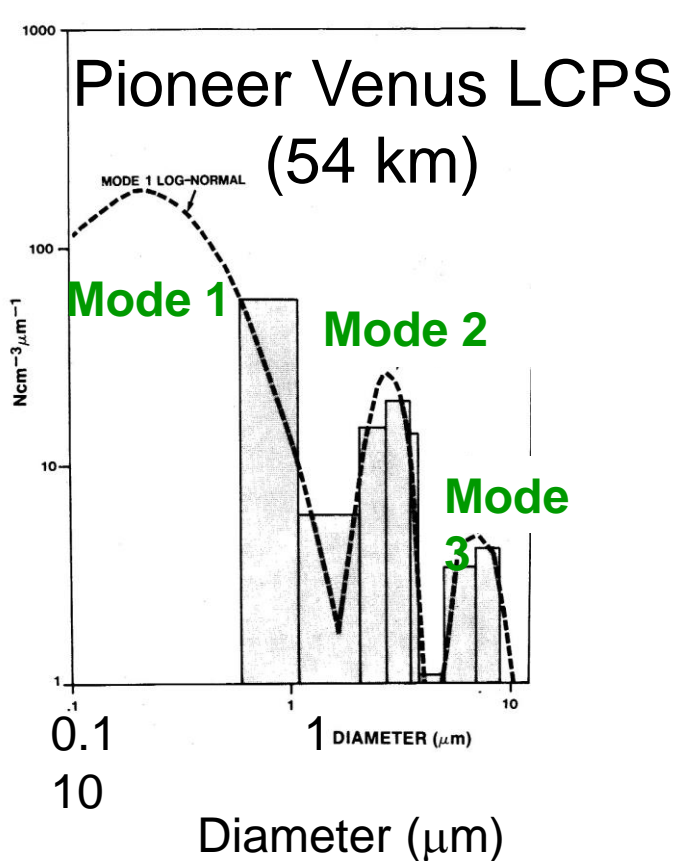
Pioneer Venus LCPS
(54 km)

Mode 1
Mode 2
Mode 3

0.1
1
10
Diameter (μm)

Vega ISAV
(48-52 km)

0.5   1   2   3 μm 4 5
Diameter (μm)

# Three-layered structure – Different dynamical and chemical regimes at different altitudes?

The bulk of the mass exists in Mode 2 (r ~ 1 μm)

The bulk of the mass exists in Mode 2 and 3 (r = 1-5 μm)
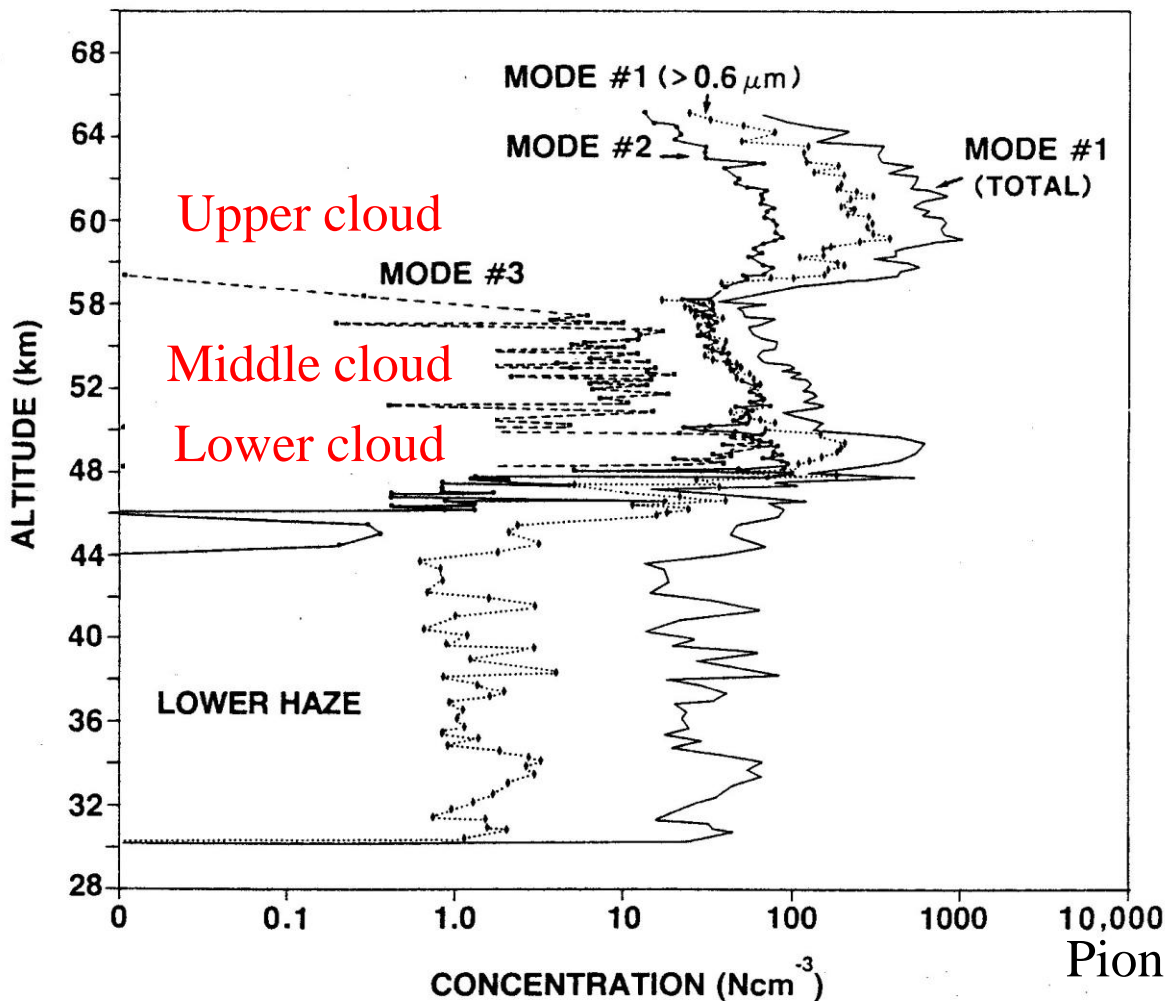
Pioneer Venus LCPS
(Knollenberg and Hunten, 1980)

Three-layered structure – Different dynamical and chemical regimes at different altitudes?

Upper cloud

Middle cloud

Lower cloud

Static stability measured by entry probes

赤外加熱と日射加熱

太陽光

安定化

雲層

不安定化

対流

赤外線
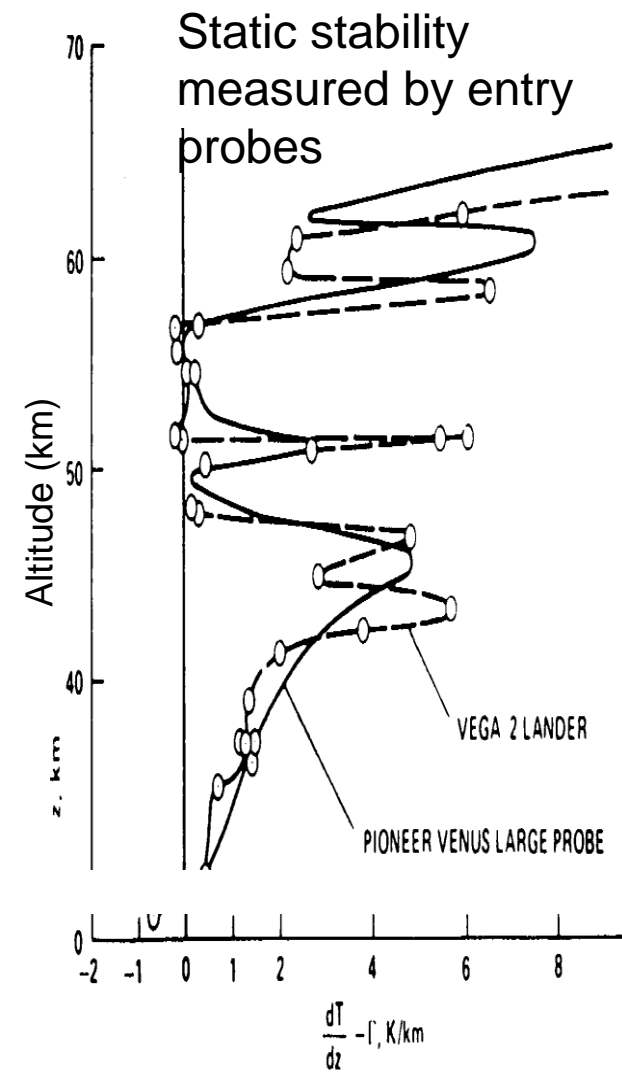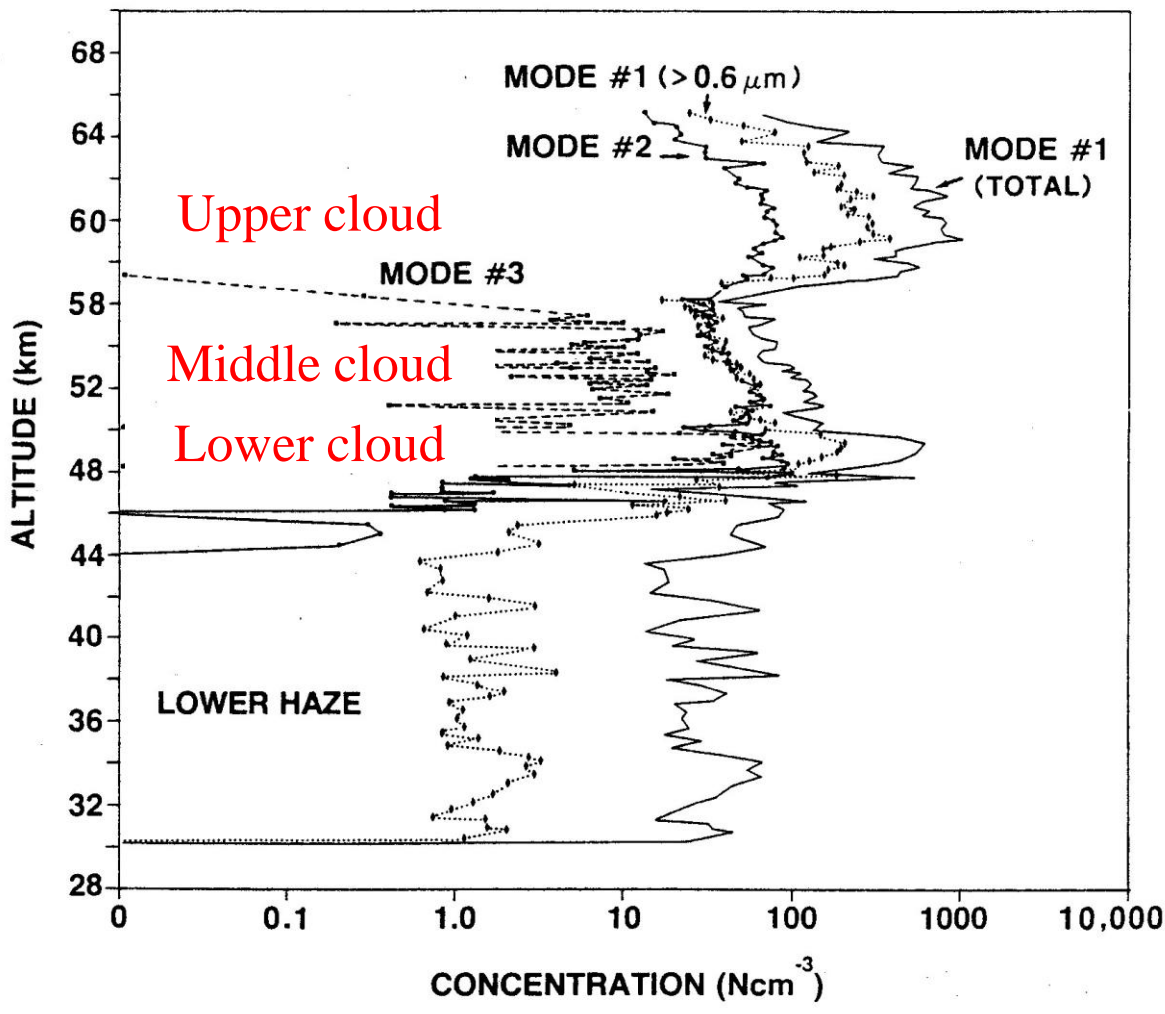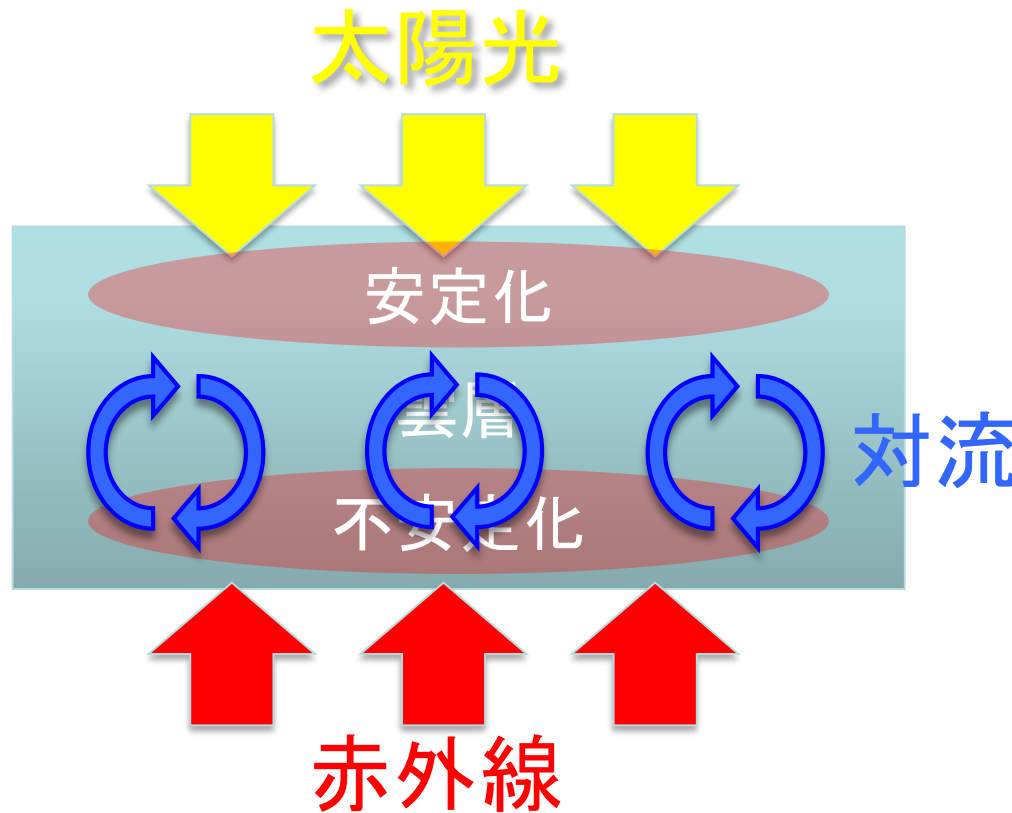
- 下層大気からの赤外線は雲層下部を加熱して成層を不安定化
- 日射は雲層上部を加熱して成層を安定化
→これらのバランスで対流強度が決まる

全球平均条件での対流構造

鉛直速度
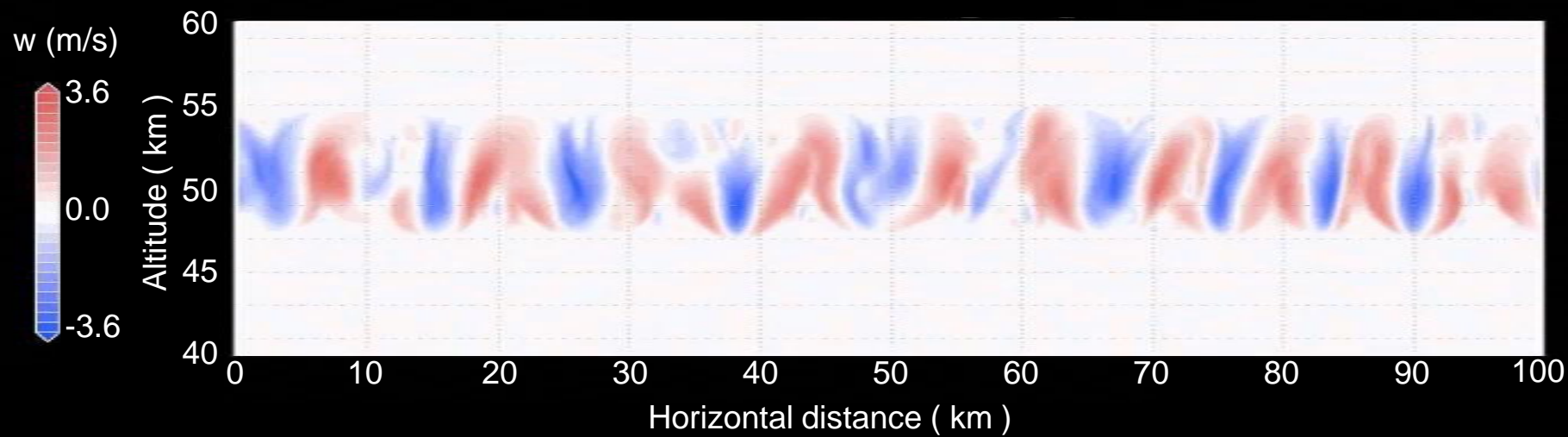
温位擾乱
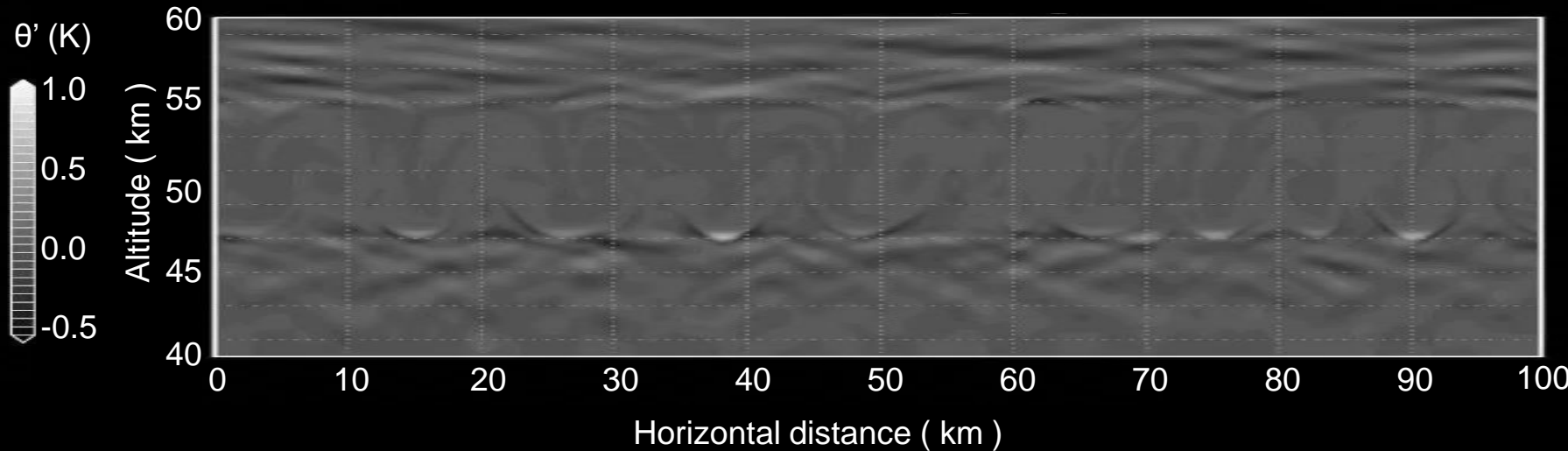
H$_2$SO$_4$ vapor profiles

67°N by Magellan

Equator by Mariner 10

by Pioneer Venus

Equator

High lat.

50 km

40 km
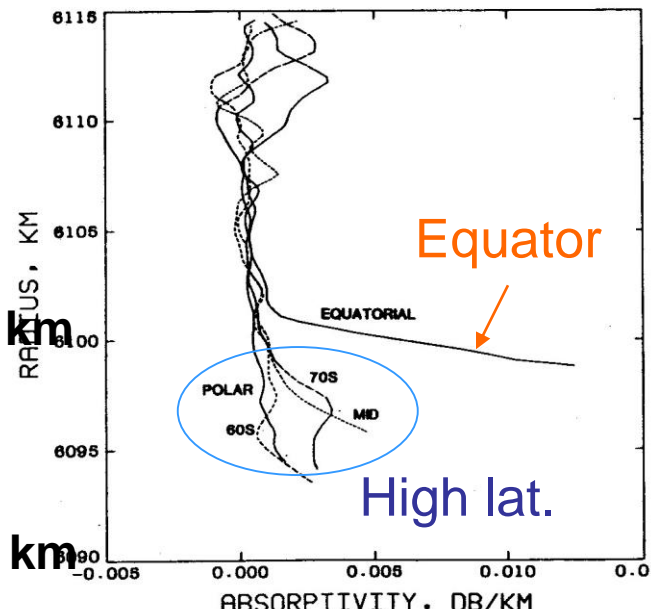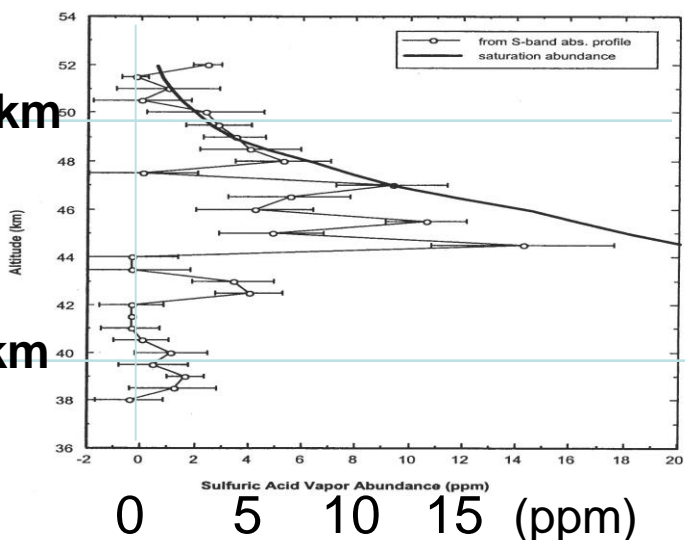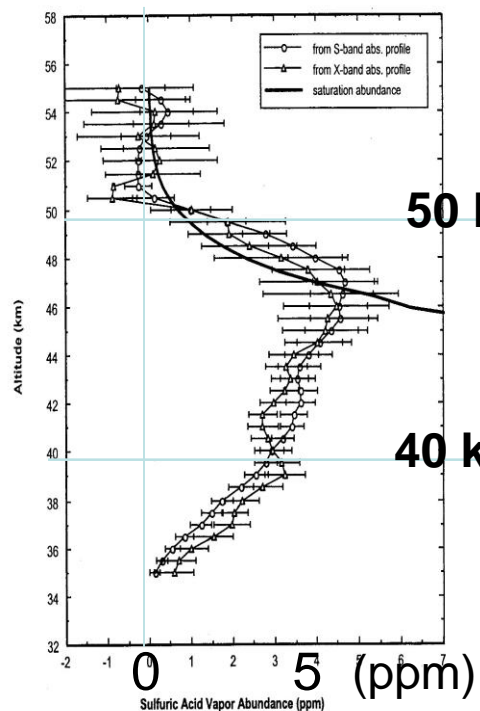
Kolodner & Steffes (1998)

Jenkins & Steffes (1991)

Sulfur-rich atmosphere: origin of H_2SO_4

SO_2 measurements by Vega landers
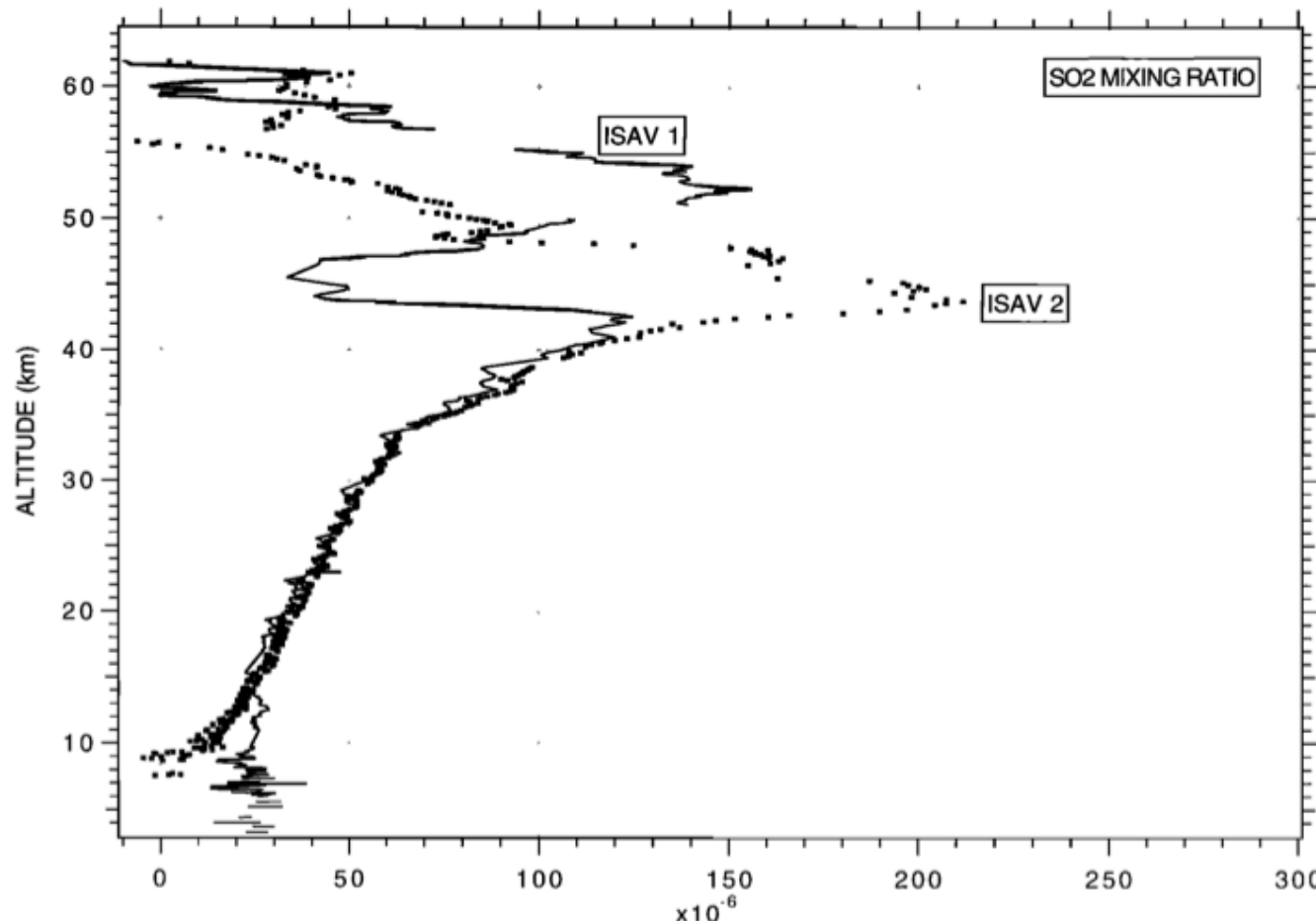
Figure 24. The SO_2 mixing ratio vertical profile retrieved for ISAV 2 (data points) is compared to that determined for ISAV 1. There is a large difference of structure above 40 km, while the profiles are nearly identical below 40 km. A peak of 210 ppm is observed at 43 km in the ISAV 2 data.

Bertaux et al. (1996)

Origin of clouds

(km)

70

60

50

40

Photochemistry above clouds

Scenario #1 (Net reaction driven by catalytic cycles including ClOx, HOx, NOx)

$$2CO_2 + h\nu \rightarrow 2CO + O_2$$

$$CO + SO_2 + O_2 + h\nu \rightarrow CO_2 + SO_3$$

$$\overline{CO_2 + SO_2 + h\nu \rightarrow CO + SO_3}$$

Scenario #2

$$SO_2 + h\nu \rightarrow SO + O$$

$$SO + h\nu \rightarrow S + O$$

$$SO_2 + O \rightarrow SO_3 \ (\times 2)$$

$$\overline{3\ SO_2 + h\nu \rightarrow S + 2SO_3}$$
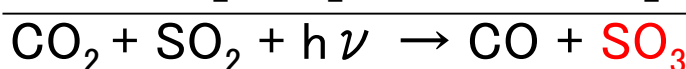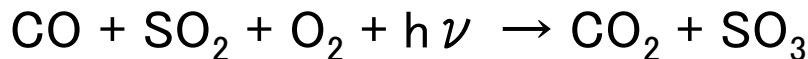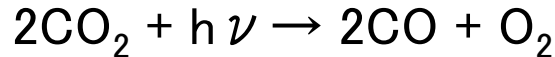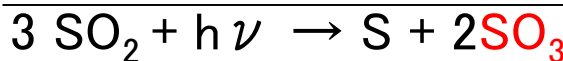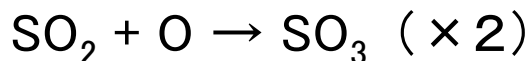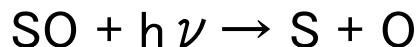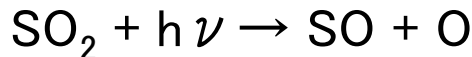
・SO_3 rapidly reacts with H_2O: $\boxed{SO_3 + H_2O \rightarrow H_2SO_4}$

・Elemental sulfur (S) can serve as condensation nuclei.

Origin of clouds

(km)

70

60

50

40

H$_2$SO$_4$ vapor and H$_2$O vapor condenses onto condensation nuclei.

Growth of particles via collision during gravitational sedimentation

Evaporation around 50 km altitude due to high temperature

Thermochemistry below clouds (Net reaction driven by catalytic cycles

$H_2SO_4 \rightarrow H_2O + SO_3$

$SO_3 + CO \rightarrow CO_2 + SO_2$

$SO_3 + OCS \rightarrow CO_2 + (SO)_2$ etc

_____

$H_2SO_4 + 4CO \rightarrow H_2O + 3CO_2 + OCS$

金星の硫黄サイクル

Zhang et al. (2012)
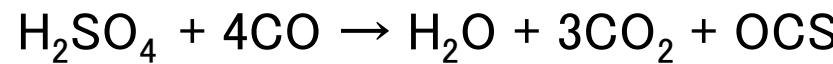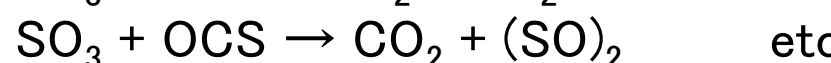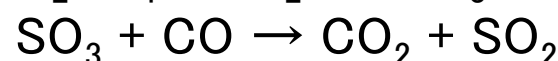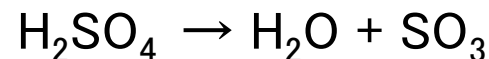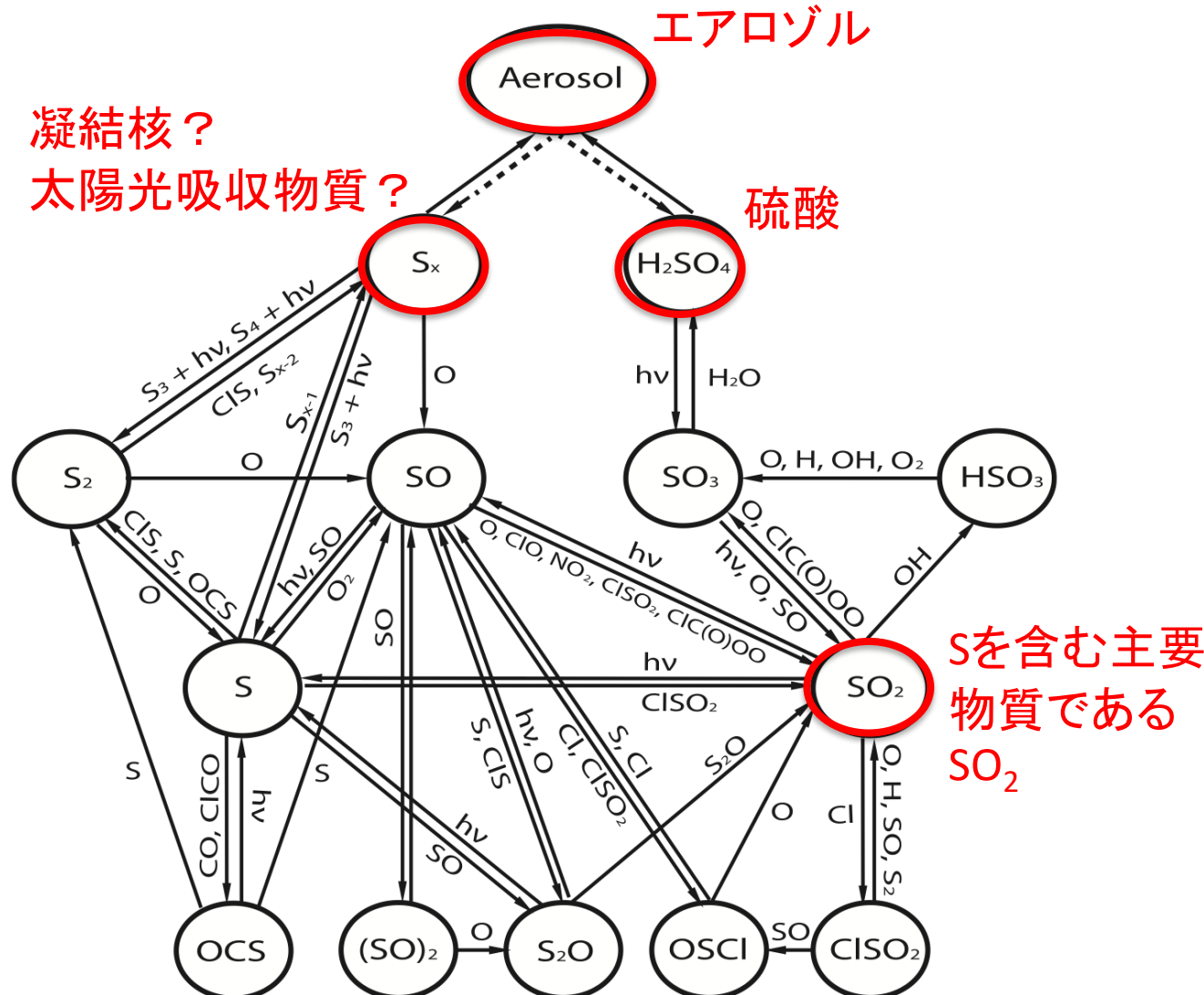
Ground-based observations of cloud-related gaseous species

Pollack et al., Icarus 103, 1, 1993
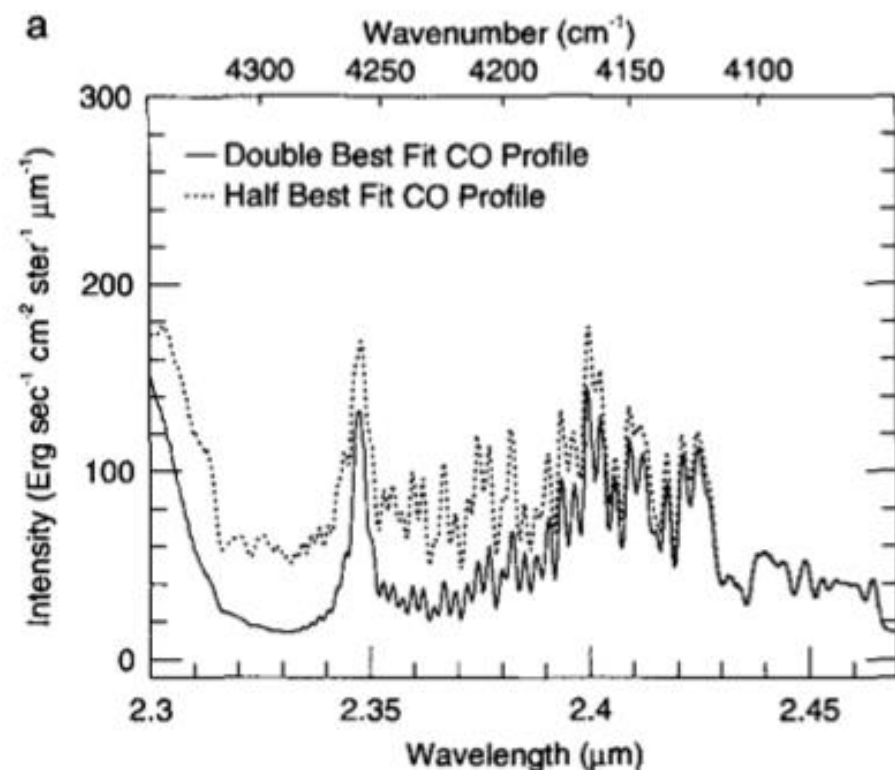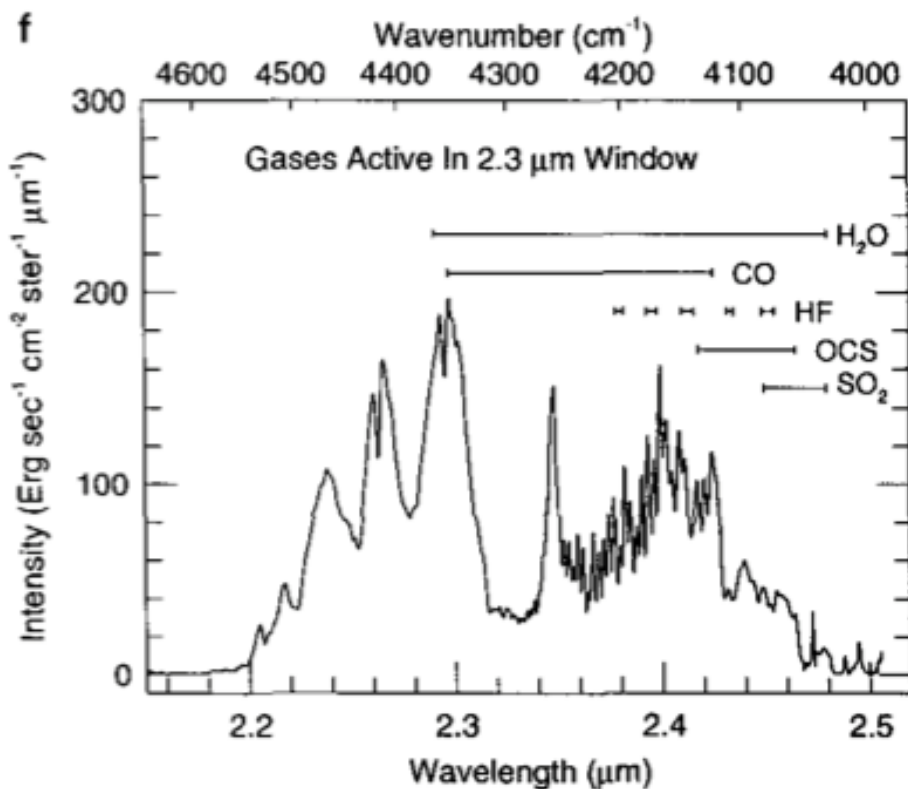
Retrieved vertical profiles
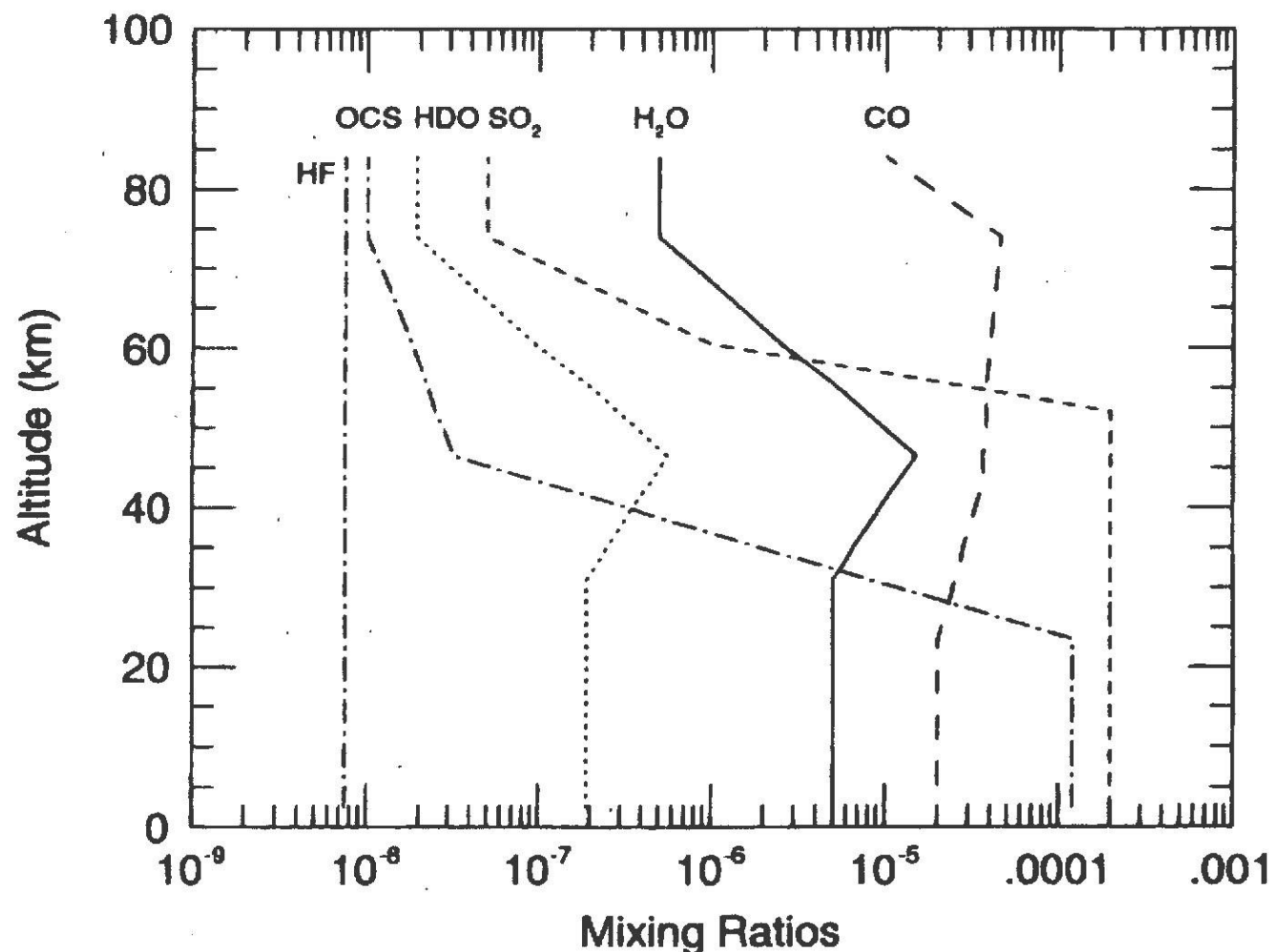
Pollack et al., Icarus 103, 1, 1993

SO, SO$_2$ profiles above cloud observed by Venus Express solar occultations (Belyaev et al. 2011)

SO: black
SO$_2$: blue
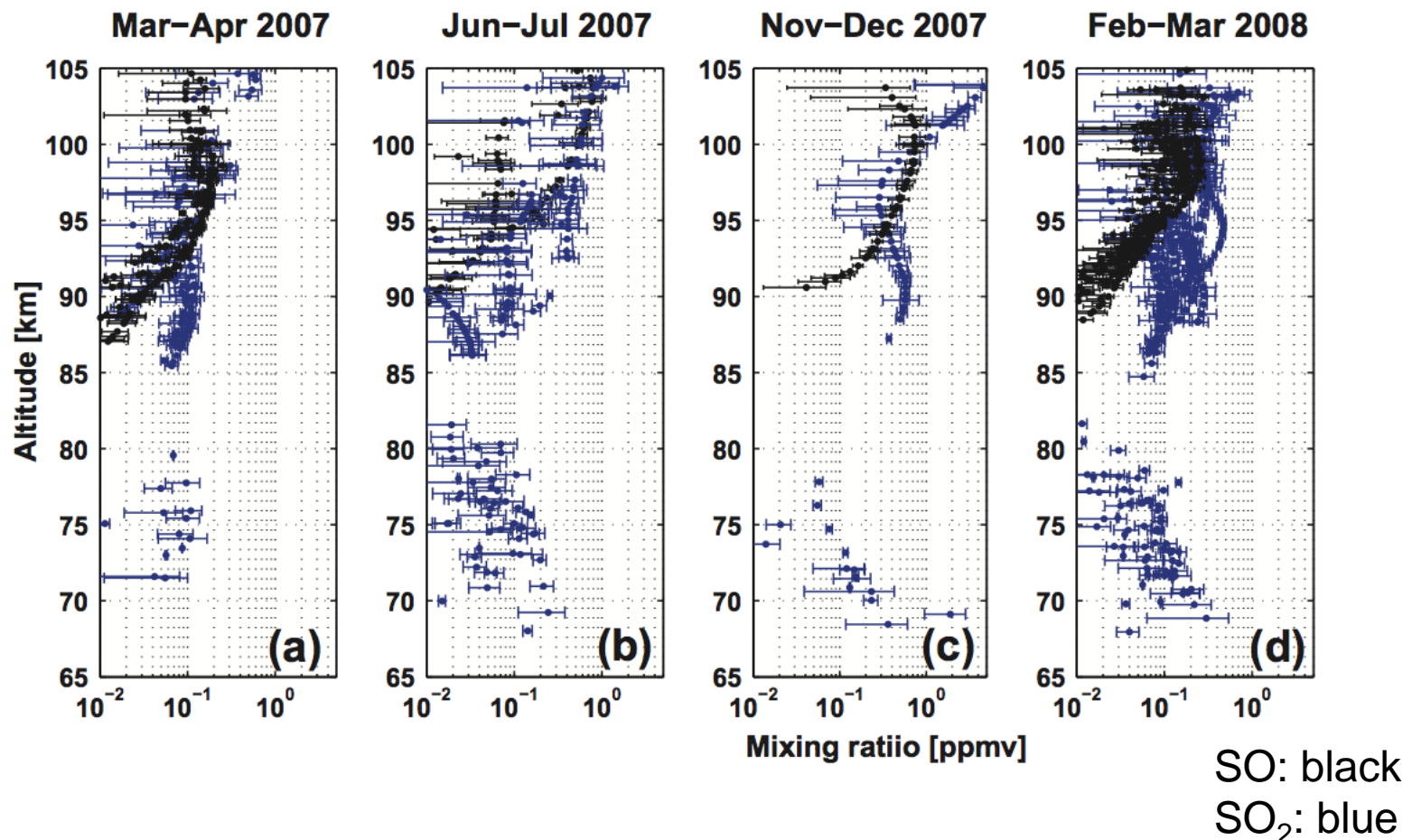
- Enhancement at high altitudes cannot be explained by traditional photochemical models.

(Zhang et al. 2012)

Artificial H_2SO_4 source added above 90 km:
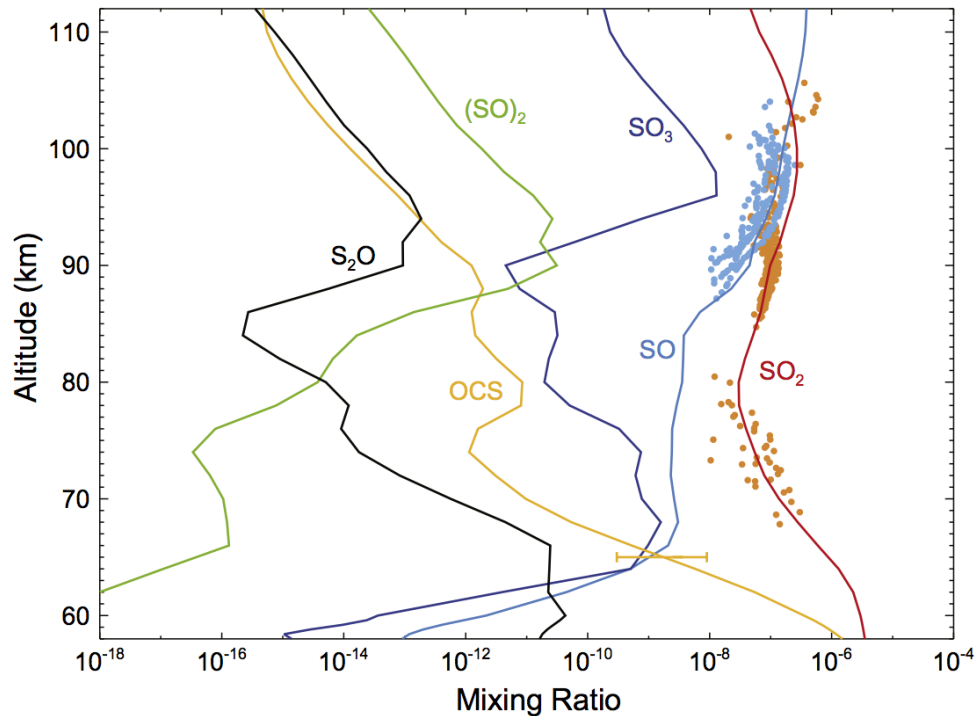
Fig. 8. Same as Fig. 2, for the sulfur oxides. The SO_2 and SO observations with errorbars are from the Belyaev et al. (2012). The temperature at 100 km is 165–170 K for the observations. The OCS measurement (0.3–9 ppb with the mean value of 3 ppb) is from Krasnopolsky (2010).

Transport of cloud particles to the upper atmosphere by winds ?
→ Open question

Material transport by meridional circulation

Akatsuki UVI 283nm

HYPOTHETICAL
LOWER ATMOSPHERE
HADLEY CELLS
AND INDIRECT CELLS

CLOUD LEVEL
HADLEY CELL

WESTWARD
SUPERROTATION
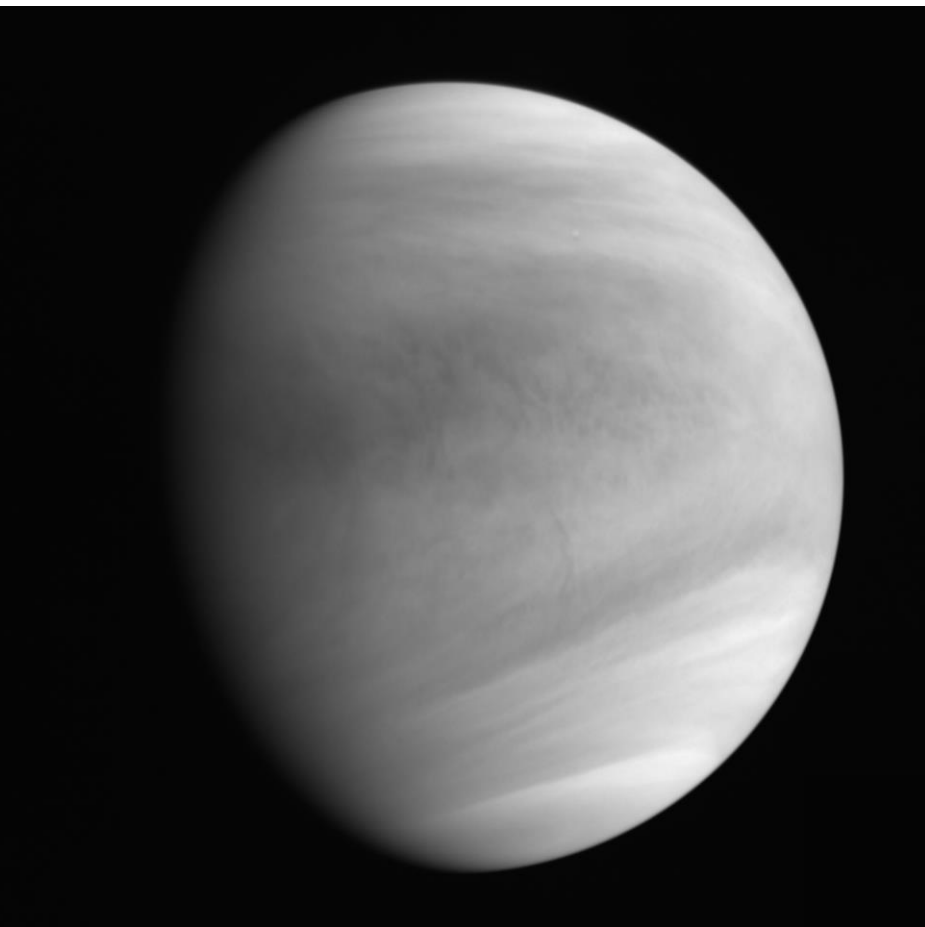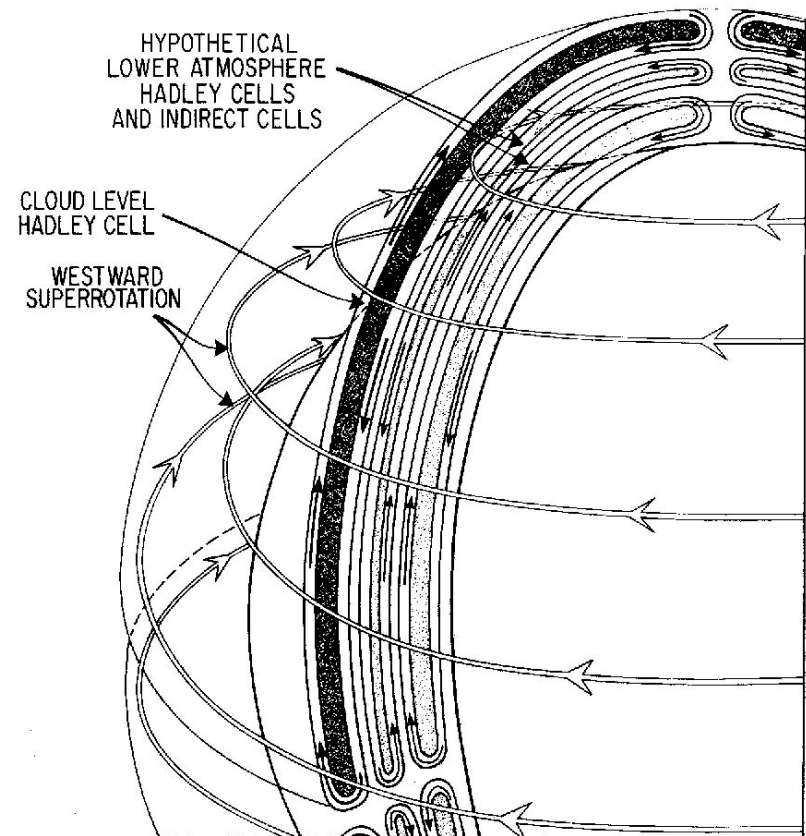
Schubert (1983)

2次元モデルによる考察

(Imamura & Hashimoto, *J. Geophys. Res.*, 1998)

Mass stream function

Vertical wind (mm/s)

EQ   POLE
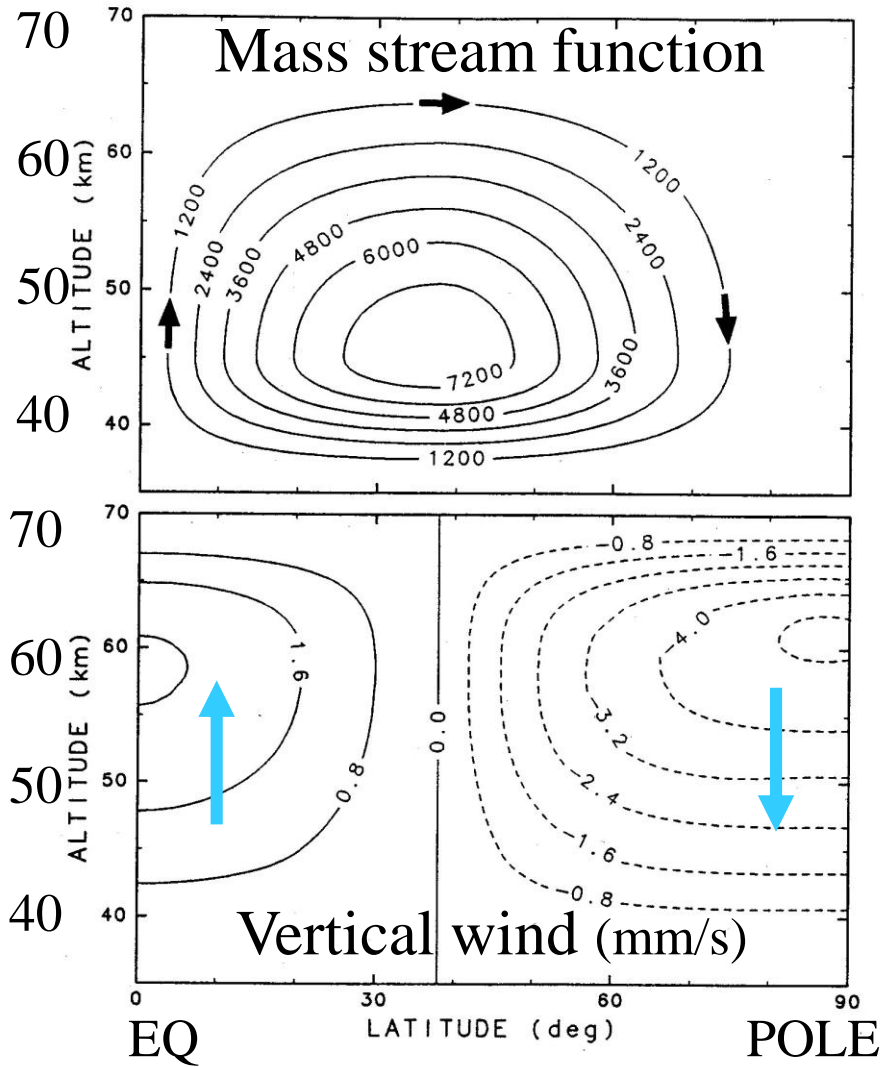
- Transport and condensation of H_2SO_4 and H_2O

- Particle radius is fixed:

    r = 1.15 μm for z > 58 km
    r = 3.65 μm for z < 58 km

- H_2SO_4 production at 60-64 km

結果

Cloud Mass Loading

Advection

Precipitation

Unit: 10^{-6} kg m^{-3}

Equator

Pole

CONTOUR INTERVAL = 2.000E+00

H$_2$SO$_4$ Vapor

Unit: ppm

Advection/Diffusion

Evaporation

Advection

Equator

Pole

CONTOUR INTERVAL = 2.000E+00
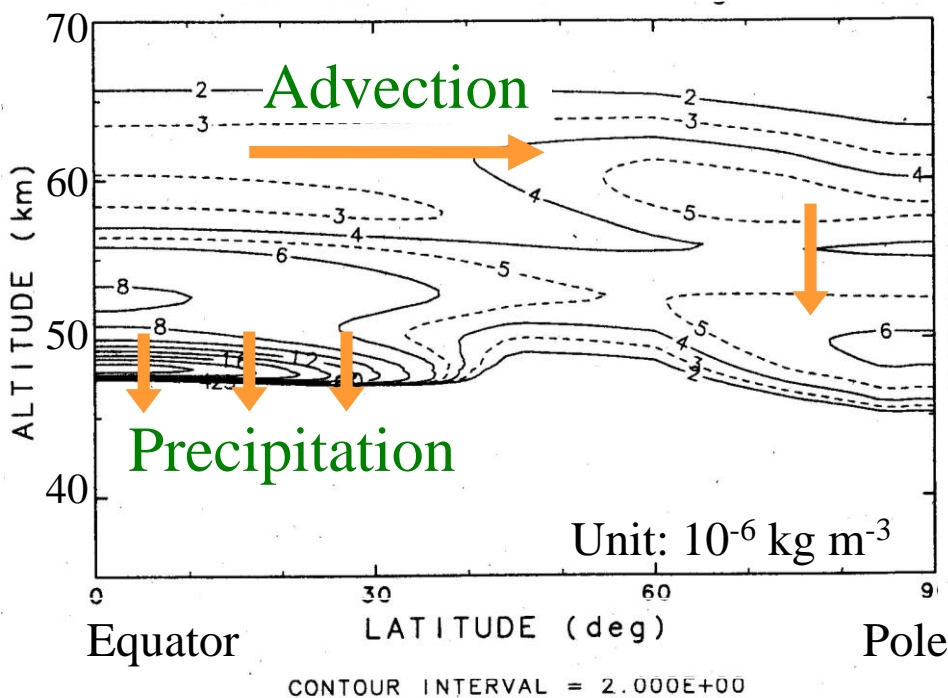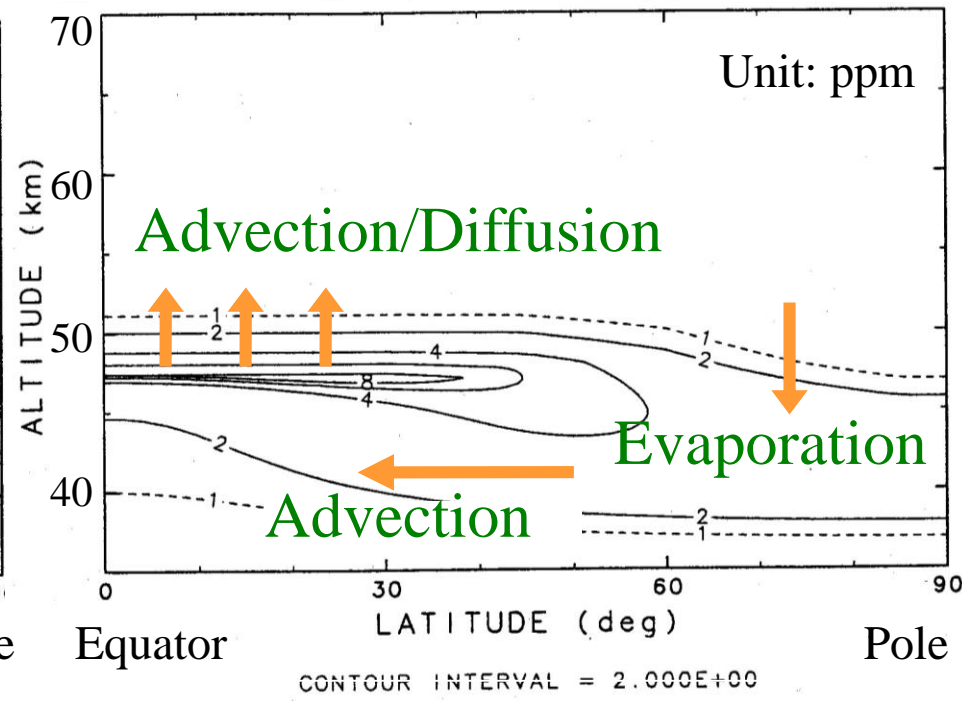
Possible planetary-scale H_2SO_4 cycle

Imamura & Hashimoto (2001)

← : Droplets
←⋯ : H_2SO_4 vapor

70km

Upwelling

Poleward advection

Photochemical production

60km

Condensation

Sedimentation
Convection
Downwelling

Convection
Upwelling

Sedimentation

50km

Stagnant region

Evaporation

Upwelling

Downwelling

40km

Equatorward advection

Diffusion

Thermal decomposition

Equator

Pole
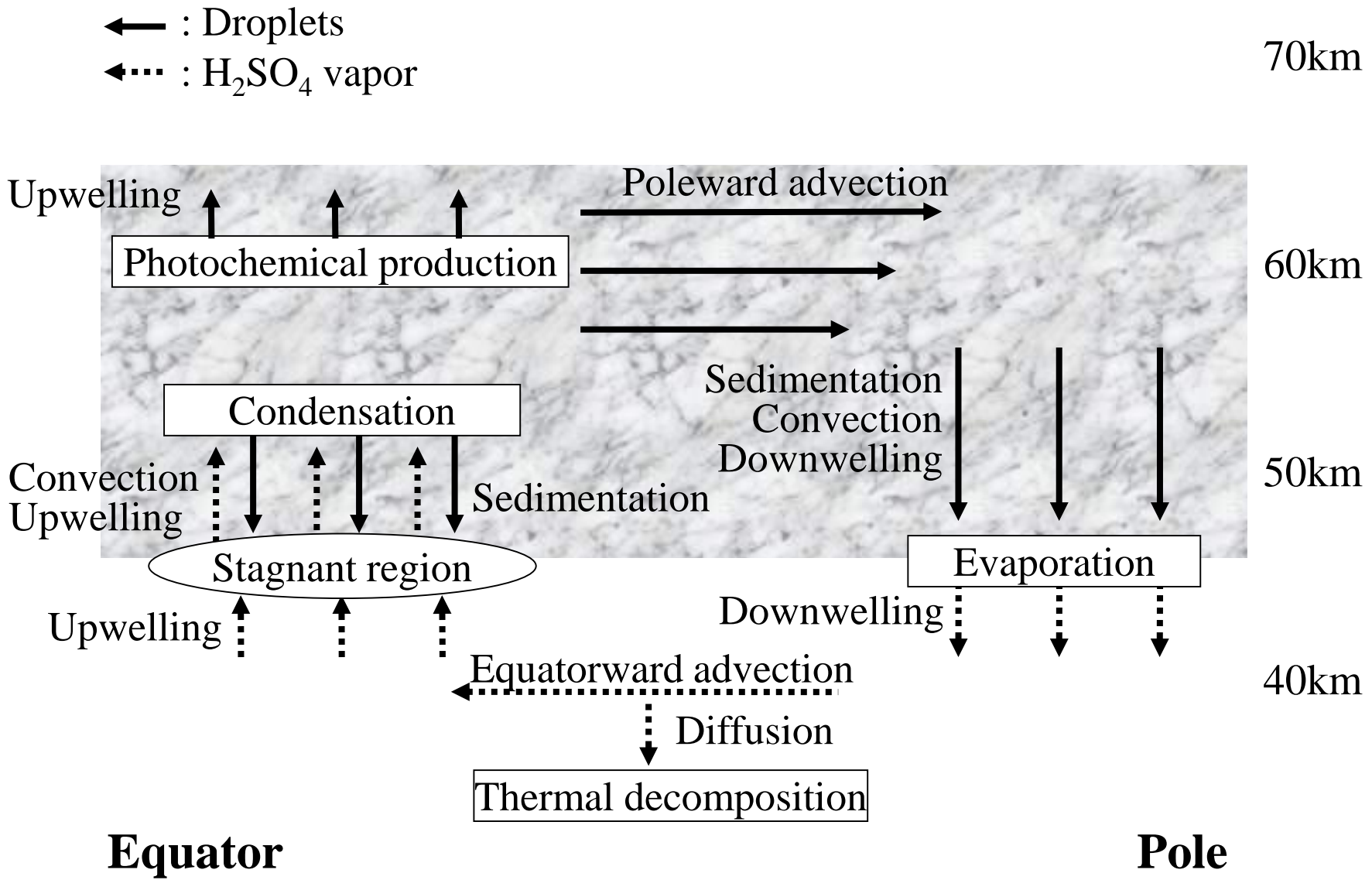
Earth's stratospheric aerosol lifecycle
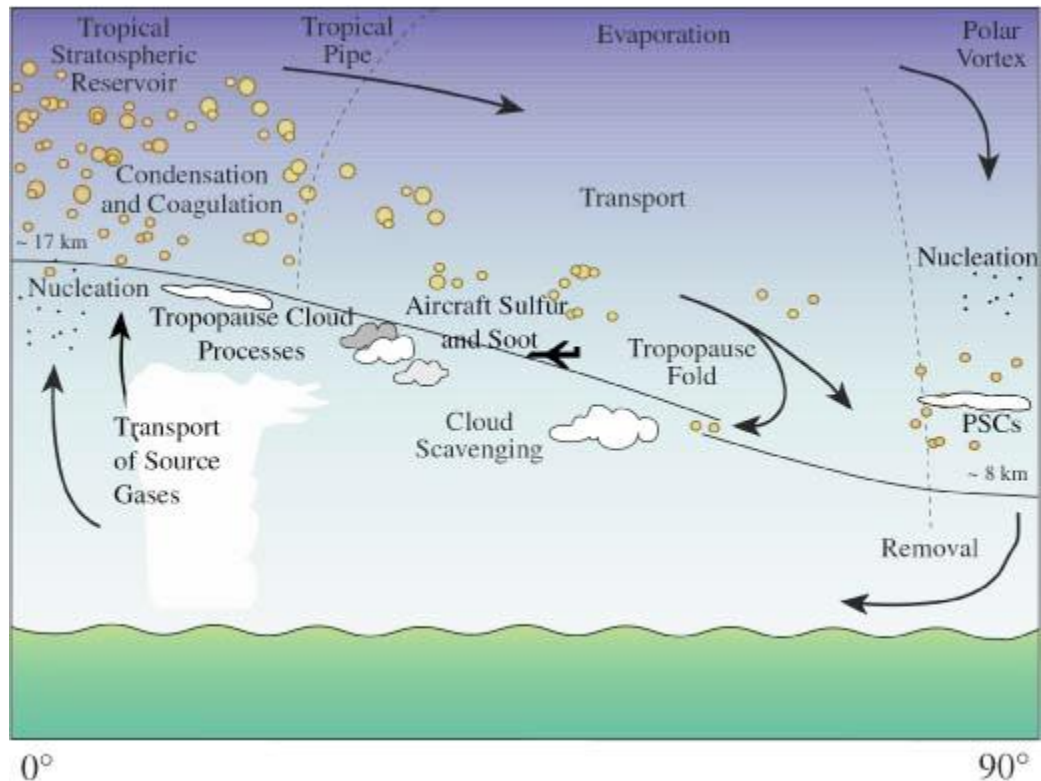
Hamill et al. (1997)
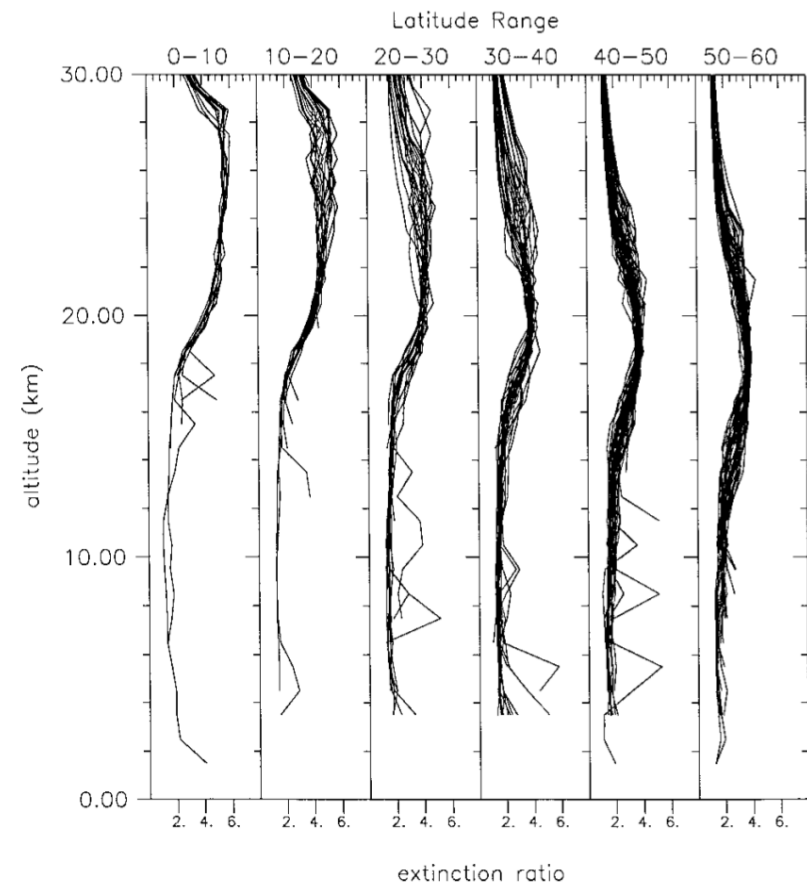
FIG. 9. Extinction ratios from the SAGE II satellite system in various latitude ranges. The extinction values were measured in April 1989 in the Southern Hemisphere. We have removed extinction ratios greater than 7 at lower altitudes for these are indications of tropospheric clouds.

あかつきIR2による2.26μm夜面画像
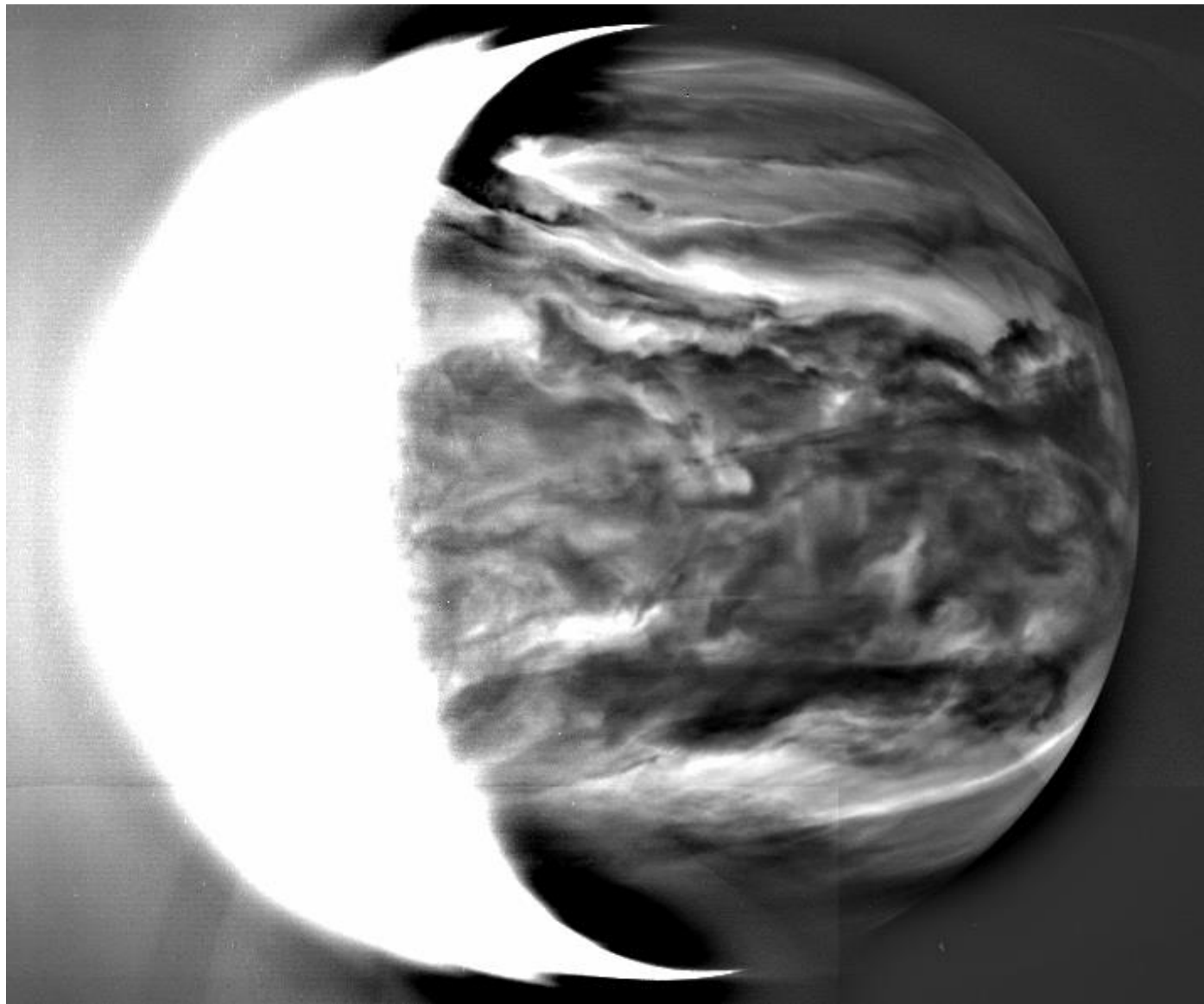
その他の輸送過程
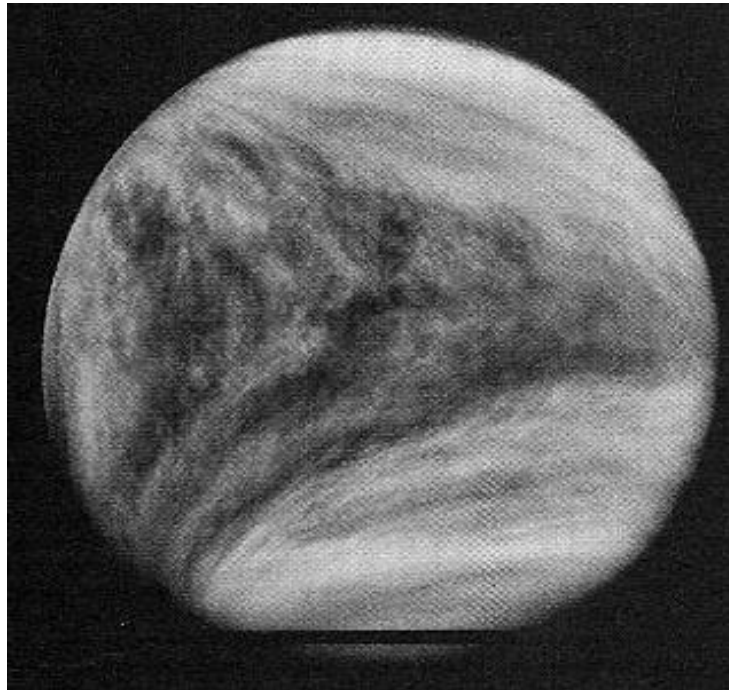
Y-feature

- Kelvin wave?
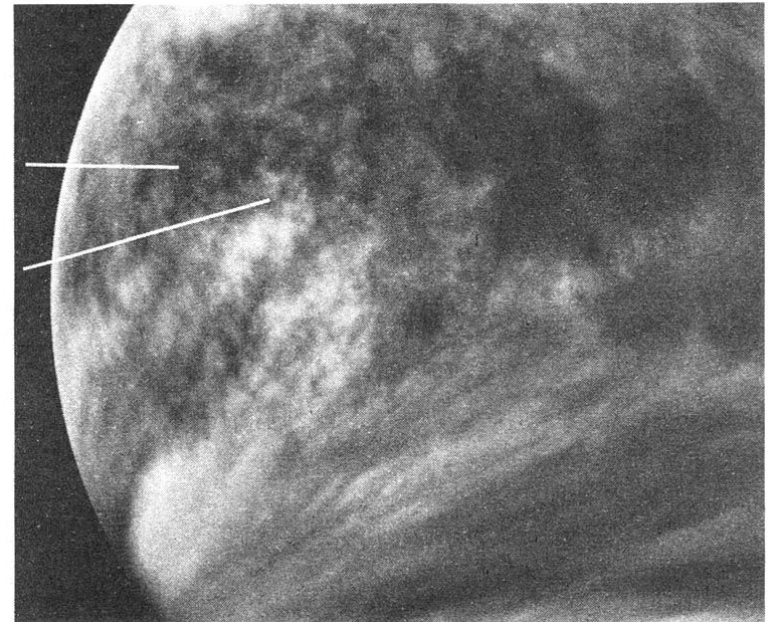
'Cells' near sub-solar region

全球平均条件での対流構造

鉛直速度
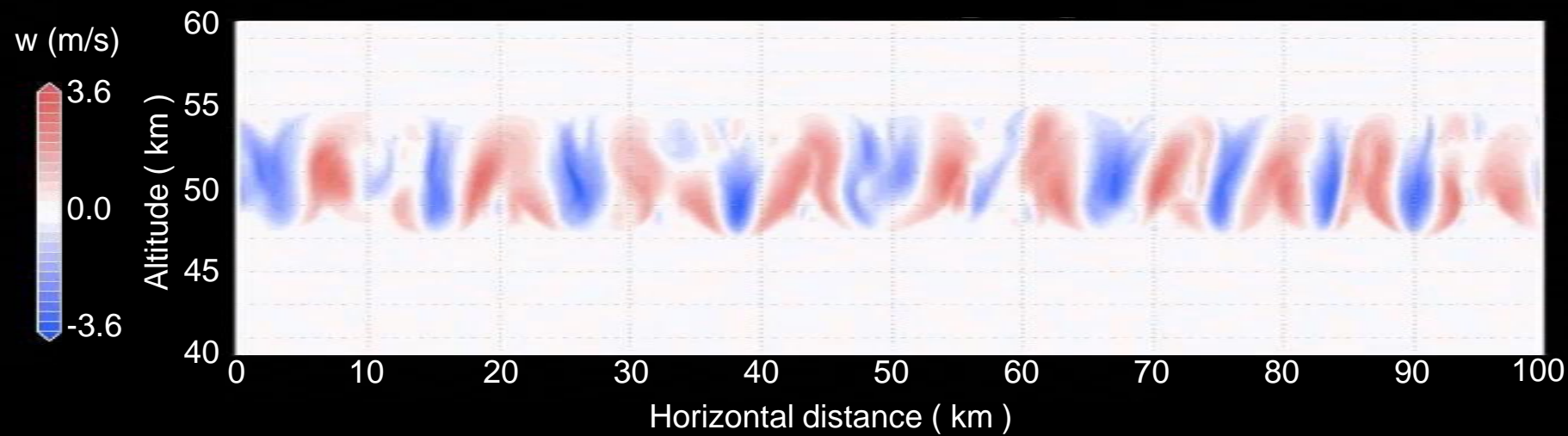
温位擾乱
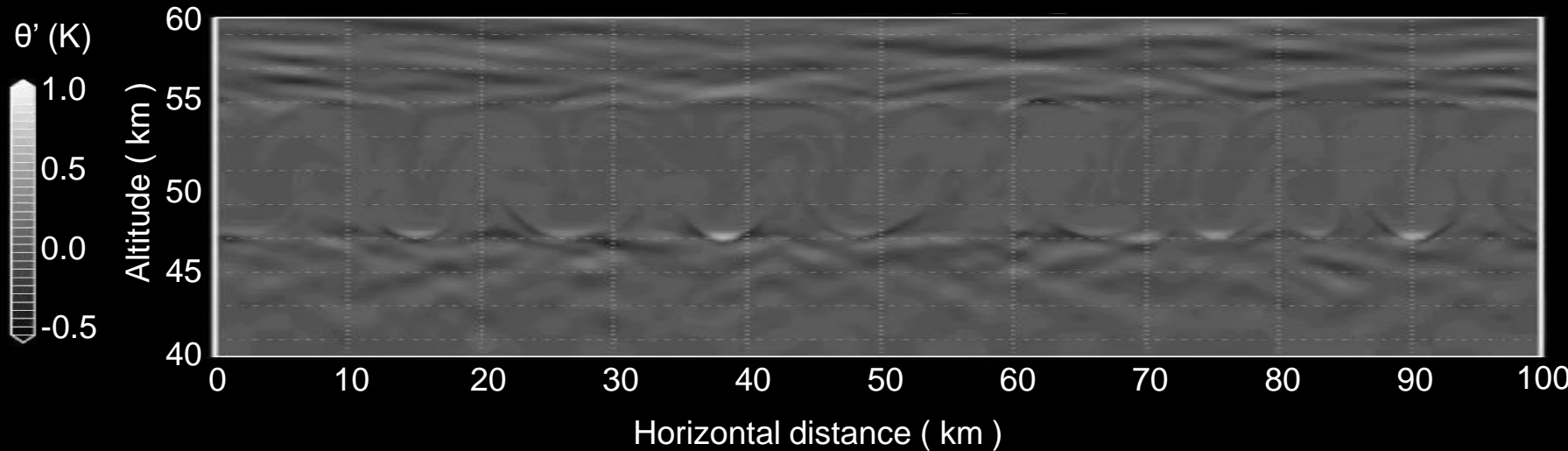
How are SO$_2$ and H$_2$O transported upward across the cloud layer ?

Photo-chemistry

Thermo-chemistry

Alt. (km)

90

80

70

60

50

40

30

20

Photochemical production of H$_2$SO$_4$ from SO$_2$, H$_2$O, CO$_2$

Upward transport of SO$_2$, H$_2$O

Downward transport

unknown meridional circulation

H$_2$SO$_4$ aerosols

H$_2$SO$_4$ condensation

H$_2$SO$_4$ evaporation

circulation of SO$_2$, H$_2$O, CO

?

Equator

Pole

production of SO$_2$ and H$_2$O from decomposition of H$_2$SO$_4$
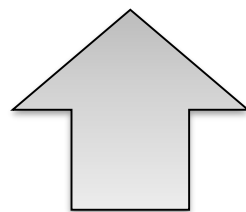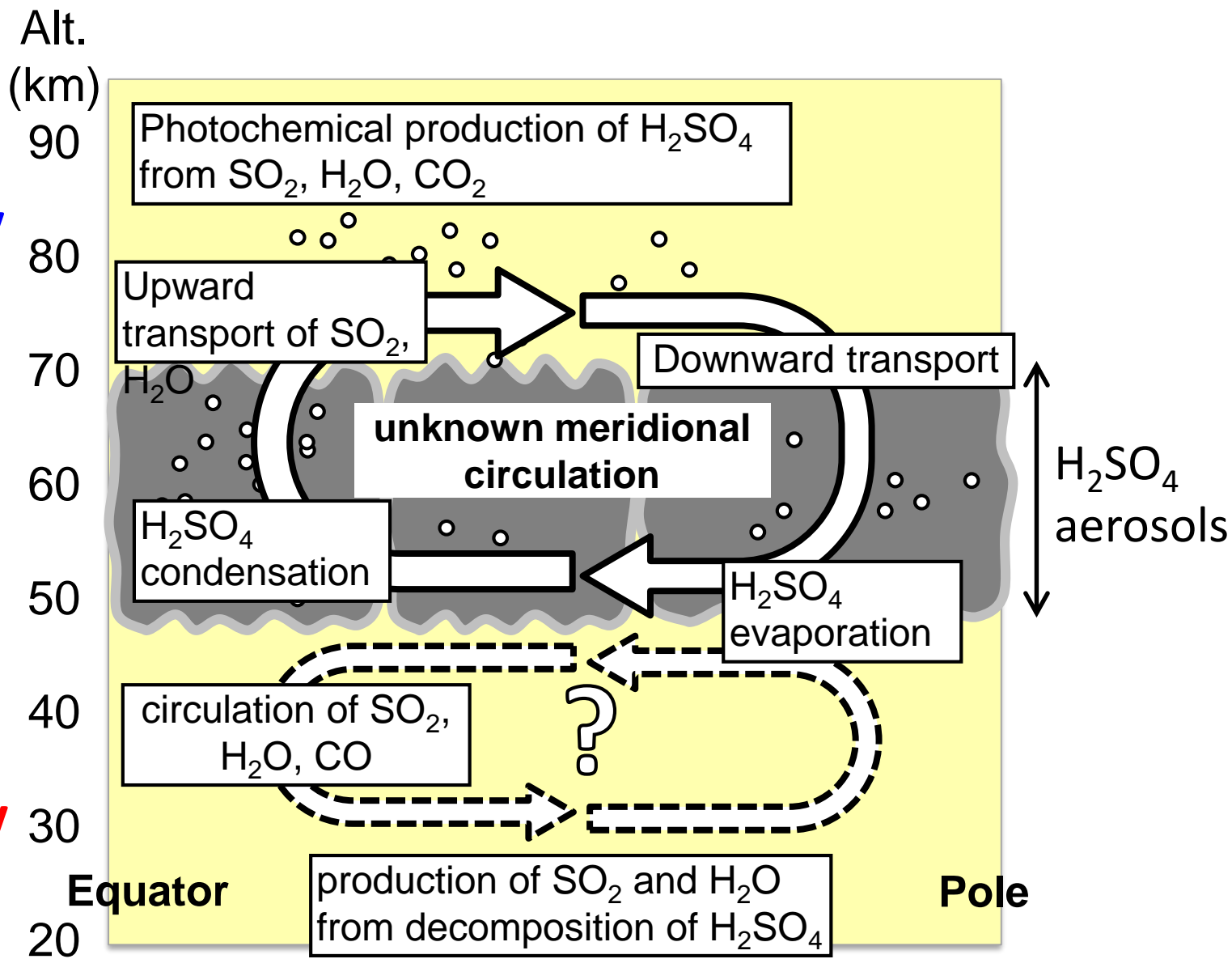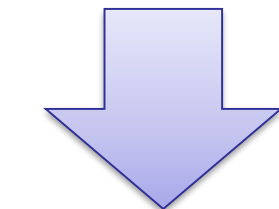
Venus in UV

"Venus is completely covered by clouds that are featureless in the visible but exhibit variable near-ultraviolet features long known to ground-based observers"
(Rossow et al. 1980)
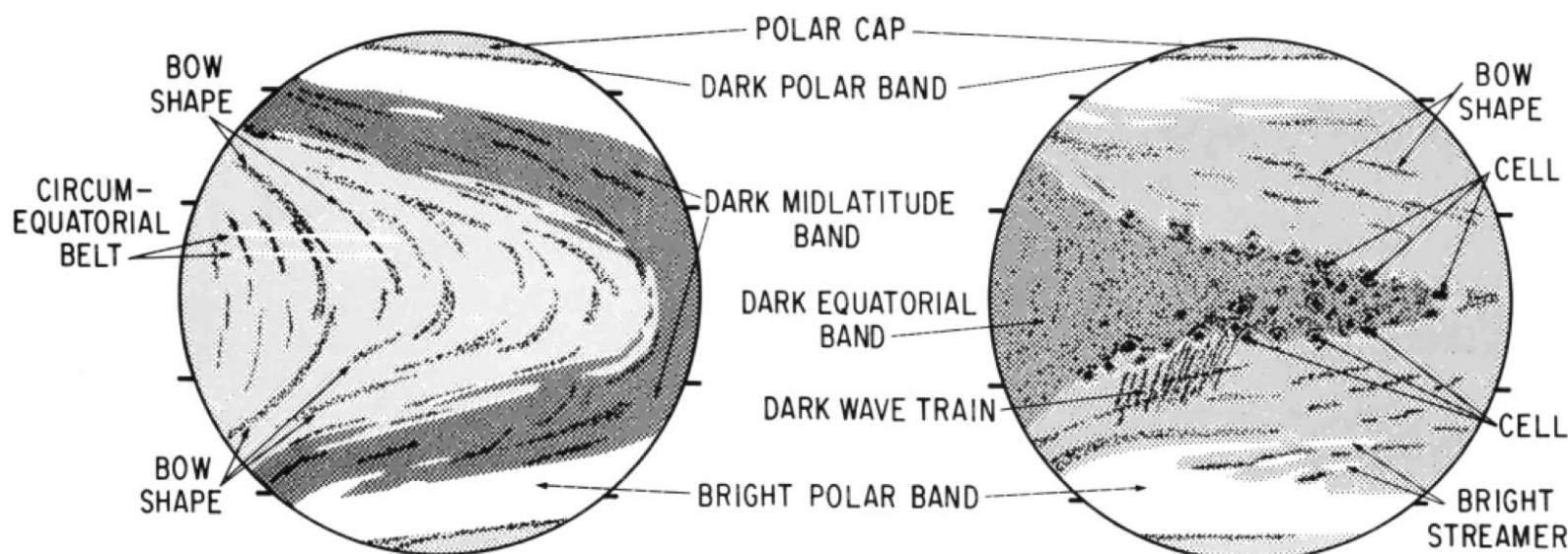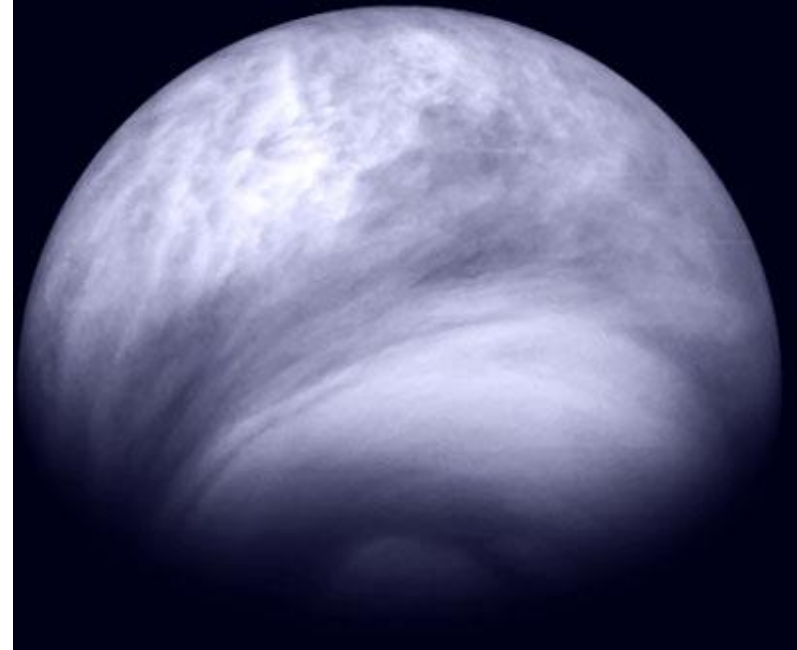
Fig. 4. Schematic diagram defining the basic types of cloud features observed in Venus ultraviolet images. The two views depicted here typically occur 2 days apart and represent the maximum and minimum tilt configurations, respectively. The tick marks on each circle indicate 20° and 50° of latitude in each hemisphere.

Origin of visible-UV absorption

- Absorbing material at far UV (<320nm) is mostly SO_2
- Absorption at near UV (>320nm) is a mystery. Candidate species are S, S_2O_2, S_2O, $FeCl_2$, etc.
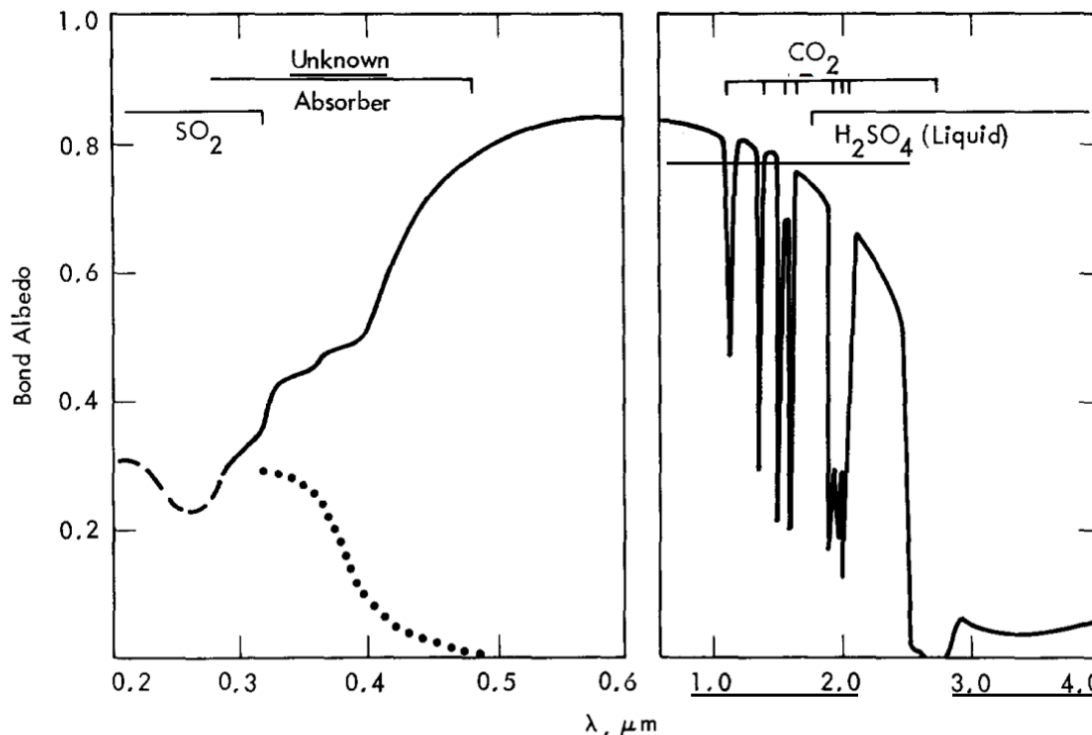
Moroz et al. (1985)

Figure 6-1. The Monochromatic Bond Albedo of Venus as a Function of Wavelength (Moroz, 1983 – Normalized to the Integrated Albedo A = 0.76). The points show the wavelength dependence of the maximum contrast between dark and light UV features (Coffeen, 1977).

Variability of SO$_2$ above clouds

SO$_2$ vs. Time

Legend:
- ▽ Anderson et al.
- ◁ Owen&Sagan
- ○ Balloon
- △ Venera 15
- ☆ HST
- □ Rocket
- ◇ IUE
- × PV
- ● SOIR (68 km)
- • SOIR (70 km)
- ✳ SPICAV UV (100–110 km)

Y-axis: SO$_2$ abundance at 40 mbar, ppb

X-axis: YEAR

upper limits

Volcanic eruptions ?
Change of atmospheric dynamics ?
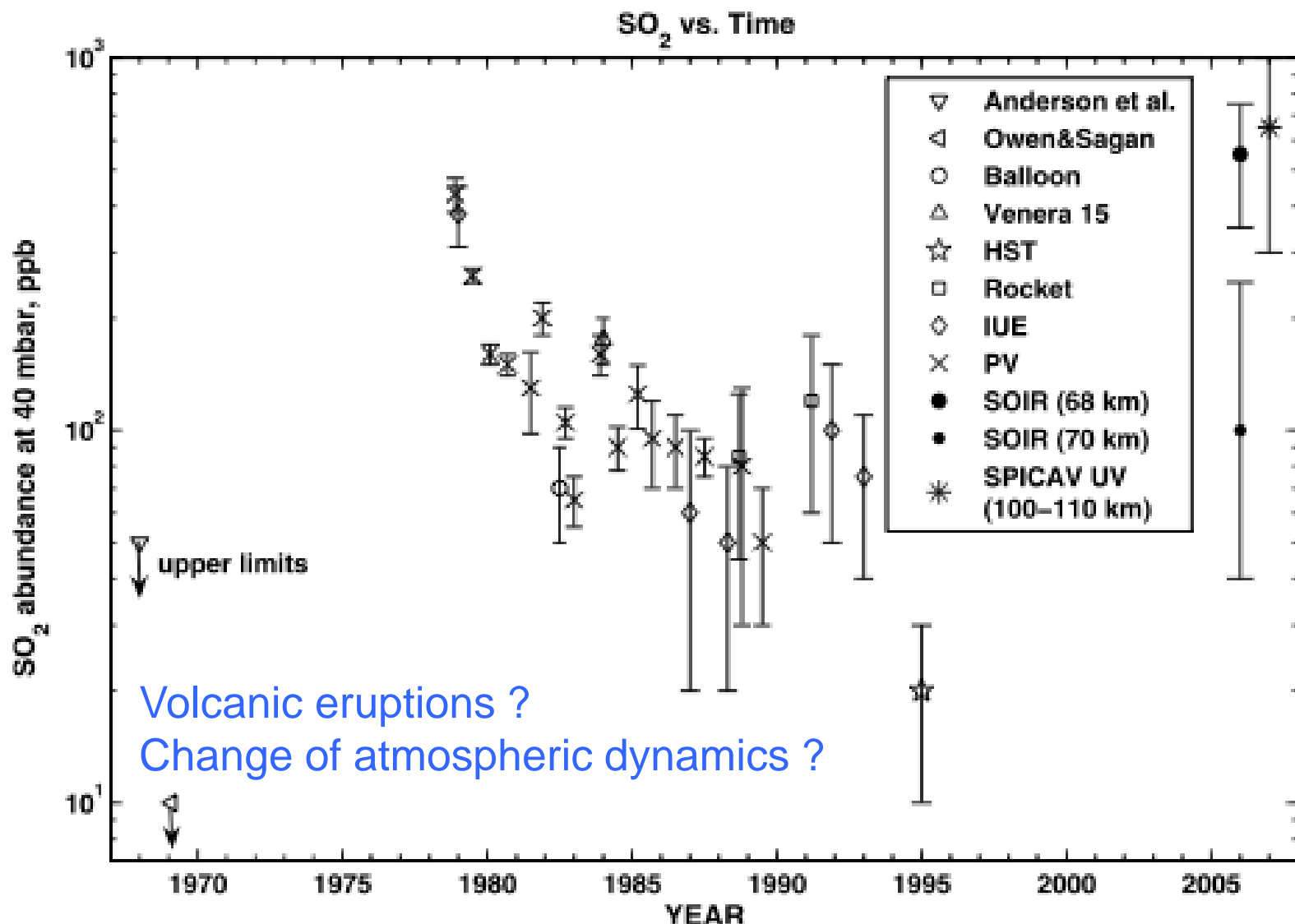
Key Points:
- VMC was able to sound Venus surface through the atmosphere transparency window
- Transient bright phenomena were observed in the Ganiki Chasma zone
- They are consistent with hypothesis of lava lakes on the surface

Correspondence to:
E. V. Shalygin,

Active volcanism on Venus in the Ganiki Chasma rift zone

E. V. Shalygin[1], W. J. Markiewicz[1], A. T. Basilevsky[1,2,3], D. V. Titov[4], N. I. Ignatiev[5], and J. W. Head[3]

[1]Max-Planck-Institut für Sonnensystemforschung, Göttingen, Germany, [2]Vernadsky Institute, Moscow, Russian Federation, [3]Department of Earth, Environmental and Planetary Sciences, Brown University, Providence, Rhode Island, USA, [4]ESA-ESTEC, Noordwijk, Netherlands, [5]Space Research Institute, Moscow, Russian Federation

Abstract Venus is known to have been volcanically resurfaced in the last third of solar system history and to have undergone a significant decrease in volcanic activity a few hundred million years ago. However, fundamental questions remain: Is Venus still volcanically active today, and if so, where and in what geological and geodynamic environment? Here we show evidence from the Venus Express Venus Monitoring Camera for transient bright spots that are consistent with the extrusion of lava flows that locally cause significantly elevated surface temperatures. The very strong spatial correlation of the transient bright spots with the extremely young Ganiki Chasma, their similarity to locations of rift-associated volcanism on Earth, provide strong evidence for their volcanic origin and suggests that Venus is currently geodynamically active.
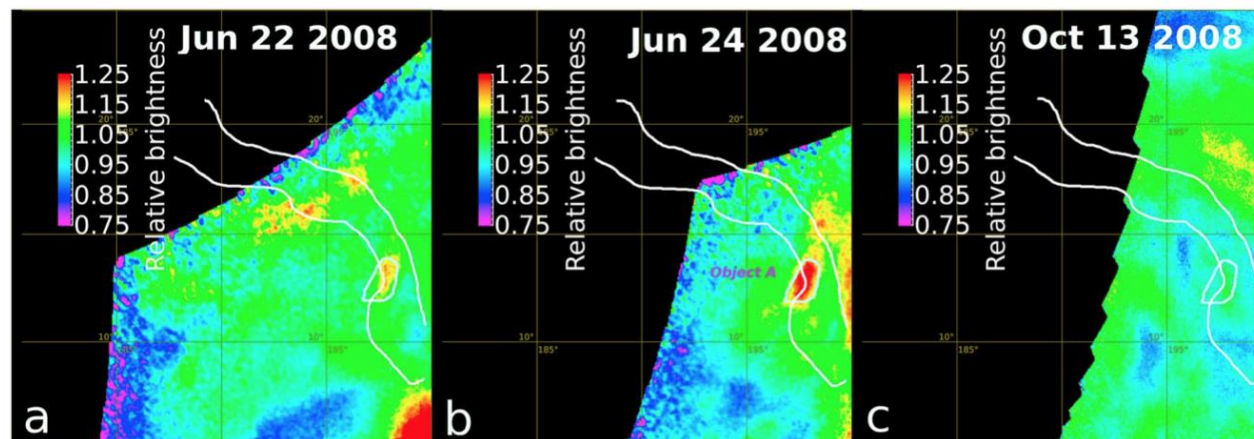
Figure 2. Maps of relative brightness in the VMC IR2 channel. Each panel shows the ratio of the mosaic composed from images obtained in the given to the averaged VMC mosaic of the region. Orbital mosaics were obtained for specified dates in orbits: (a) 793, (b) 795, and (c) 906. Ganiki Chasma and object "A" in orbit 795 are outlined with white lines in each panel. The grid size is 5° by 5°, that is ≈528 km at the equator.

Massive eruptions several hundred million years ago ?
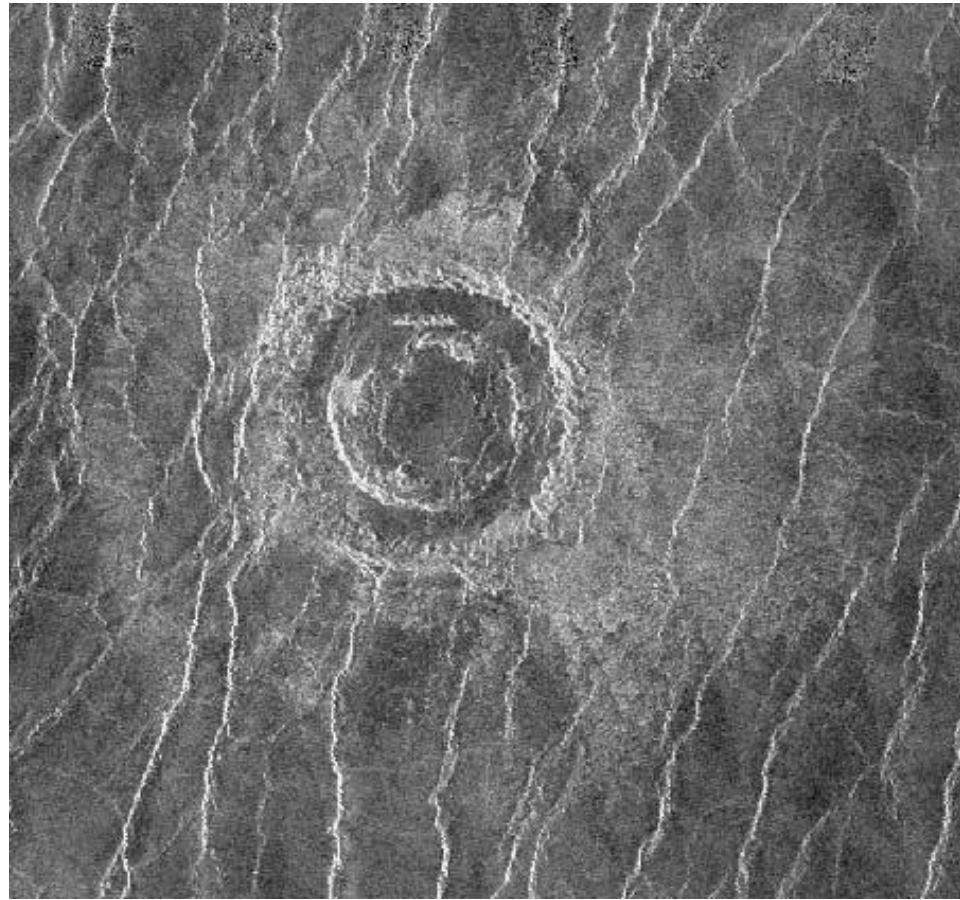
Radar image of Venus surface by NASA's Magellan spacecraft

Wrinkle ridges may have been formed by thermal stress caused by a sporadic enhancement of greenhouse effect (H_2O?) in the past.
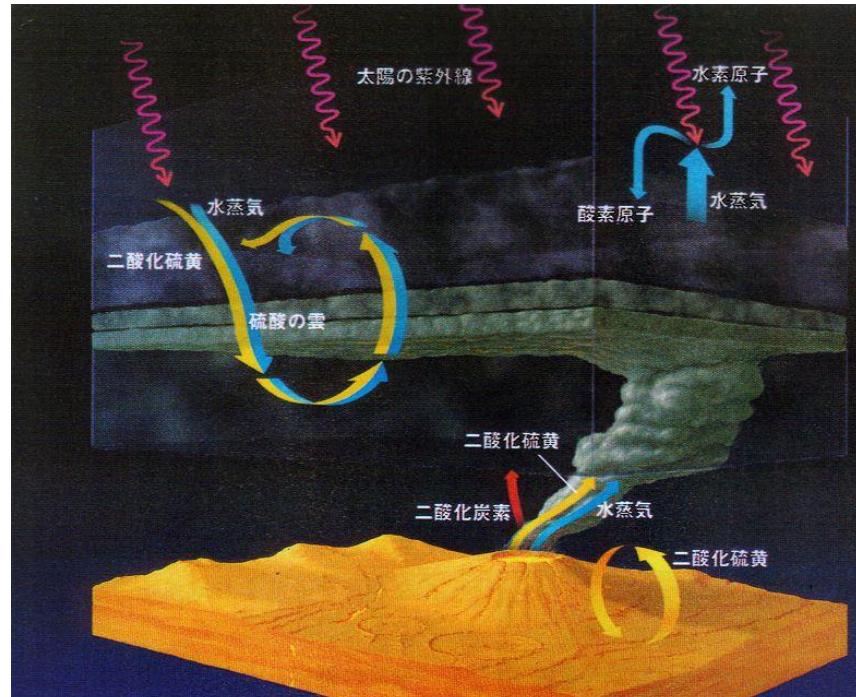
Bullock & Grinspoon (2001)
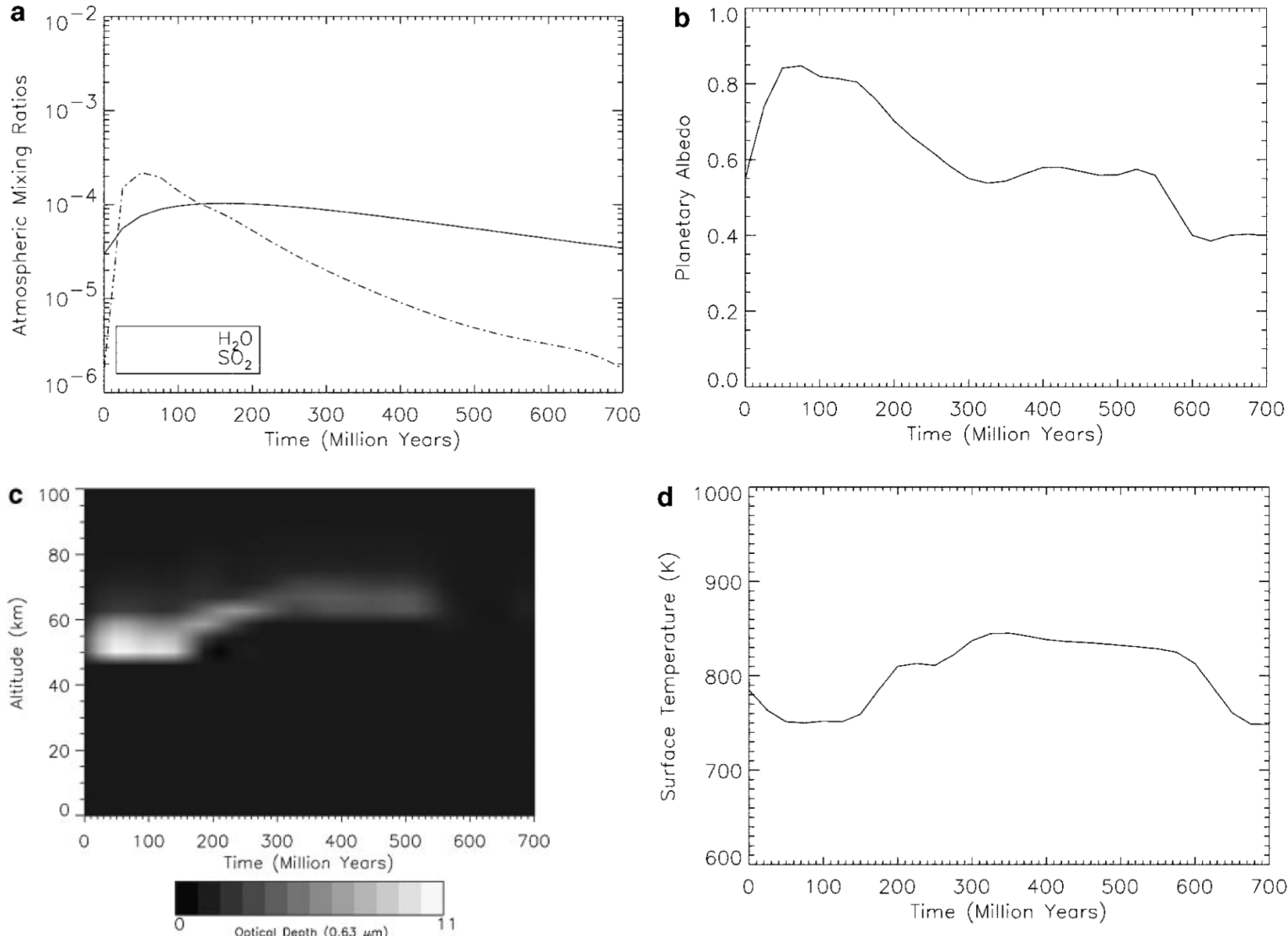
FIG. 11.   Case 3: Rapid outgassing (100 Myr, 1 km), with exospheric escape (160 Myr) and SO_2 reactions with the surface. (a) is the evolution of atmospheric mixing ratios as a function of time. The solid line is for H_2O, dot–dashed line is for SO_2. (b) is the evolution of planetary albedo. (c) shows the evolution of cloud optical depths as a function of time. (d) shows the evolution of surface temperature as a function of time.

Stabilization of Venus' climate by a chemical-albedo feedback

(Hashimoto & Abe, 2000）

雲アルベド・温室効果

$$SO_2 + O + H_2O \rightarrow H_2SO_4$$

H_2SO_4 の 雲

SO_2

May stabilize the climate

地表面化学反応

$$Fe_3O_4 + 6\ SO_2 + 16\ CO = 3\ FeS_2 + 16\ CO_2$$

FeS$_2$

Fe$_3$O$_4$
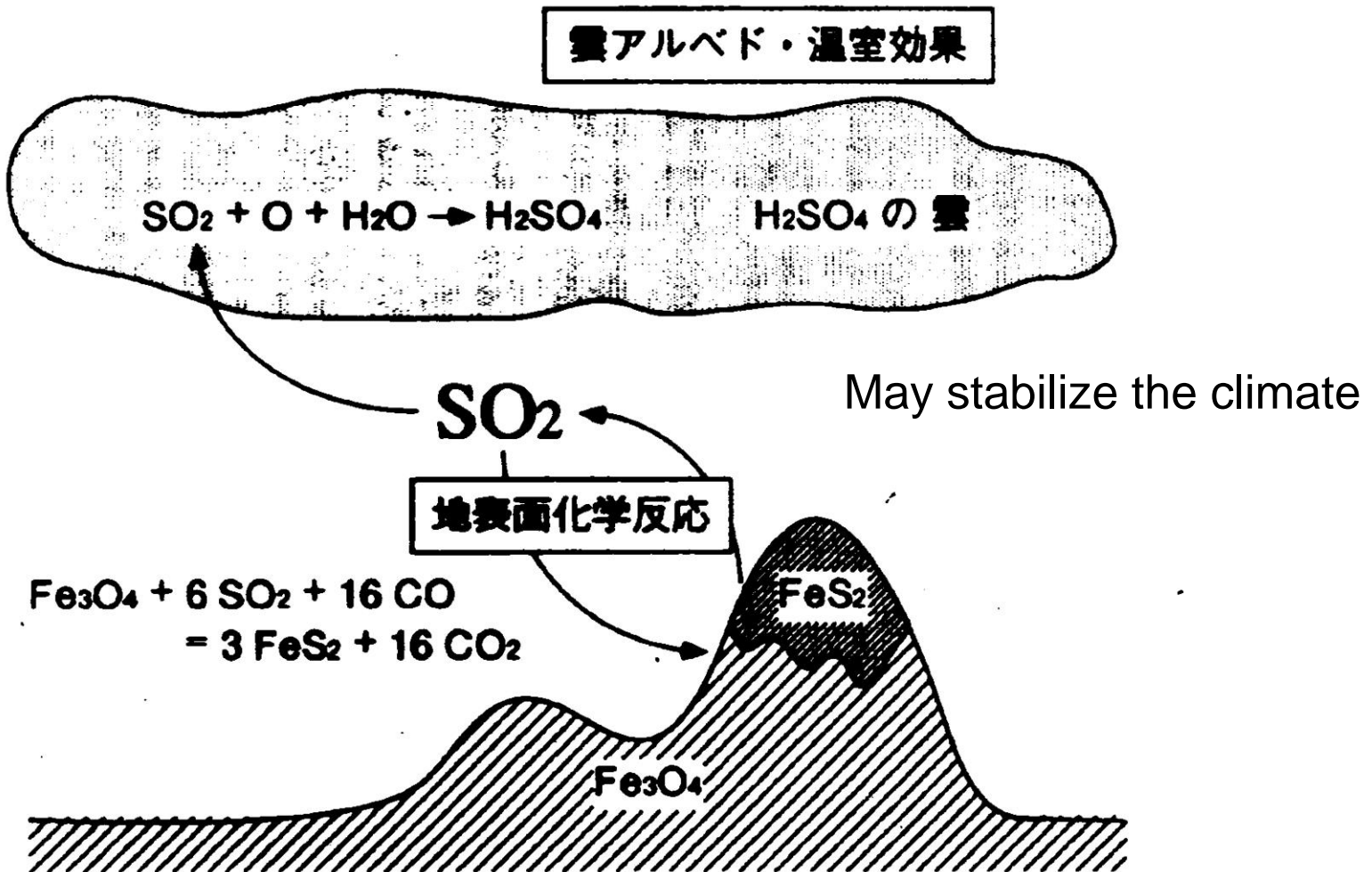
Dust in the Martian atmosphere

Seasonal variation of optical thickness in infrared
(Smith et al. 2004)

- Micrometer-sized small mineral particles float in the atmosphere with a background optical thickness of 0.1-0.5.
- The dust loading changes with time and space.
- The dust serves as a heat source in the atmosphere by absorbing sunlight.
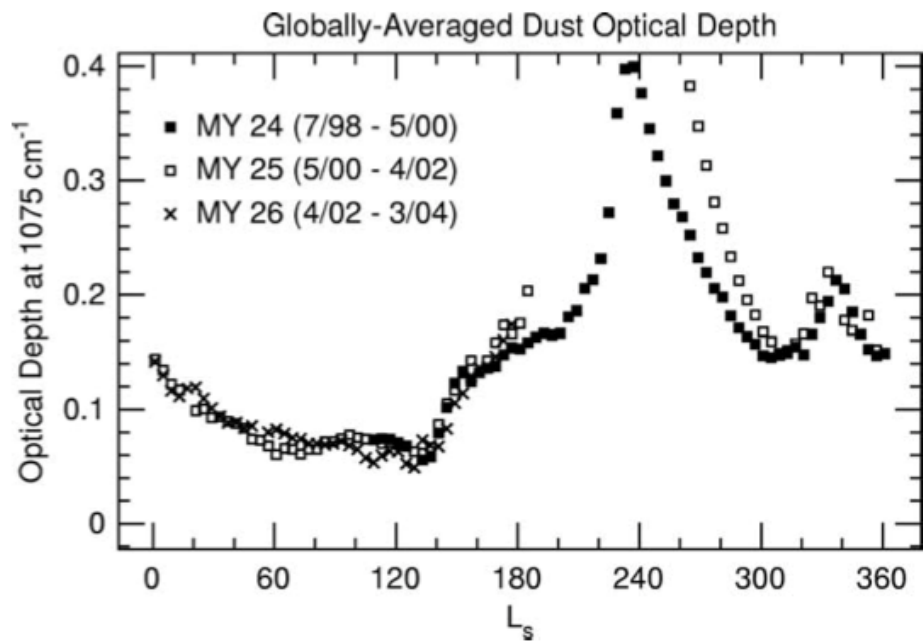
Fig. 7. Globally-averaged daytime (local time ~ 1400) dust optical depth at 1075 cm^{-1} (scaled to an equivalent 6.1-mbar pressure surface) as a function of season (L_s). Three martian years are represented: Mars Year 24 (MY 24) (■), MY 25 (□), MY 26 (×). During the planet-encircling dust storm of 2001 (MY 25), globally-averaged dust opacity reached 1.3 at $L_s = 205$–$215°$.

Dust as a heat source

- Absorption of solar radiation
  - much stronger than the greenhouse effect of CO_2, which is only several kelvins
 - much stronger than cloud albedo effect and latent heat

thick dust

thin dust

20°-40° N   20°-40° S
0°-20° N   40°-60° S
0°-20° S   0°-20° S (1999)

Temperature at 0.5 mbar

Solar longitude（Season）

40 K difference between thick-dust year and thin-dust year
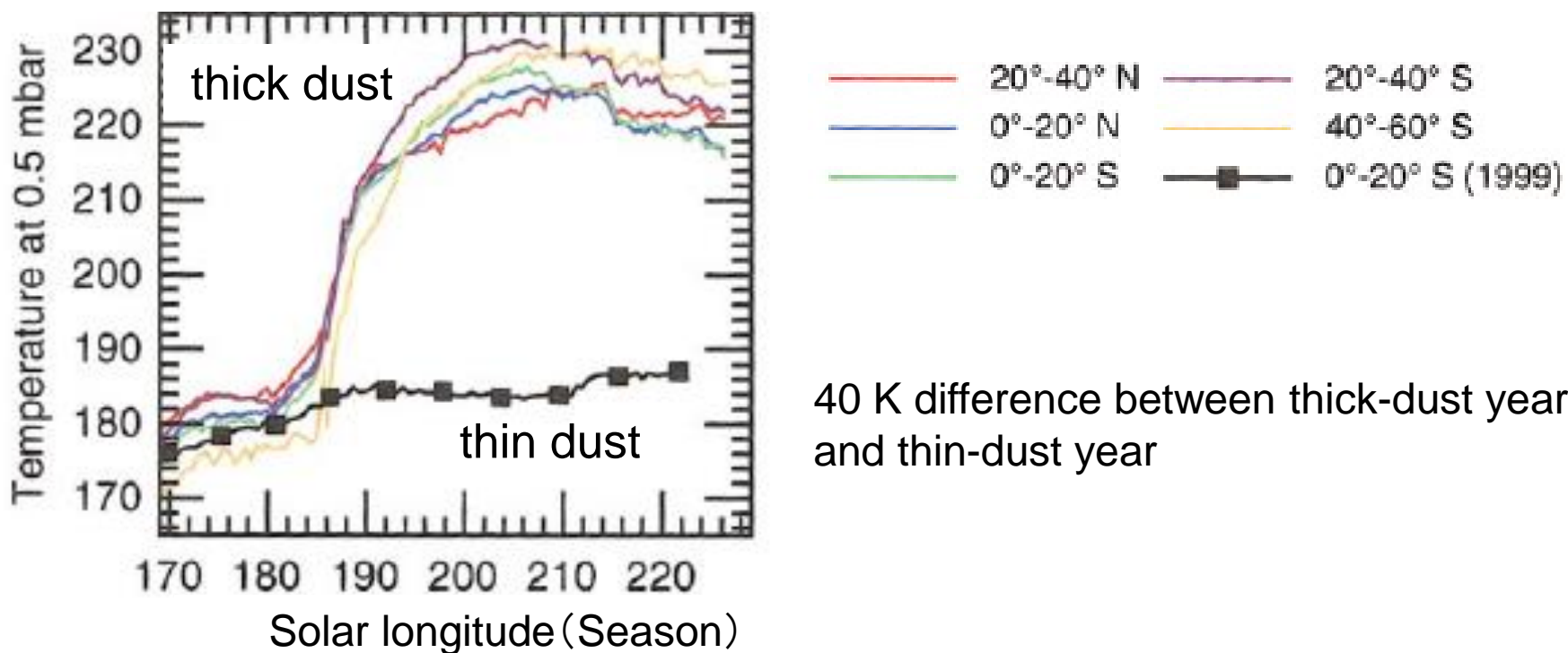
Smith et al. (2002)

Radiative-convective model

## Gierasch & Goody (1972)

without dust
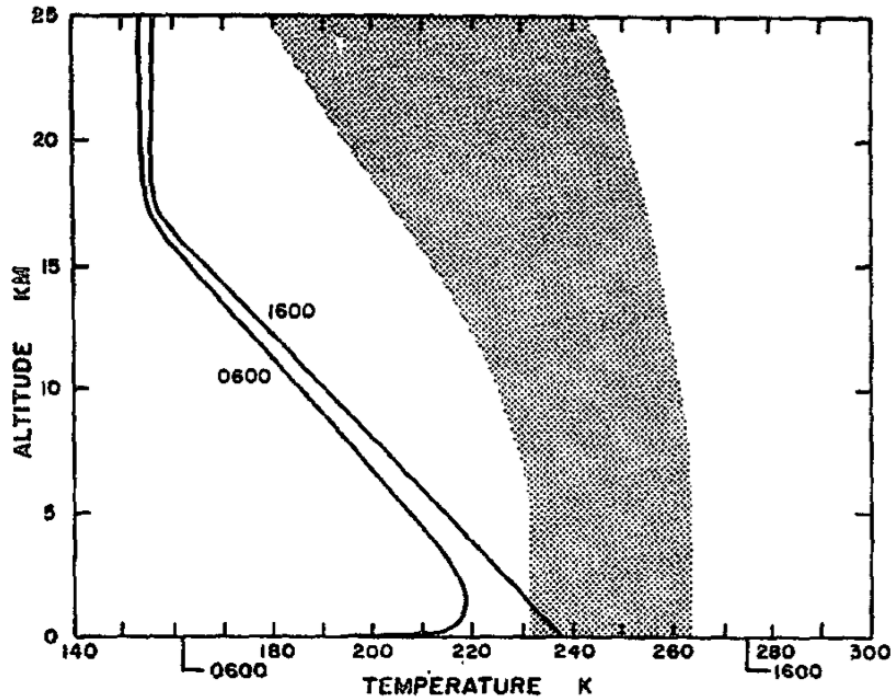
with dust
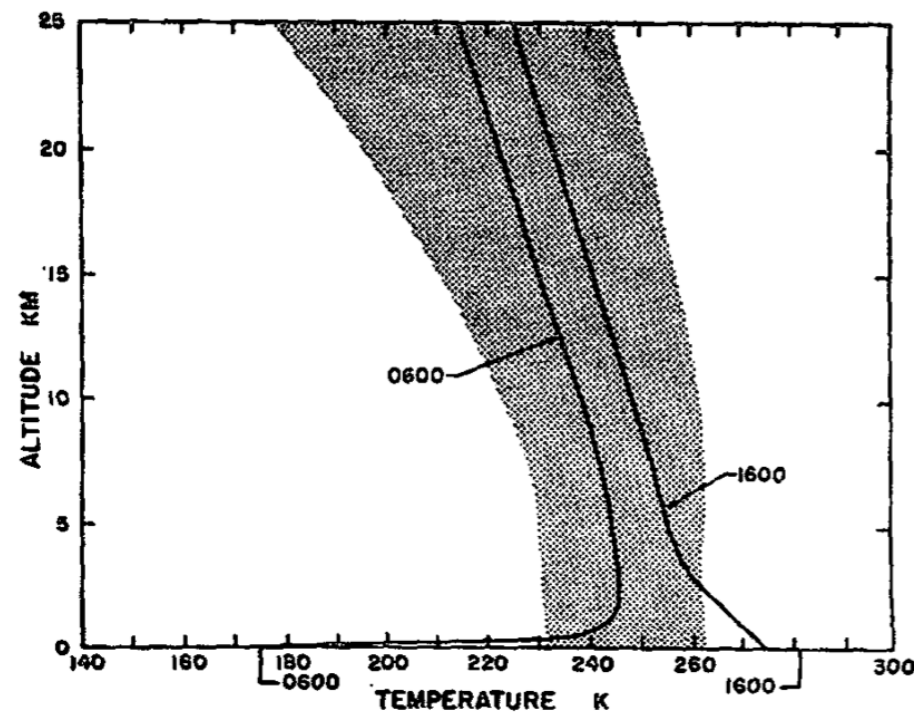
FIG. 1. Martian temperature calculations. The stippled area represents temperatures reported by Kliore *et al*. (1972) and Hanel *et al*. (1972). The lines are theoretical profiles for a pure CO_2 atmosphere, at 1600 and at 0600 hours (the coldest time). Both theory and observation refer to mid-latitude summer conditions. The tags indicate the ground temperatures. In the case of the 1600 theoretical profile a strong boundary layer is indicated.

FIG. 2. Same as Fig. 1 except that the atmosphere contains an extra solar absorber, evenly mixed with the atmosphere at all levels, and having an optical depth of 0.10 at all wavelengths. Note the weak boundary layer at 1600.

# Phobos-2 infrared sounding

## Titov et al. (1997)

Morning limb
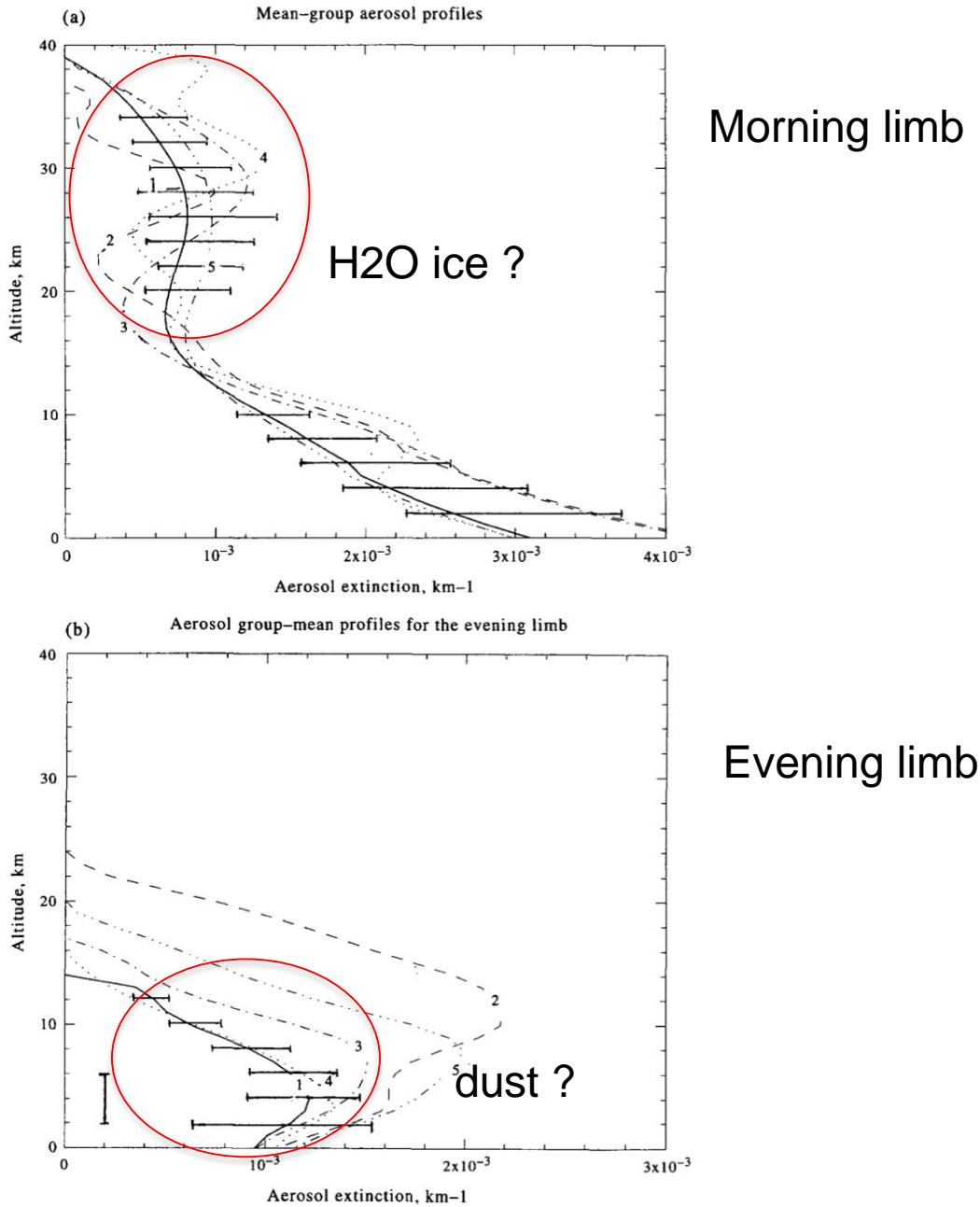
Evening limb

Fig. 11. Aerosol extinction profiles retrieved from the group-mean brightness profiles (a) at the morning limb, and (b) at the evening limb. The confidence intervals are shown for the aerosol profiles retrieved from the group 1 brightness profiles. These error bars are based on the analysis of all uncertainties of the retrieval procedure. The vertical bar shows the uncertainty in the limb positioning. Numerals by the curves correspond to the group numbers in Tables 1 and 2

Dust storms

6/30/1999 06:51:59 UTC   6/30/1999 08:49:34 UTC   6/30/1999 10:47:11 UTC   6/30/1999 12:44:52 UTC
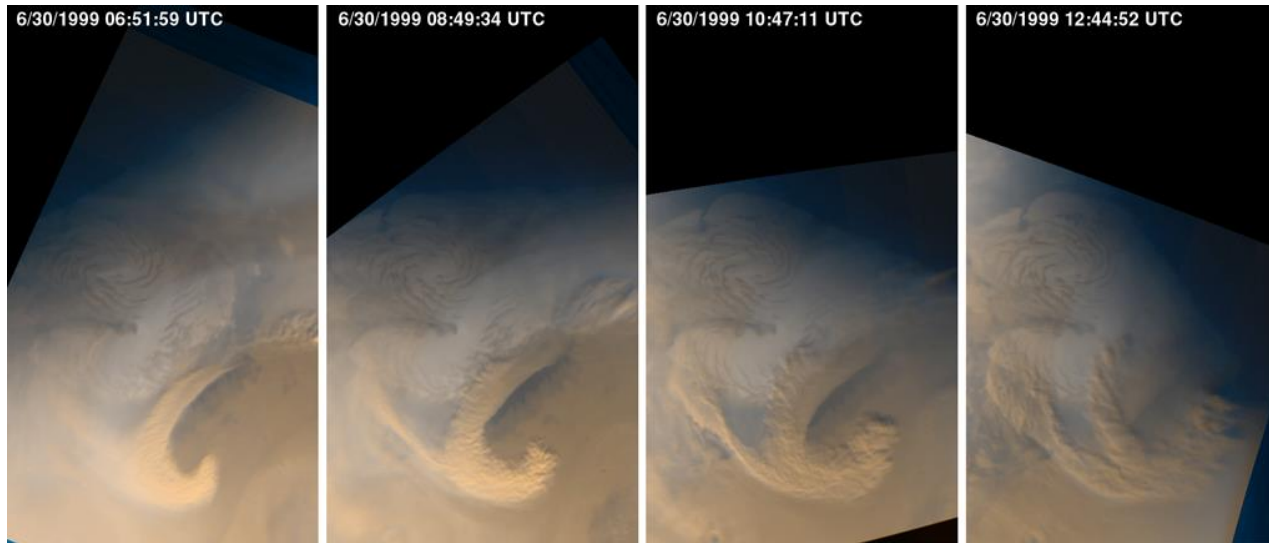
regional storm

Seasonal variation of optical
thickness in infrared
(Smith et al. 2004)

Globally-Averaged Dust Optical Depth

- MY 24 (7/98 - 5/00)
- MY 25 (5/00 - 4/02)
- MY 26 (4/02 - 3/04)
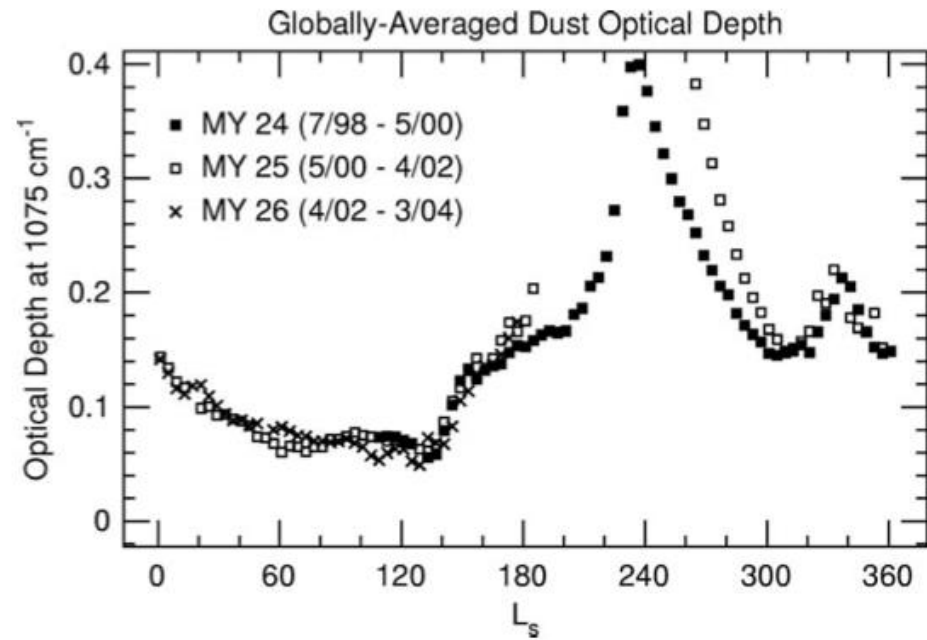
Dust devils

- Source of background atmospheric dust ?

MOC2-141a   Malin Space Science Systems/NASA

大気ダストの分布

- 年間通して存在する背景ダストの供給源は謎
- 高度10–20kmに混合比極大

背景量

Smith et al. (2004)
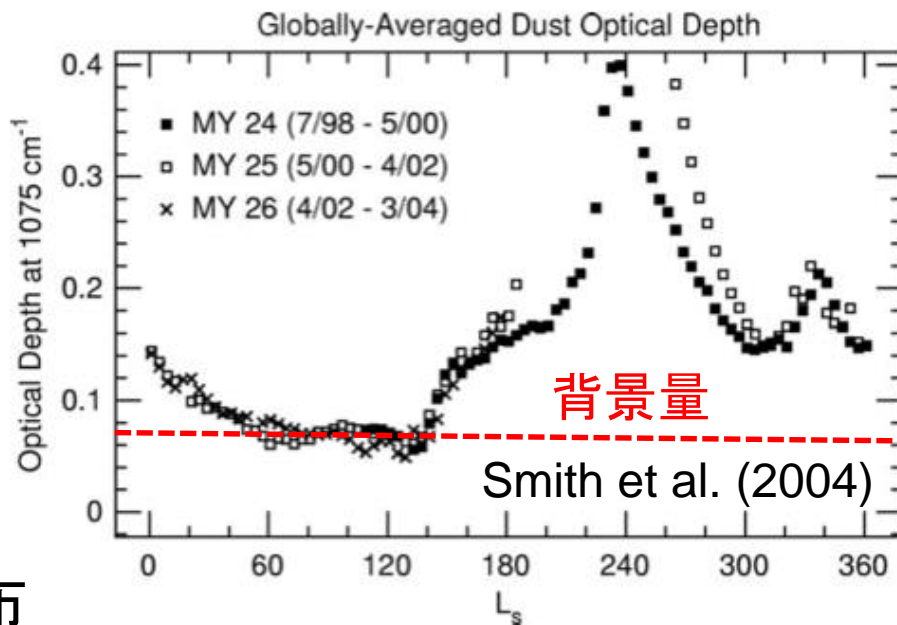
ダスト混合比の子午面分布
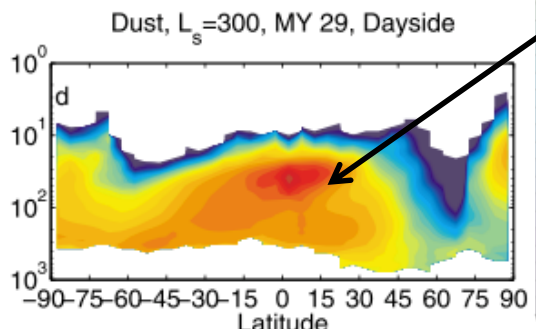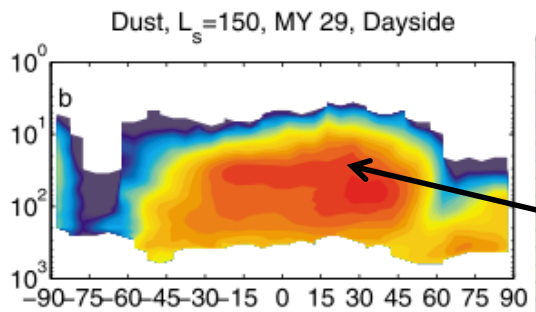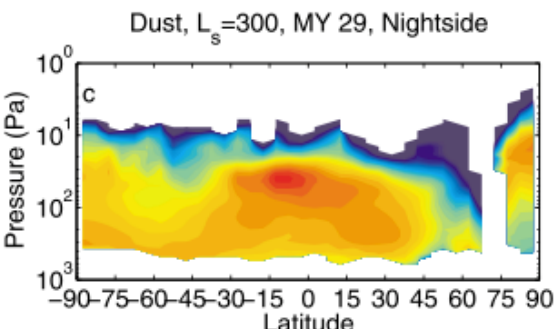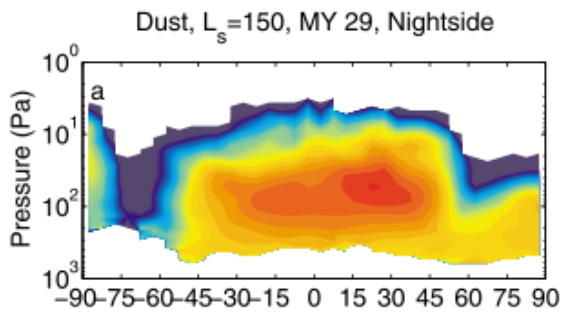
Detached dust layers

Heavens et al. (2011)
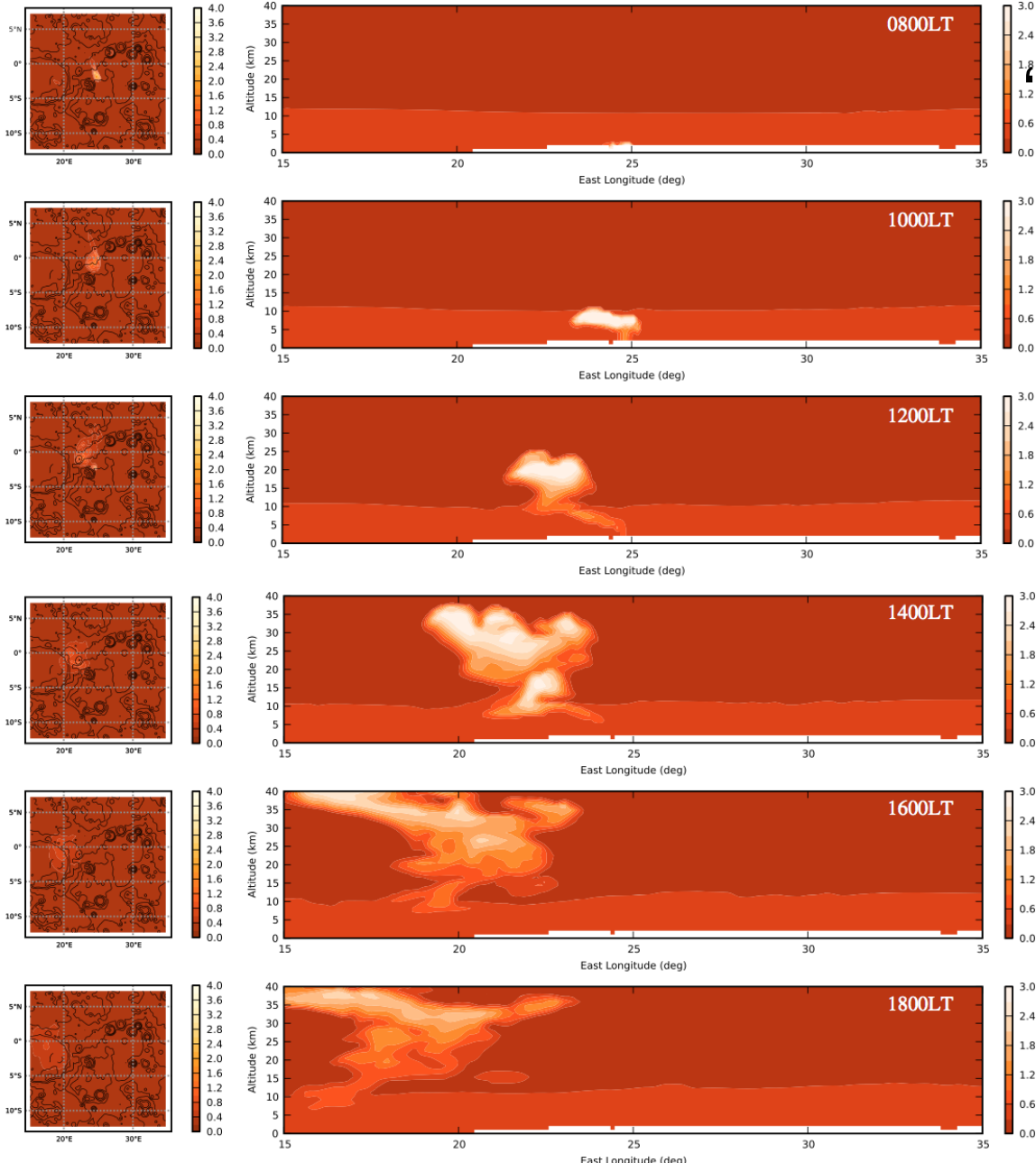
"Rocket dust storm"
Spiga et al. (2013)

数十km～数百kmスケールの急発達プルームが鍵？

Figure 12. The LMD-MMM storm simulation with lifting and no initial dust perturbation. Same as Figure 4 except that local times range from 0800 to 1800 and longitude-altitude sections are obtained at latitude 1.5°S.

Global dust storm

Mars • Global Dust Storm

June 26, 2001

September 4, 2001

Hubble Space Telescope • WFPC2

NASA, J. Bell (Cornell), M. Wolff (SSI), and the Hubble Heritage Team (STScI/AURA) • STScI-PRC01-31
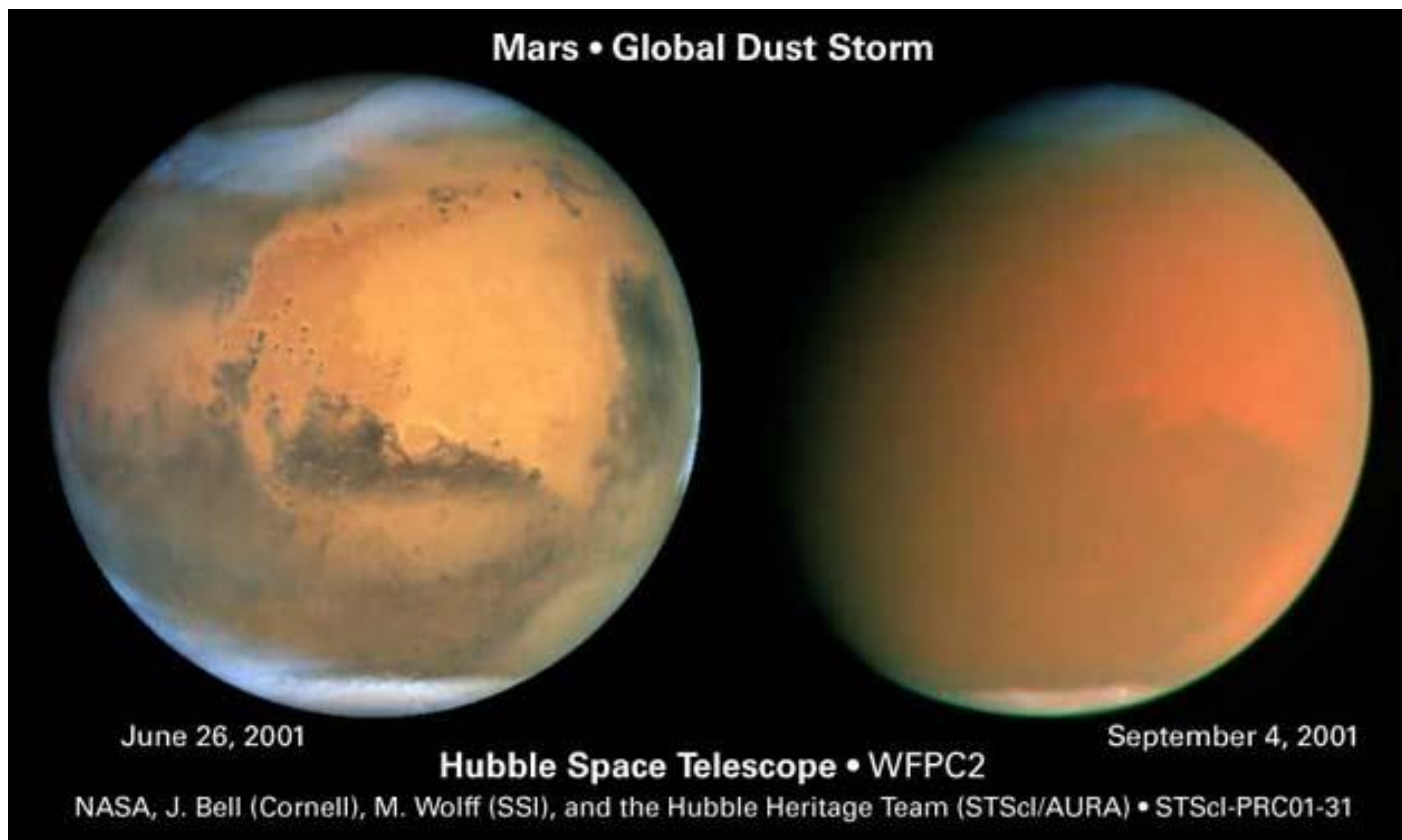
- Global dust storms tend to occur in southern spring-summer
- Positive feedback between dust heating and the intensification of winds is expected in the development of global dust storms.

# Episodic occurrence of major dust storms
→ irregular nature of Martian meteorology
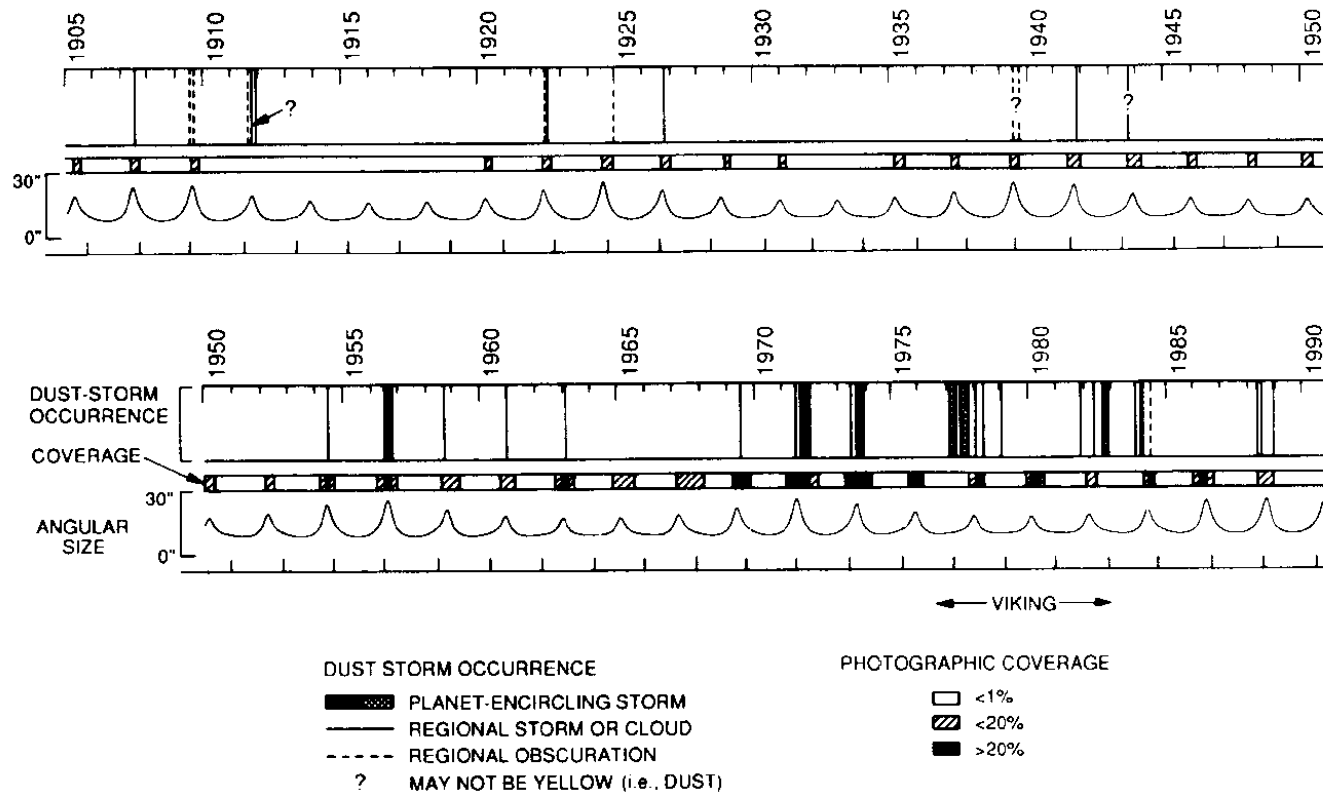
Fig. 7. Timeline of the detection of regional and planet-encircling obscurations, clouds and storms. These events are listed in Table III. Earth dates are indicated at the top, and perihelion (and thus Mars years) at the bottom of the dust-storm timeline. The second timeline indicates periods of photographic coverage of Mars, defined in terms of the percentage of L_s degrees that photographs were taken. Coverages of <1%, of 1 to 20% and >20% are indicated. The third timeline indicates the apparent size of Mars, as seen from Earth, on a scale of 0 to 30 seconds of arc (figure from Zurek and L. Martin 1992).

Dust storms in numerical models
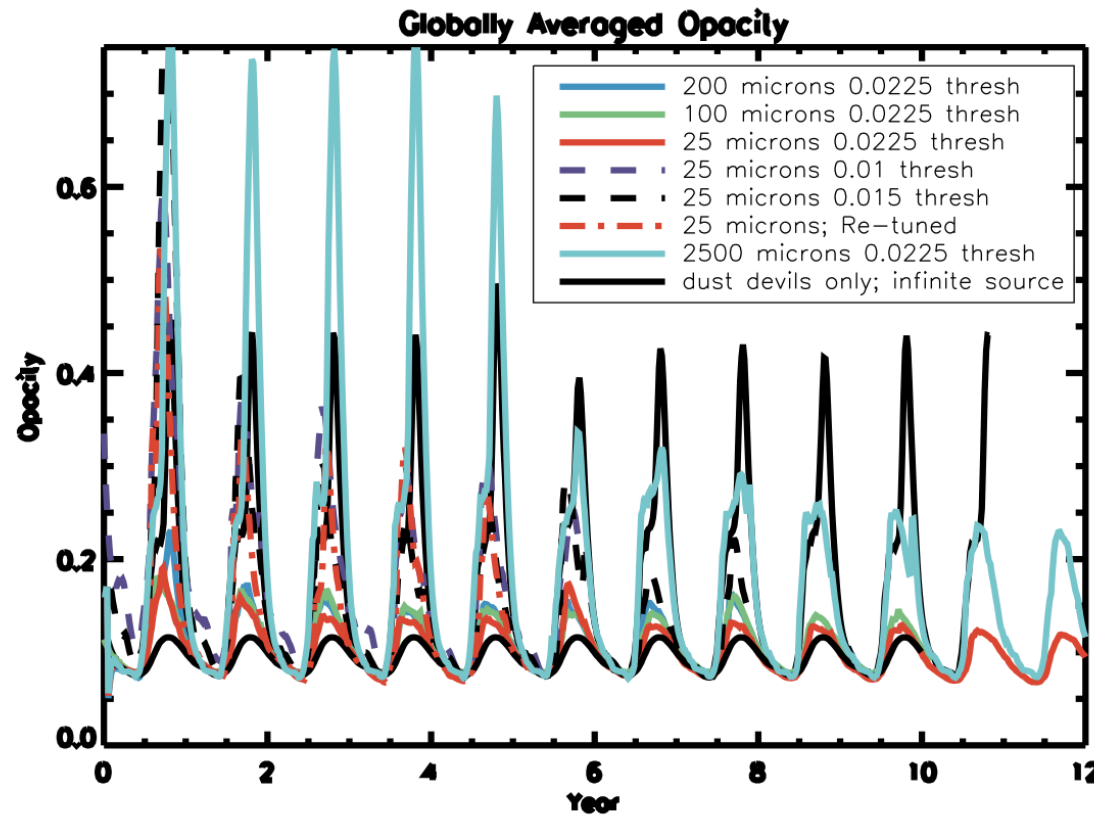
Figure 3. Multi-year globally averaged 9 μm opacity for the infinite surface dust simulation (black solid) the finite surface dust simulations (colored solid and dashed lines).

Kahre et al. (2005)

Spatial Net Deflation/Deposition: Baseline Simulation

Max: 280.408 Min: −89.5374

GCM Topography
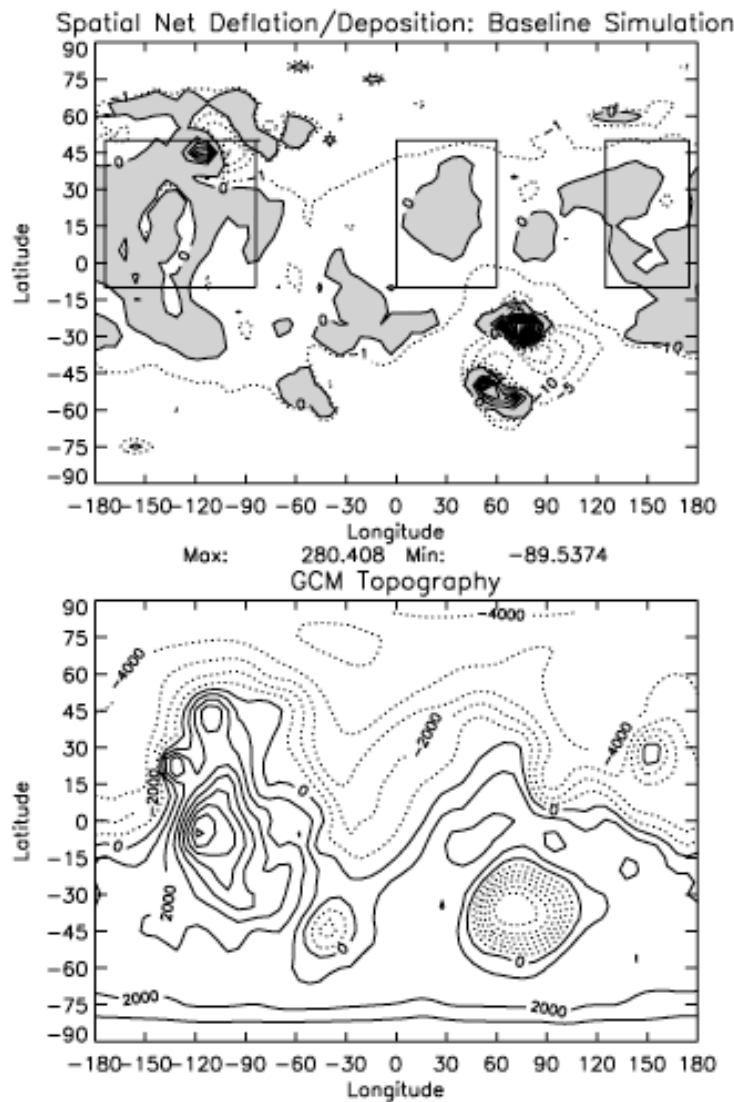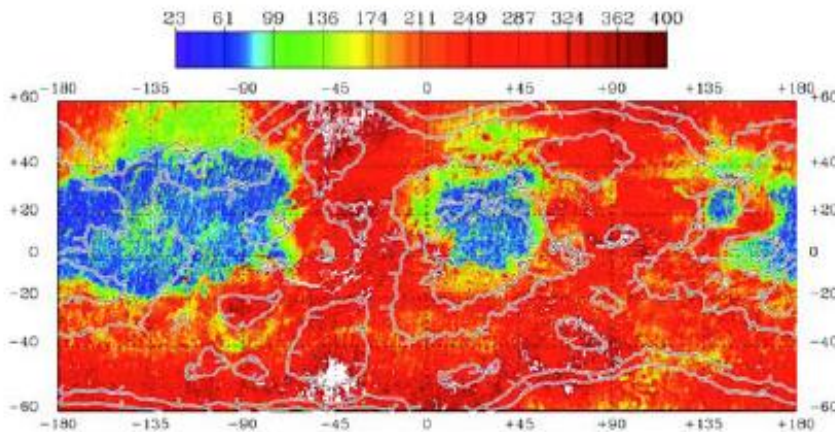
Thermal Inertia

Observation by Mars Global Surveyor

Figure 7. (top) Map of net annual dust deflation (shaded regions) and deposition (nonshaded regions) for the baseline simulation. The heavy black boxes outline the three low thermal inertia regions: Tharsis (left), Arabia (middle), and Elysium (right). (bottom) MOLA topography smoothed to the model's resolution. Contours indicate height above (solid) or below (dotted) the MOLA geoid in meters. The contour interval is 1000 m.

Long-term change of surface dust ?

Surface dust tendency between pre- and post-global dust storm in 2001
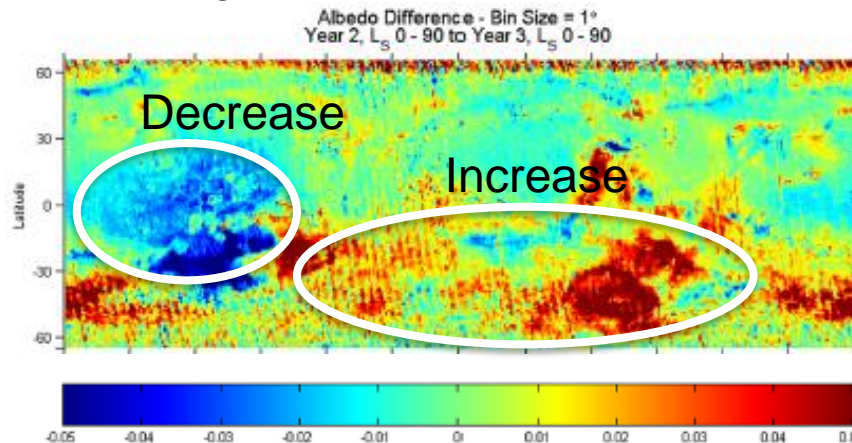
Surface dust tendency during one year after 2001 dust storm
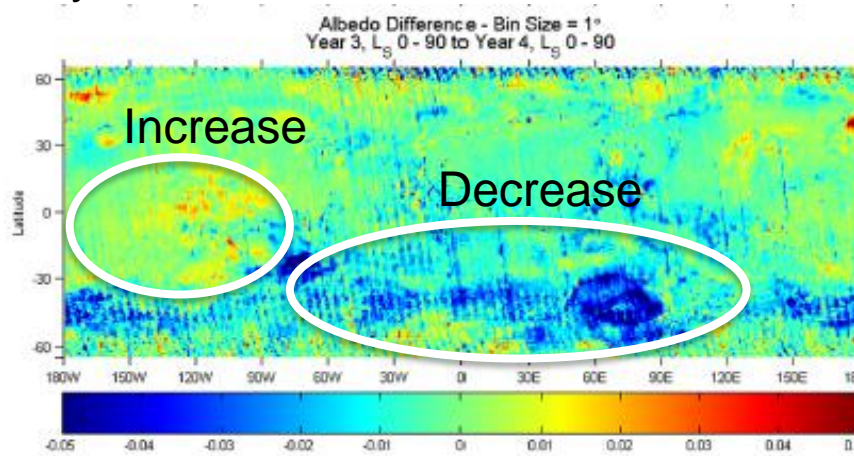
（Szwast et al., 2006）

# H$_2$O ice clouds on Mars
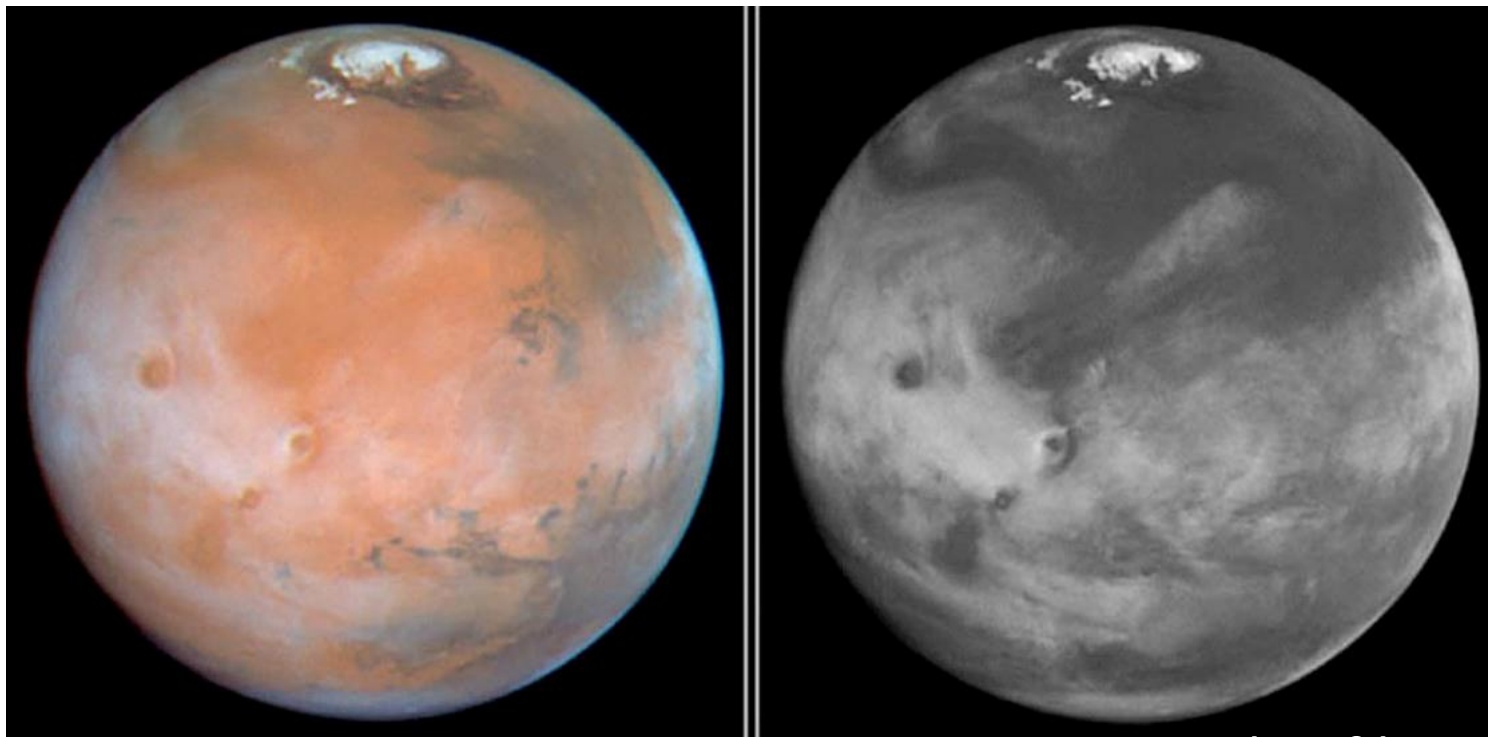
HST Mars images

Polar caps

North
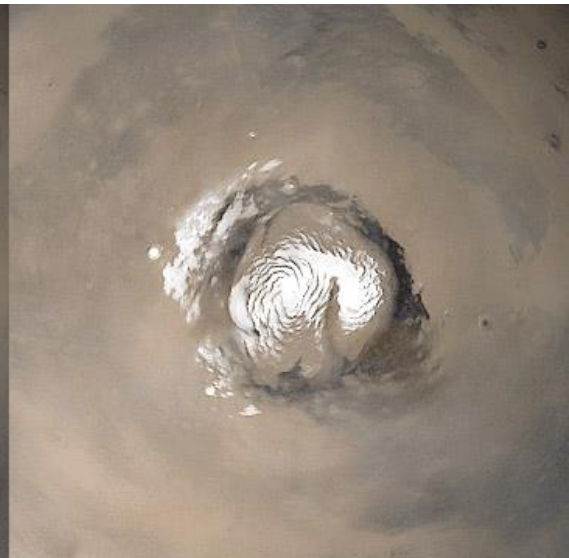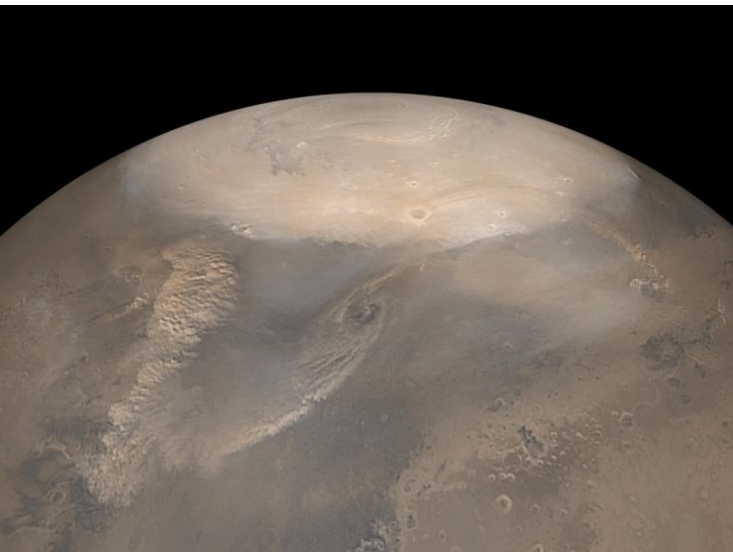
South
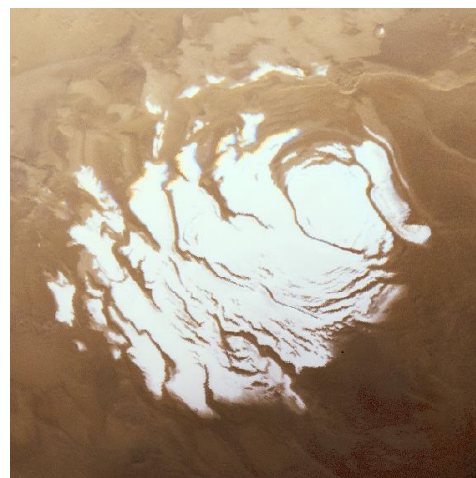
H$_2$O ice + CO$_2$ ice

- Seasonal variation
- Residual polar caps in summer
  - H$_2$O only on the north
  - H$_2$O + CO$_2$ on the south
- Southern CO$_2$ ice serves as a cold trap of H$_2$O ?
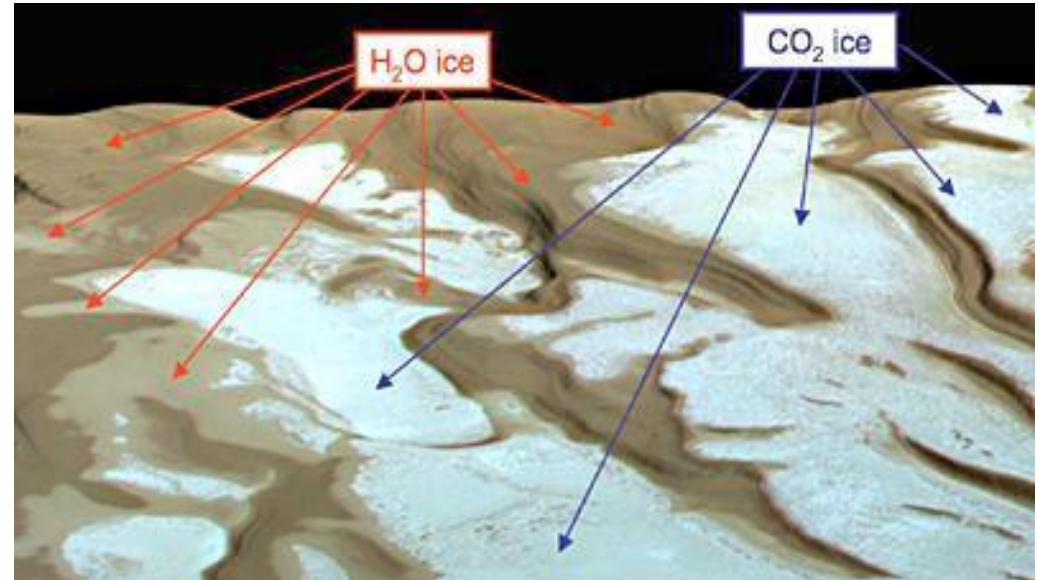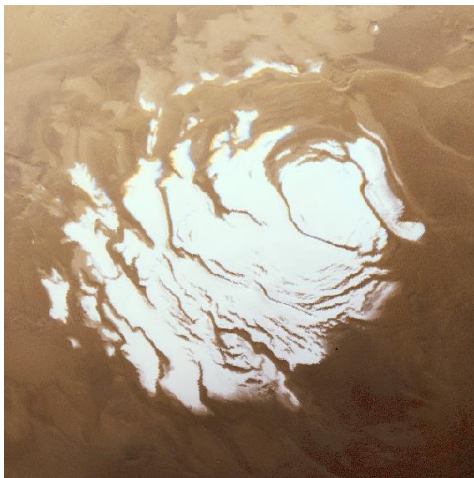
# Mars Odyssey

Neutron Spectrometer (NS) and High-Energy Neutron Detector (HEND)

Subsurface ice

Global Distribution of Water on Mars

Northern-Latitude Water Abundance (poleward of 45°)

Water Abundance (weight percent)

Southern-Latitude Water Abundance (poleward of -45°)

Los Alamos
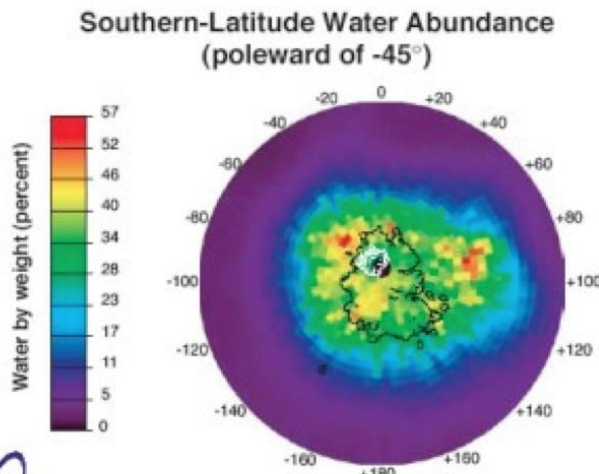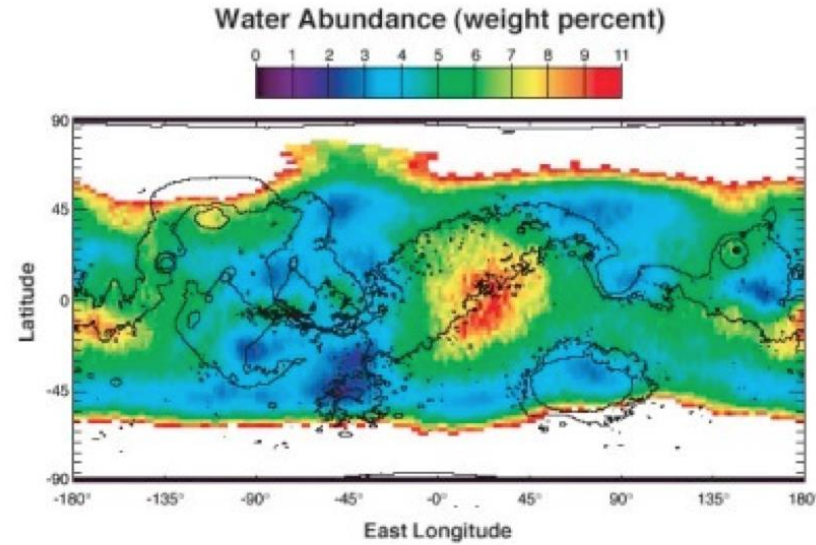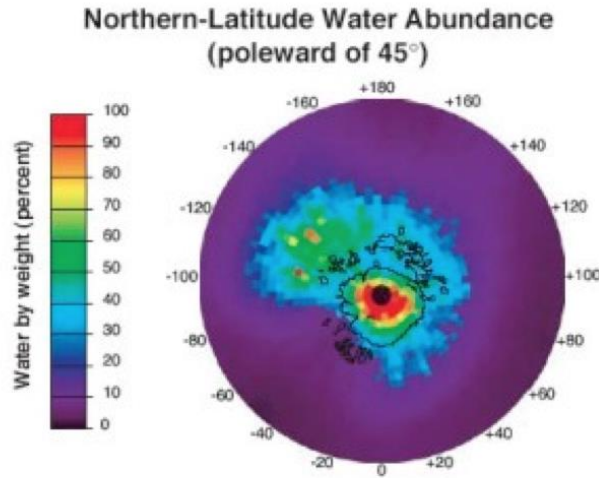
Phoenix Mars Lander
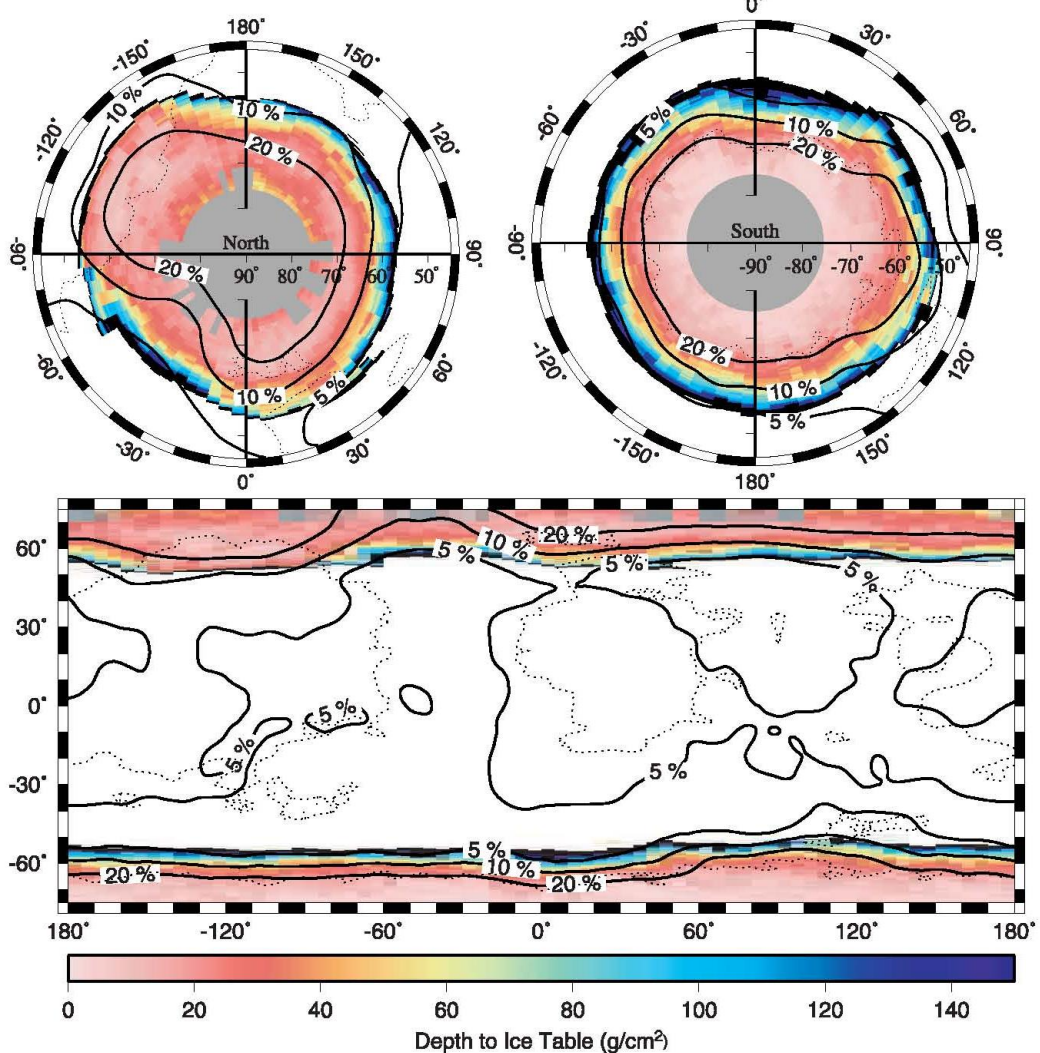
Figure 8. Color indicates depth to the ice table in g cm⁻² when ice is in equilibrium with the atmospheric water vapor. Ground ice is unstable in the white area. Black segments indicate finite burial depths larger than 150 g cm⁻². Missing data points are shown in gray. Assumed volume fraction of ice is 40%, but the geographic boundary between icy and ice-free soil is independent of the ice fraction. Solid contours indicate water-equivalent hydrogen content in percent determined from neutron spectroscopy [*Feldman et al.*, 2004]. The dotted lines are 200 J m⁻²K⁻¹s⁻¹/² contours of thermal inertia.

Schorghofer and Aharonson (2005)

Comparison with models

Near equilibrium ?

色： 大気中の水蒸気との平衡状態を仮定して計算される氷床までの深さ

実線： 中性子分光観測から見積もられた水含有量

→現在の気候とだいたい平衡状態か

しかし中・低緯度の氷は説明がつかない

Seasonal variation of dust, clouds, and H₂O vapor observed by an infrared spectrometer (TES) on Mars Global Surveyor

ダスト

氷雲

水蒸気

Smith, Icarus 167 (2004) 148–165
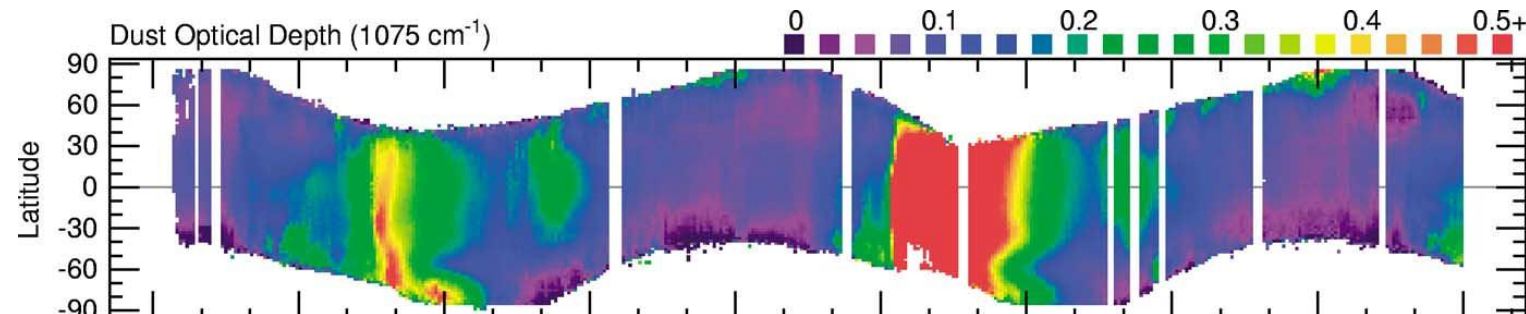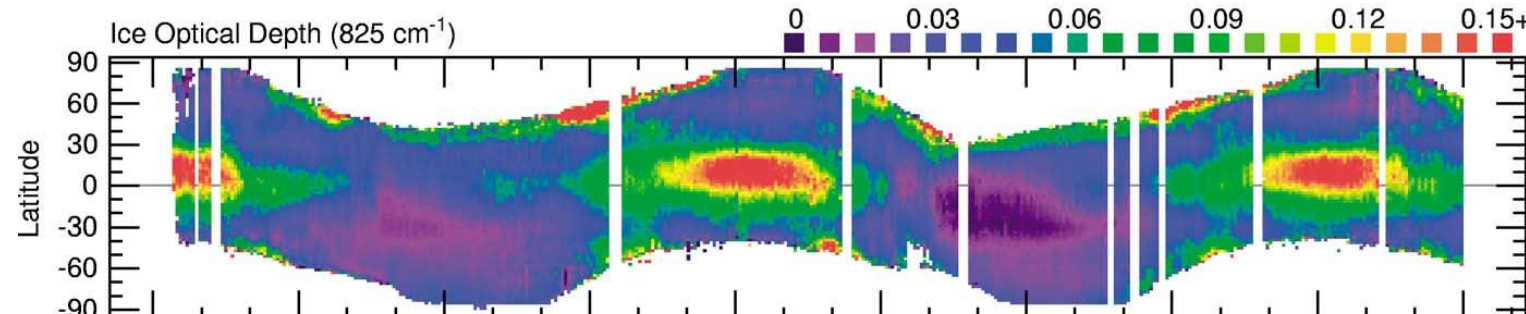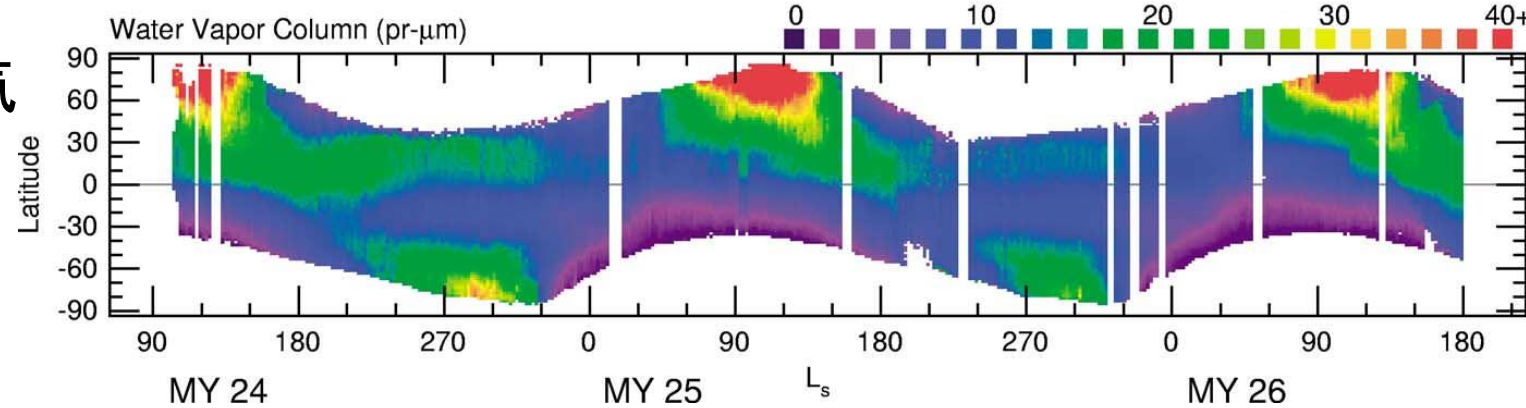
Seasonal cycle of Martian water

- 北極冠の消長が全体を駆動
- 北半球の春～夏に北極冠が昇華して北極域の水蒸気濃度が上昇、これが（この時期の弱い）水平渦で低緯度に拡散的に運ばれる。
- 低緯度に運ばれた水蒸気の一部は赤道越えのハドレー循環で南半球へ
- 北半球の秋～冬には北極冠で凝結により水蒸気濃度が低下し、南北濃度勾配が逆転するため、傾圧不安定などに伴う水平渦で低緯度から北極域に水蒸気が拡散的に戻る。低緯度の水蒸気量はそれまでの水蒸気輸送の履歴で決まる。
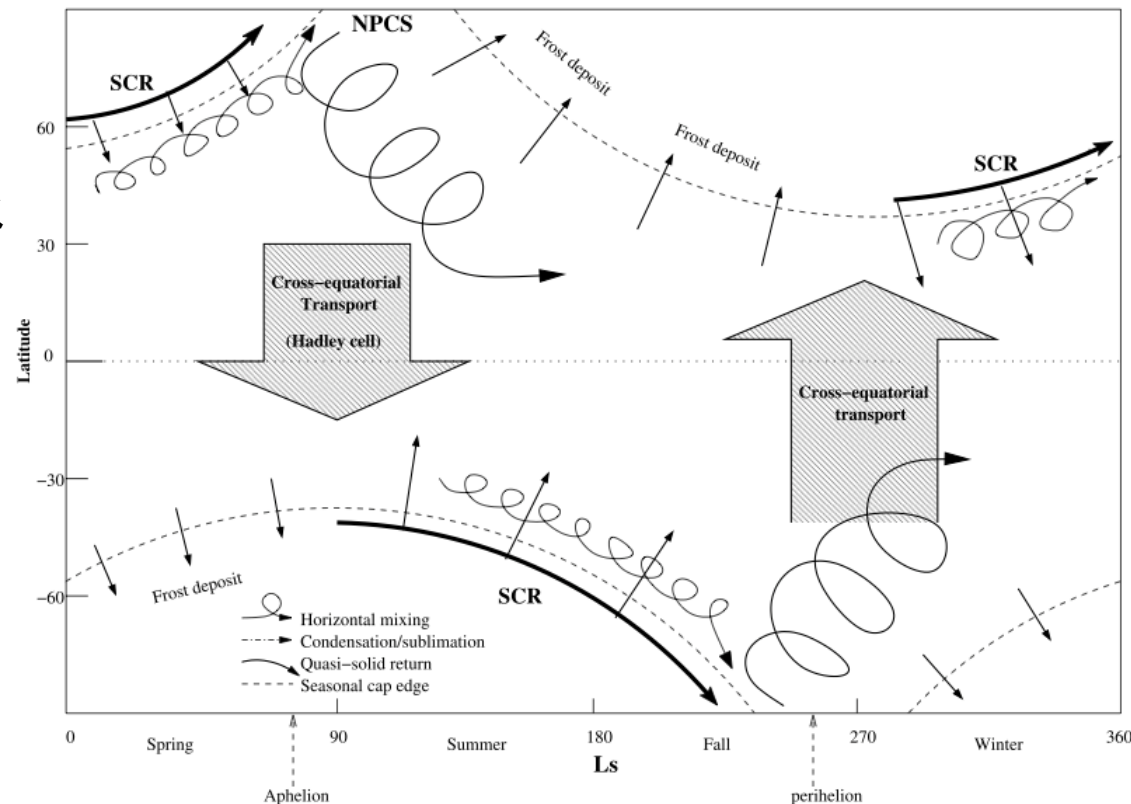

Figure 3. Chart describing the principal events affecting the Martian water cycle over the course of a year. NPCS stands for North Polar Cap Sublimation; SCR stands for Seasonal Cap Recession.

ISAS JAXA

What's MMX　Objective　Science　Probe　Member　Links　News ⧉

MMX
Martian Moons eXploration

火星衛星へのサンプルリターンを狙っている探査機です。

MMXの実現によって様々な技術的向上が期待され、

その成果によって太陽系の惑星形成の謎を解く鍵が得られるでしょう。
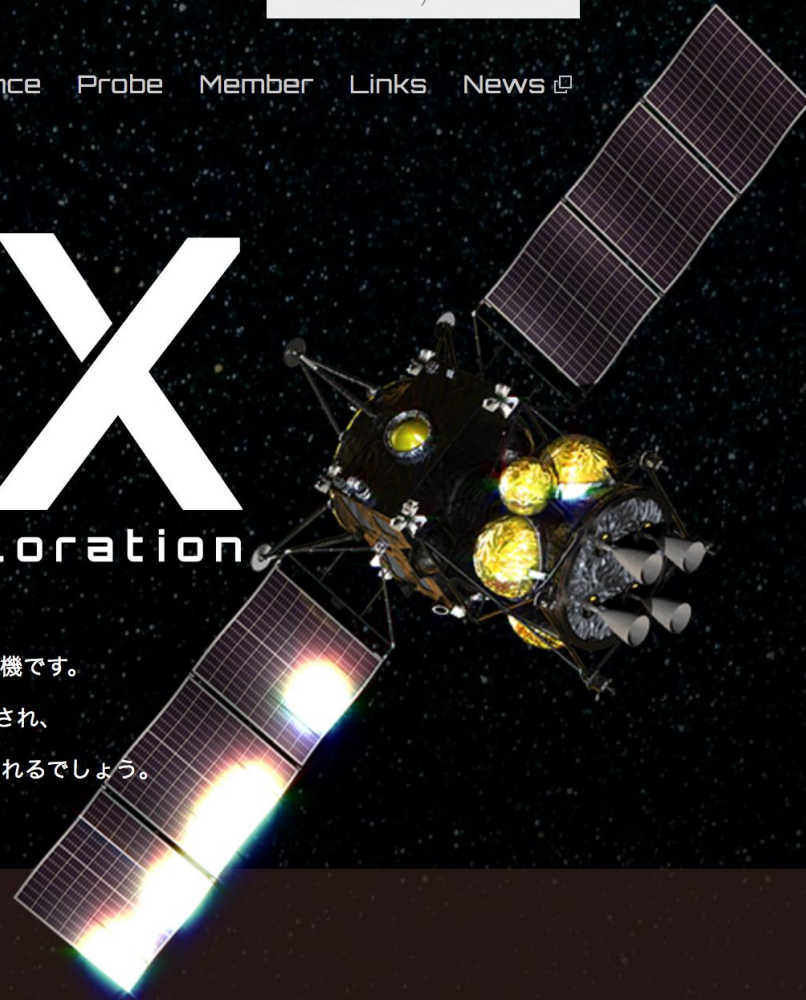
NEW　最新情報

2017.05.17	ニュースページを公開しました。上のタブのNewsから見ることができます。
2017.05.17	Twitterアカウントができました。(@mmx_jaxa_jp)
2017.04.07	メンバー写真を更新しました。
2017.04.05	ホームページを公開しました。

Twitter

Tweets by mmx_jaxa_jp

MMX ミッション機器

- ガンマ線・中性子分光計：地下の物質分布、特に氷が存在の有無を調査
- 広角分光カメラ：7つの画像センサを用いて、7色の画像を同時に取得
- 近赤外分光計：表層の水分子や水を含む鉱物を観測
- 望遠カメラ：20 km離れたところから40 cmの岩石を見つけることが可能
- レーザ高度計：表面の凹凸を調査
- ダスト計測器：ダストが浮遊しているかを観測
- イオンエネルギー質量分析：衛星周辺の粒子を調査

Controlling factors of Martian climate

- Water cycle
  - Atmosphere-surface water exchange controls the long-term evolution of water reservoirs
  - The seasonal/diurnal cycle controls the amount of water in the atmosphere, thereby influencing escape to space
- Dust lifting
  - Radiative effect of dust controls the surface/atmospheric temperature, thereby determining the stability of surface water
  - Radiative effect of dust controls the water vapor content in the upper atmosphere and the vertical transport of atmospheric constituents, thereby influencing escape to space

Water cycle on Mars
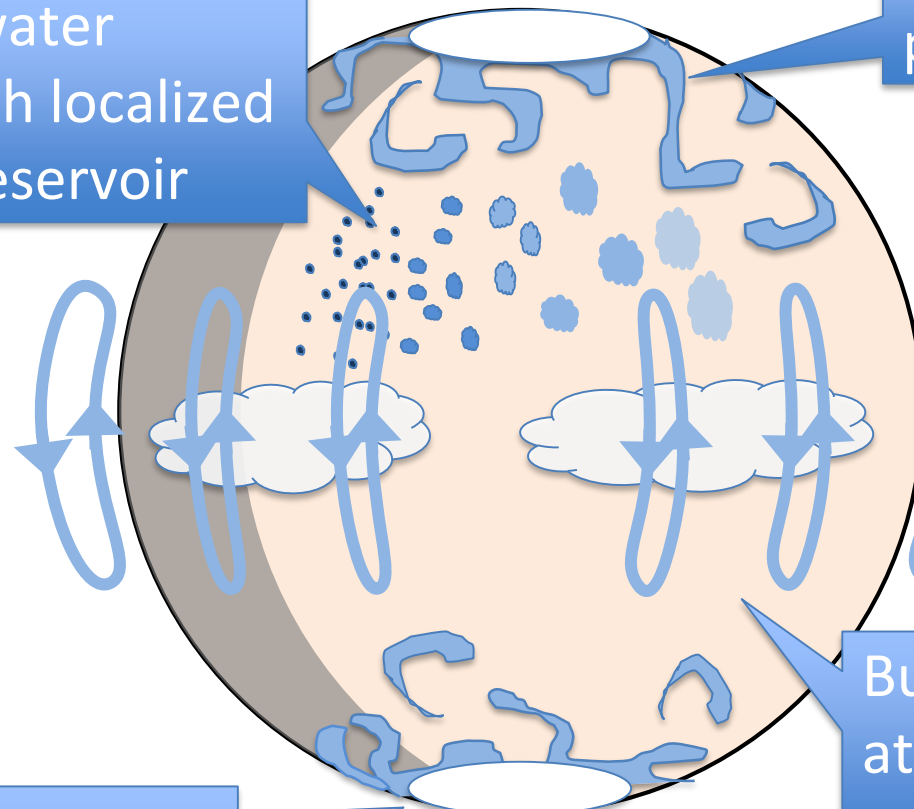
# localized water vapor transport and phase change : keys to understand water cycle and reservoir stability

Thick clouds on nightside

Cloud belt

June 27, 1997
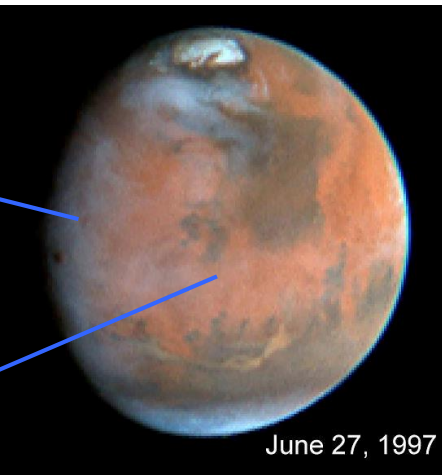
Mars Express/PFS water vapor map

H_2O column density ($L_s=330°-60°$) - PFS/LW

Fouchet et al. (2007)

Water Equivalent Hydrogen

Precipitation predicted by GCM

Feldman et al. (2005)
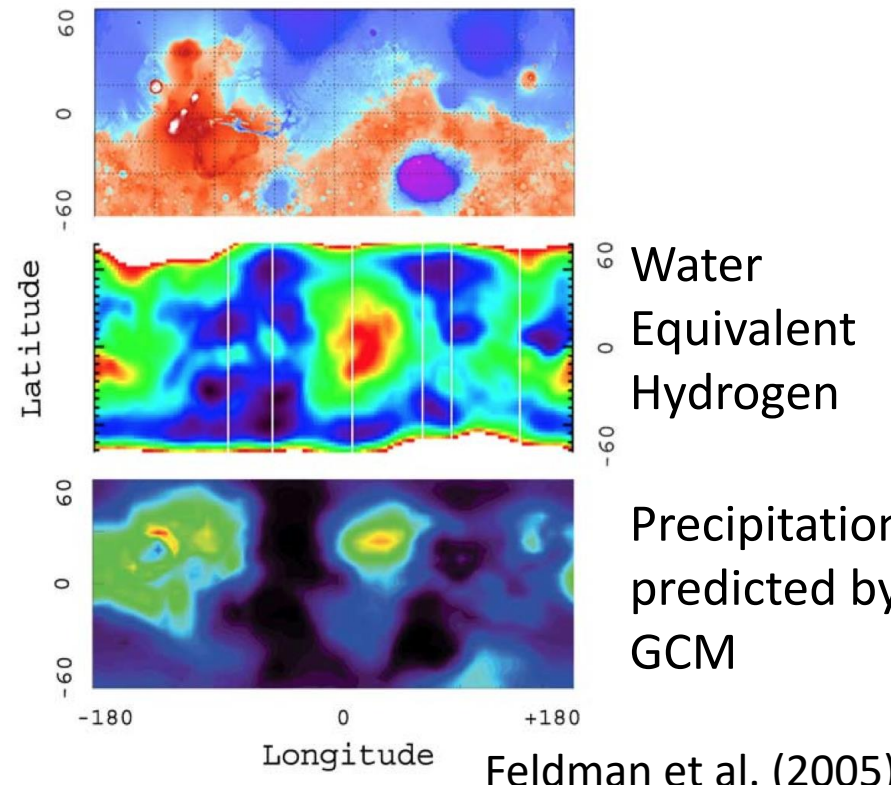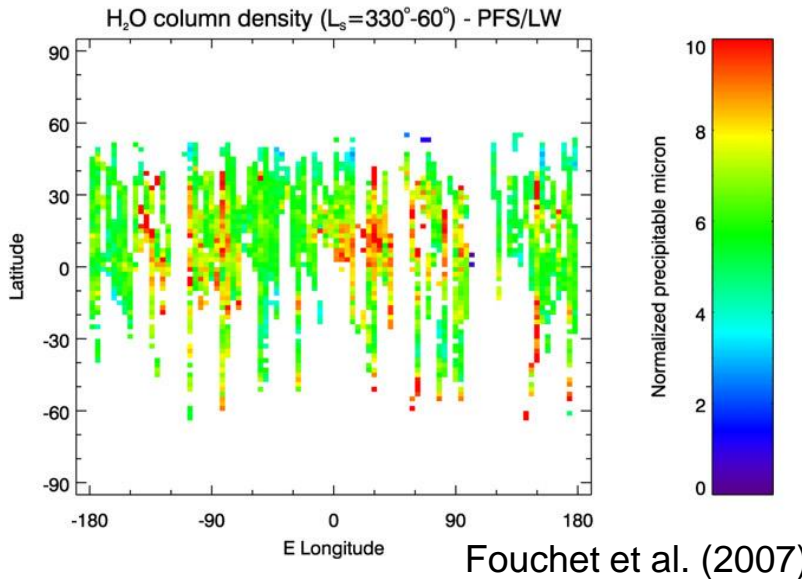
Previous observations did not obtain snapshots of high-resolution water vapor distribution and did not observe formation/evaporation of localized clouds

# Fast, localized dust storms : key to understand dust lifting and anomalous dust distribution

Meridional cross section of dust mixing ratio

Detached dust layers
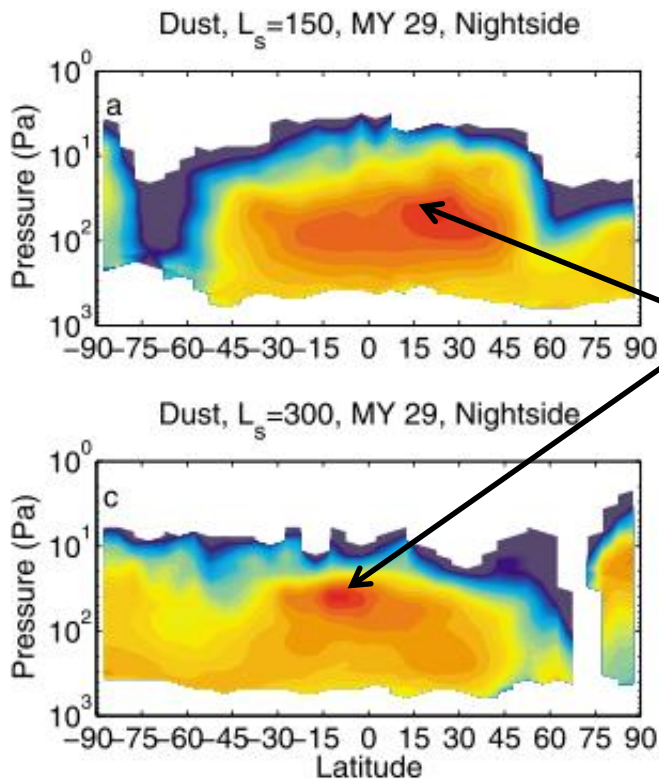
Heavens et al. (2011)

"Rocket dust storm": source of high-altitude dust ?
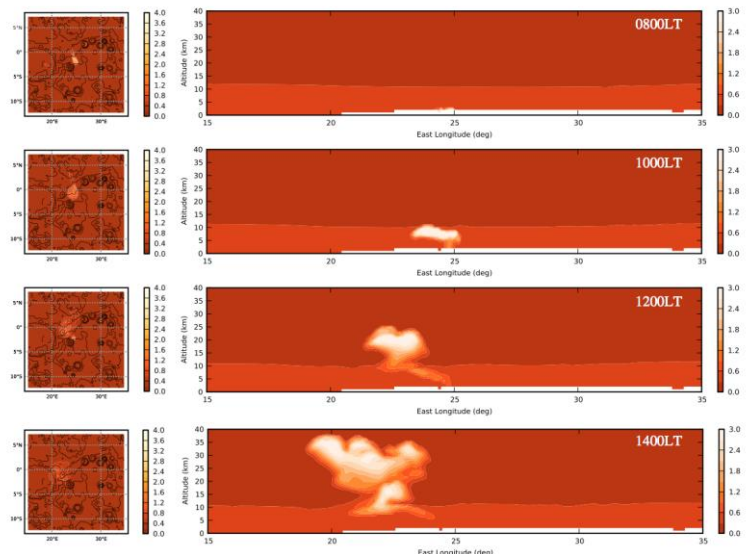
Spiga et al. (2013)

Localized dust clouds : Previous observations did not detect temporal development

# Limitation of observations from polar, low-altitude orbiters
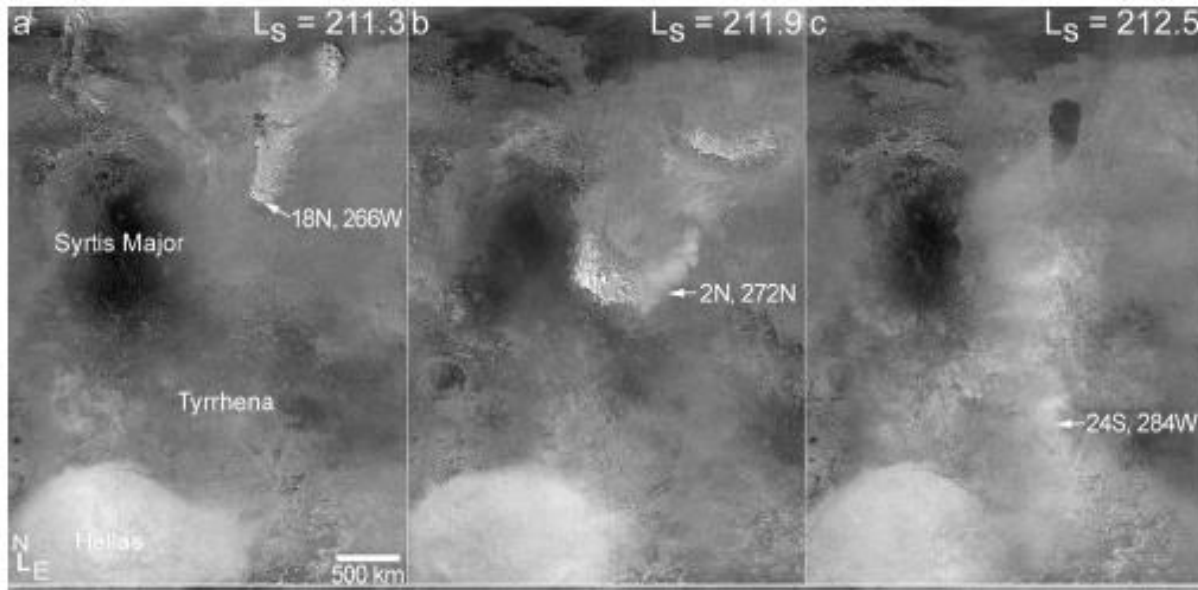

MOC images taken on three successive days
Too sparse in time

Concept of trace gas observations by Trace Gas Orbiter
*Too sparse in space*
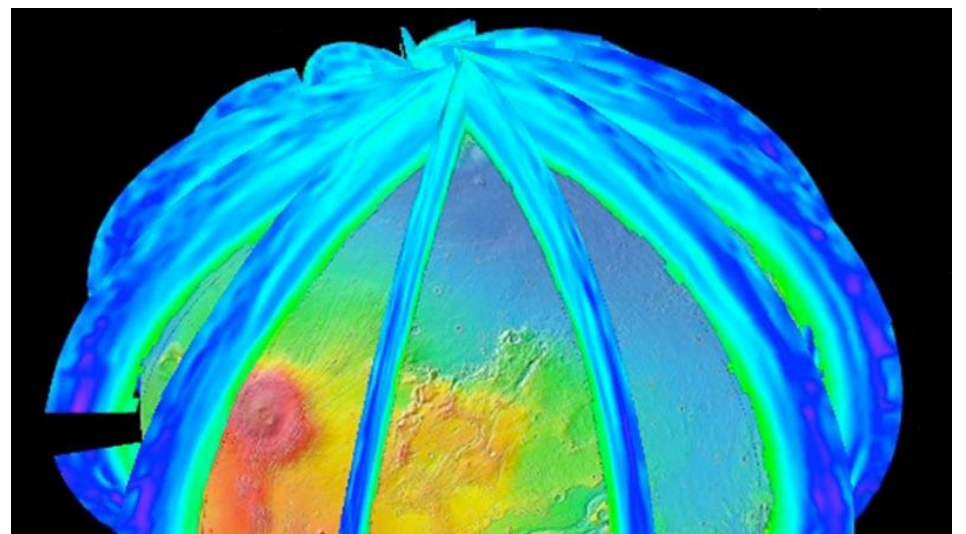
High-altitude orbit of MMX: an ideal platform for continuous, high-resolution monitoring

4-5 hours of continuous mapping with <1 h interval

Visible imaging
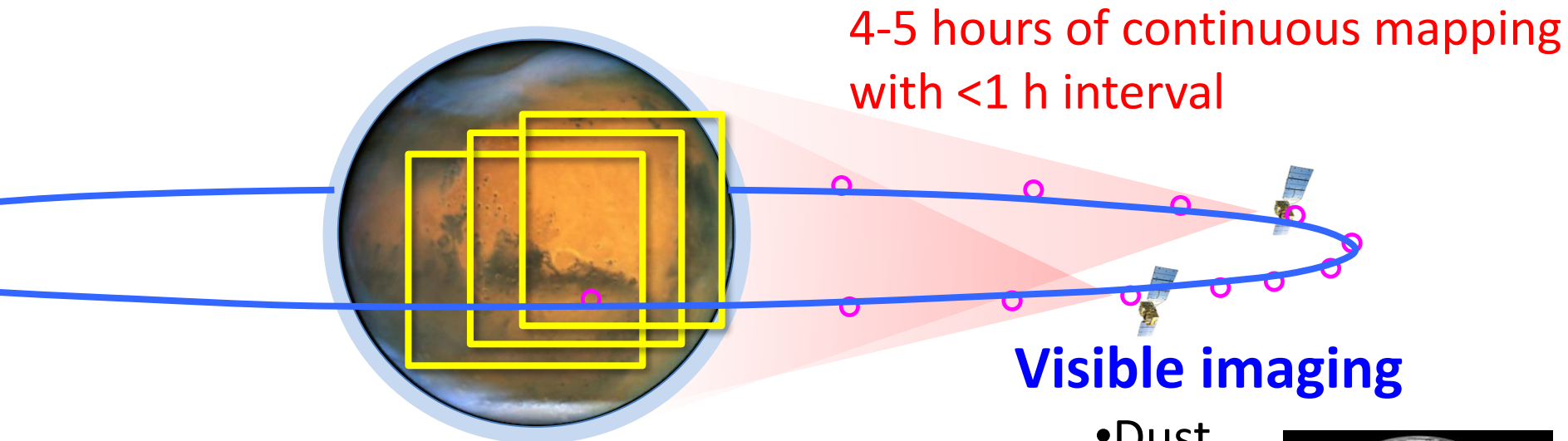
•Dust

•Cloud

Near-IR Imaging spectroscopy

•Water vapor, CO

•Dust, cloud
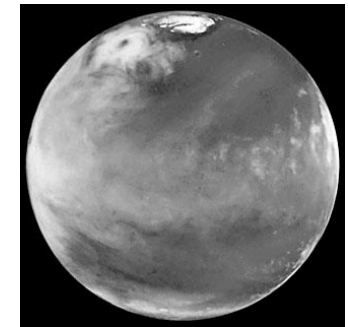
•Surface pressure

Imaging spectroscopy (MacrOmega)

- Mapping of H_2O, CO_2 (surface pressure) and CO column amounts by near-IR spectroscopy of reflected sunlight
  - Multi-pixel FOV combined with the scanning by spacecraft attitude control enables acquisition of 2-D maps
- Dust, clouds

Mars Express /OMEGA
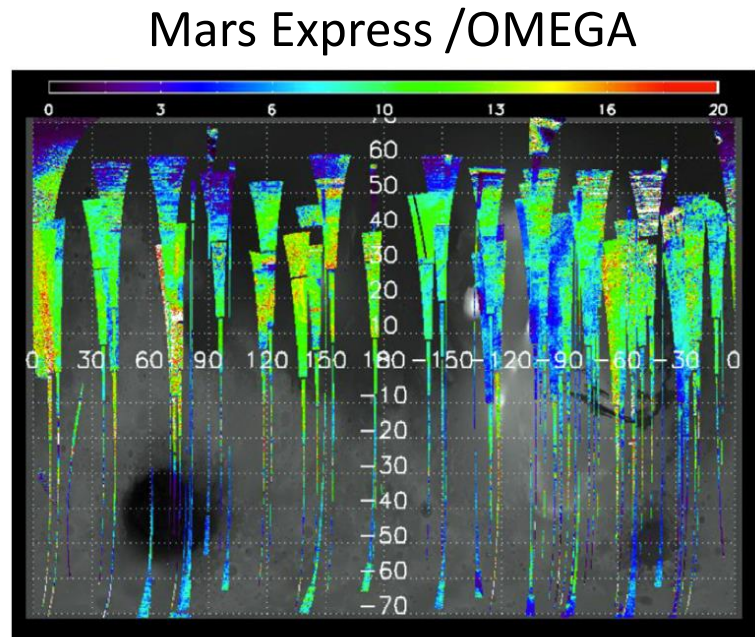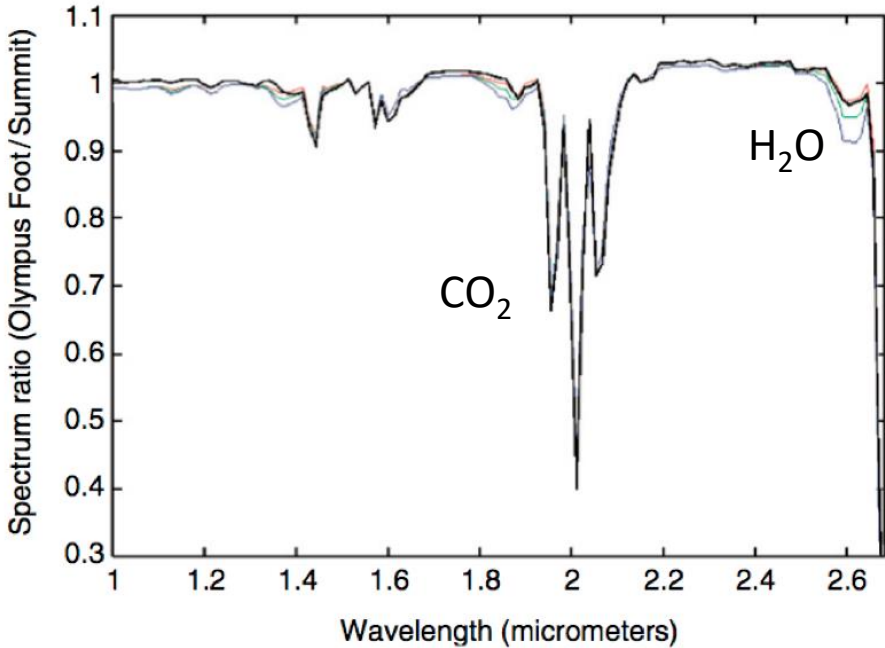
Imaging clouds and dust (WAM)

– Clouds (blue) and dust (red) are well distinguished by using multiple filters
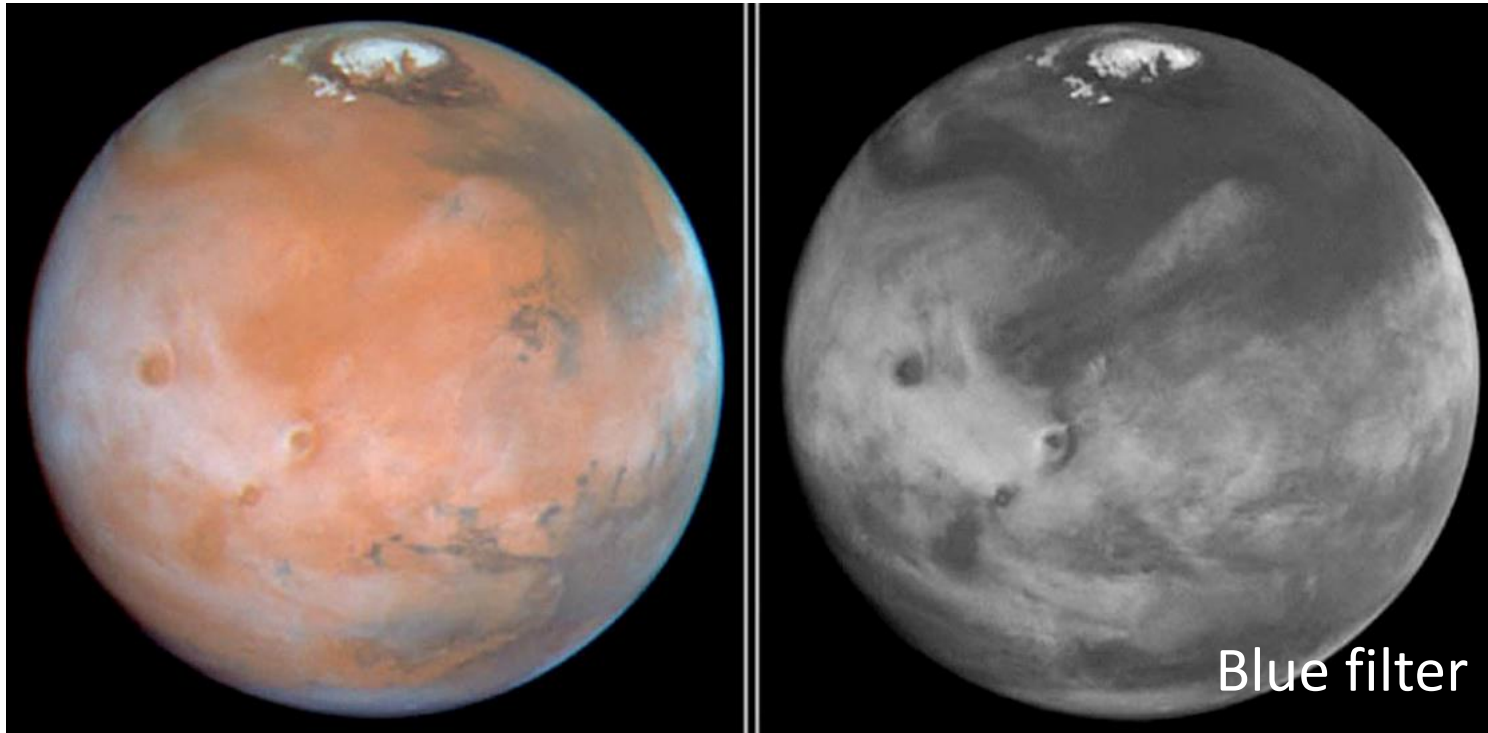

Blue filter

HST Mars images

Importance of successive imaging
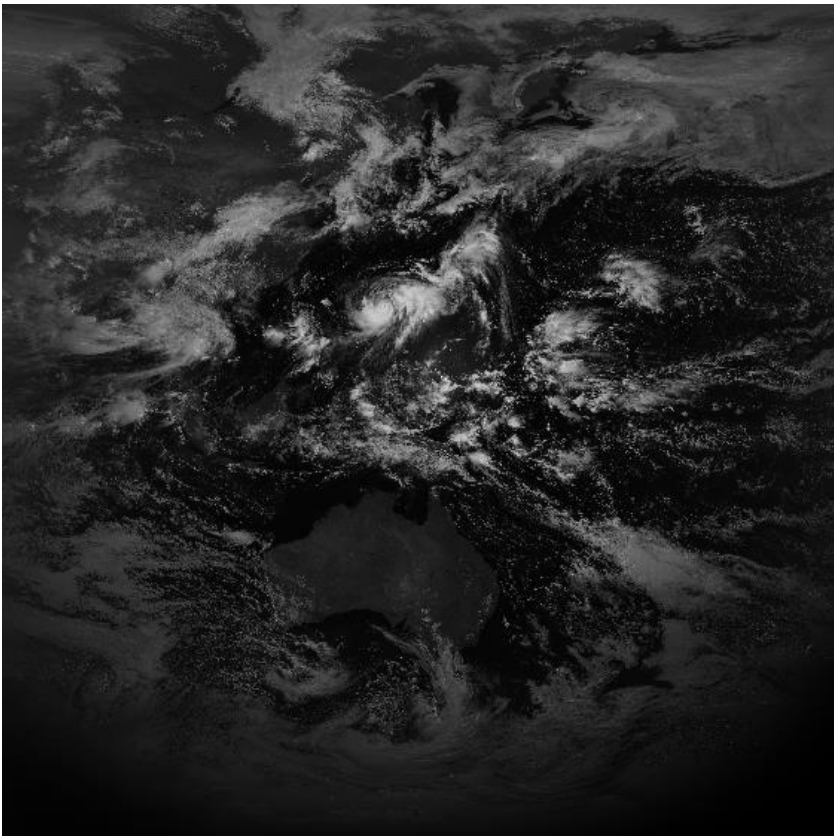
One global image per one day similar to mosaics by MOC or MARCI
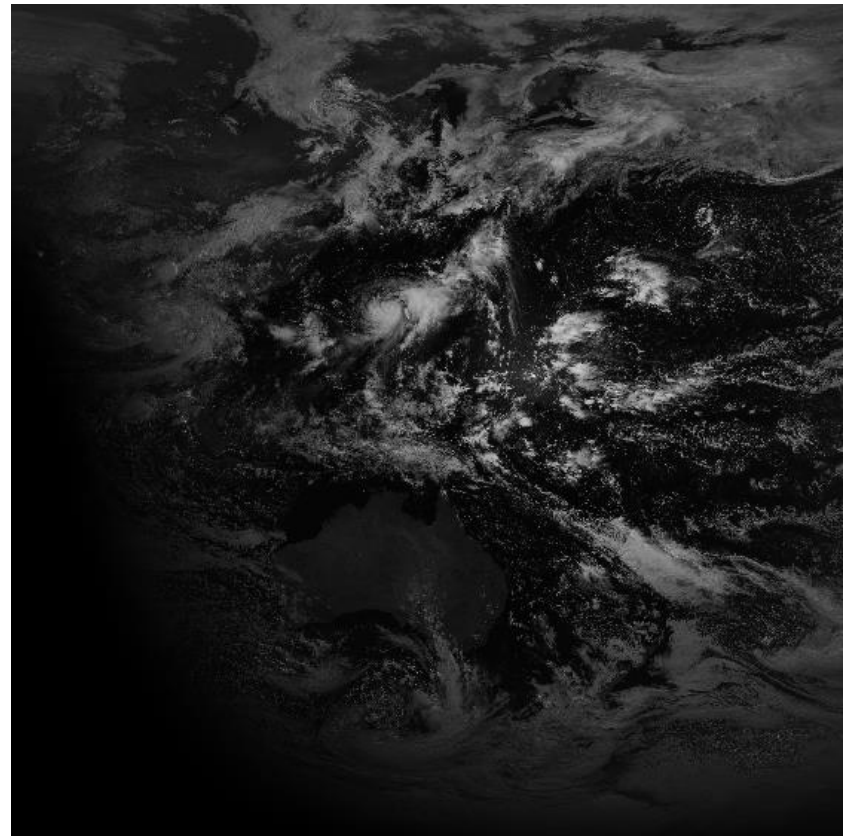
Continuous global monitoring from the Mars orbiter

(provided by Ogohara)

Changing views of Martian atmospheric science

Observed planetary-scale distributions of water vapor, clouds, dust and other species are interpreted based on numerical models
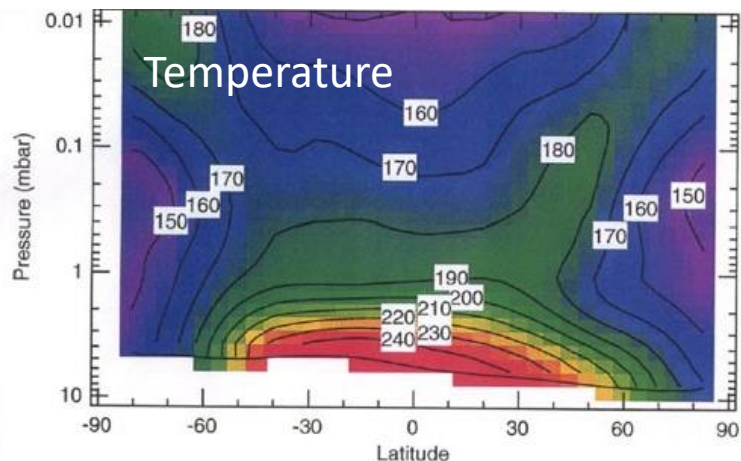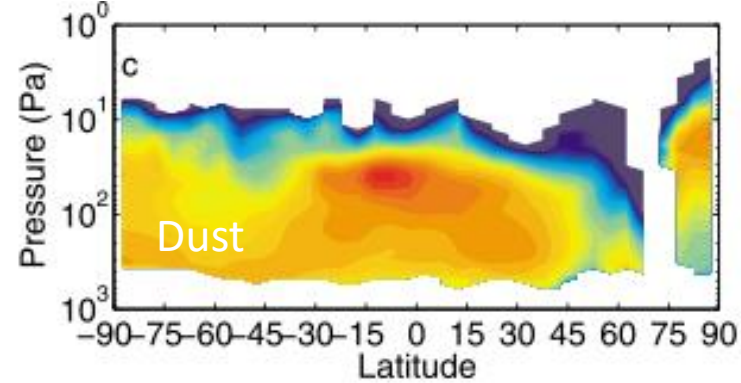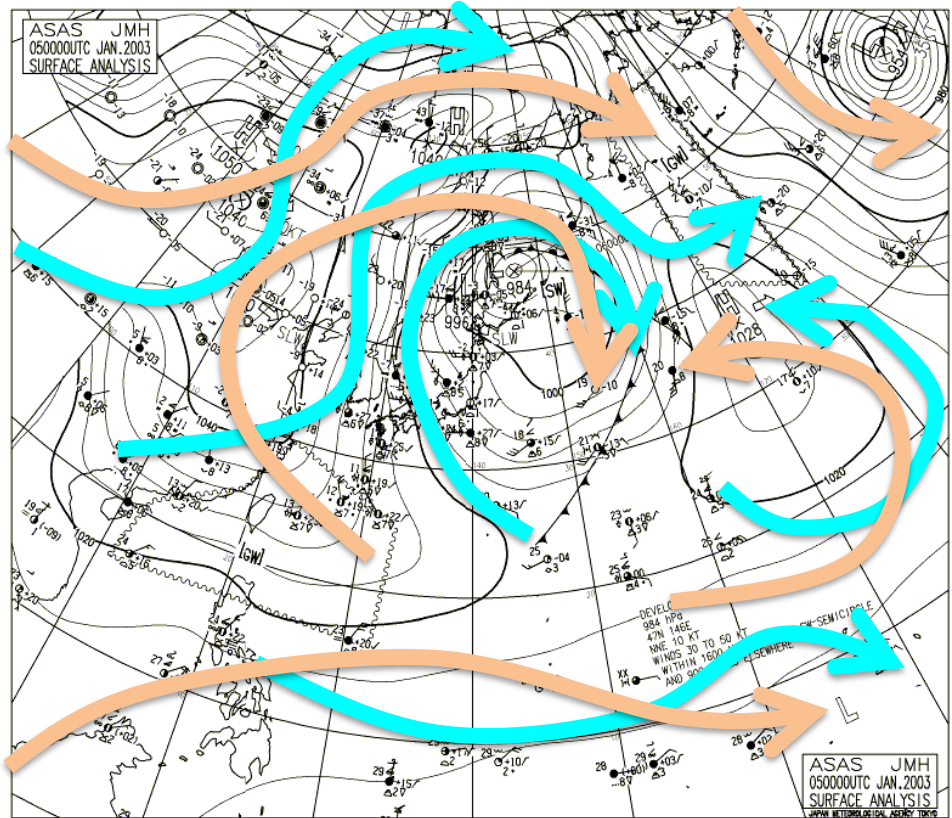

Transport processes are directly detected and combined with meteorological data (with the help of data assimilation)

Phobos and Mars as seen from the Phobos-observation orbit
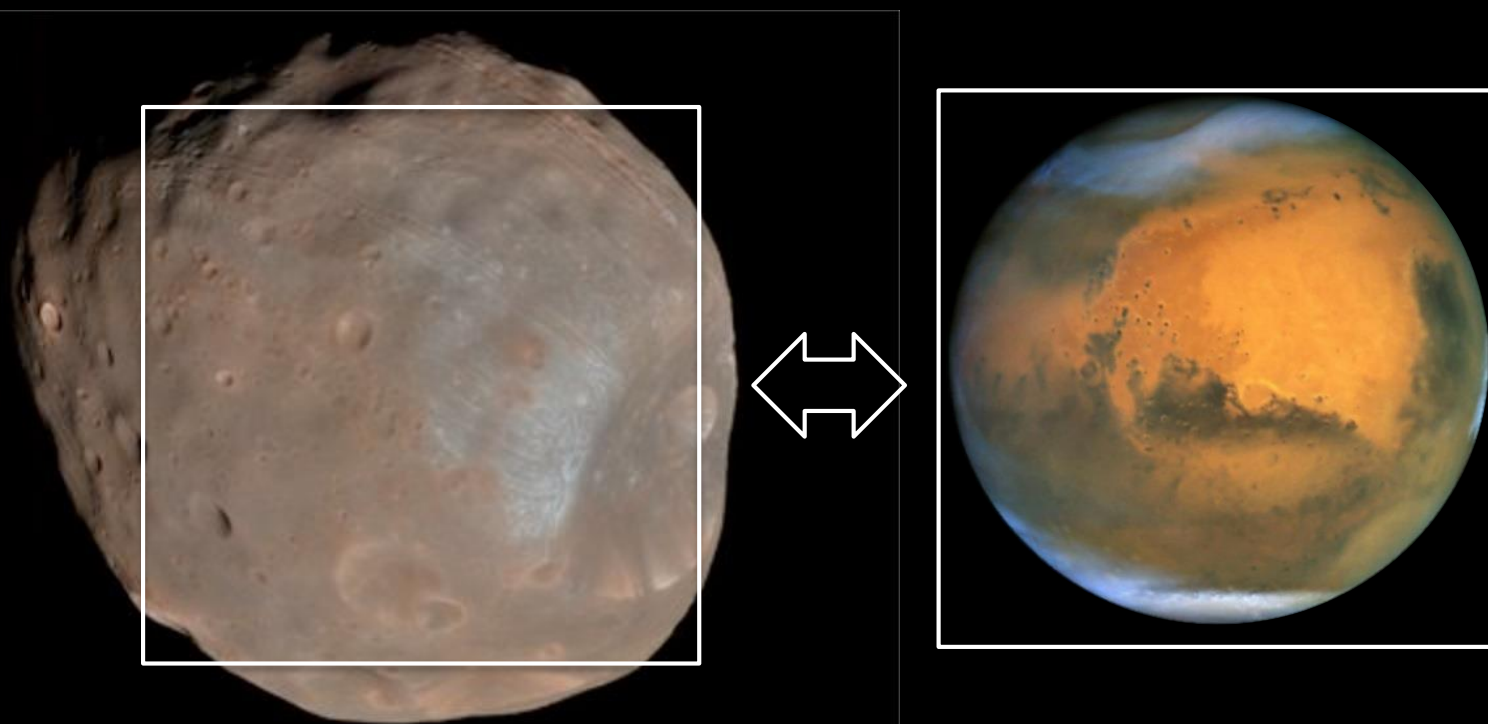
They have a similar apparent size. (Why don't you observe Mars using instruments that we already have for Phobos ?)

Summary

- Diurnal cycles and localized events are expected to play crucial roles in the Martian climate system. Such processes have not been well observed in previous Martian missions. Observations in MMX from a high orbit will achieve a breakthrough via continuous, high-resolution global monitoring of dust, clouds, water vapor, and minor gases.

- Expected outcomes
  - Spatial distribution of water vapor at fine scales
  - How water vapor emerges at specific locations, flows over long distances, and forms clouds
  - Location, local time, and timescale of localized dust lifting
  - How the lifted dust clouds spread and become diffuse